University of Peloponnese

Department of Informatics and Telecommunications

STUDY OF EM WAVE PROPAGATION IN ELLIPTICAL CORE OPTICAL FIBERS

Euripides I. Georgantzos

Doctor of Philosophy

October 2020

STUDY OF EM WAVE PROPAGATION

IN ELLIPTICAL CORE OPTICAL FIBERS

ABSTRACT

STUDY OF EM WAVE PROPAGATION IN ELLIPTICAL CORE OPTICAL FIBERS

Euripides Georgantzos

University of Peloponnese

Although initially studied as a deviation from cylindrical optical fibers, elliptical core fibers have evolved to become a basic component in numerous applications. Increased ellipticity of the core section allows these fibers to sustain polarization for long distances. Polarization, birefringence, simplicity to manufacture, structural cohesion and azimuthal stability, are the key advantages of elliptical fibers. As a result of their distinct properties, they are used in various applications including optical sensors, interferometers, rare-earth-doped fiber sources, amplifiers and communications applications.

The concept of EM wave propagation inside dielectric rods of elliptical section has been studied initially for elliptical waveguides in general by researchers including L.J. Chu, Lyubimov and Yeh; especially Yeh's analysis has provided basic mathematical tools and estimations regarding key propagation characteristics which have proved essential for further research. The specific case of optical fibers with elliptical core has also been studied initially by Dyott, Stern and Schlosser, and research continues until today targeting specific characteristics like propagation modes, dispersion, birefringence and eigenvalue equations among others. Most of the existing studies are utilizing complicated mathematical methods and make critical assumptions involving the refractive index profile, in order to achieve results of a certain level of accuracy.

The current thesis introduces a novel method that, after conducting a fundamental level of mathematical analysis, substitutes the subsequent, prevalent Mathieu functions' analysis, with the Resonant Transmission Line theory. As a result, the presented technique estimates the key characteristics of propagating modes, including the mode propagation constant β and birefringence in elliptical fibers, with remarkable speed and accuracy. Among the advantages of the applied RTL method, is the fact that it is based more on computational strength than mathematical complexity, it converges fast, it avoids the unrealistic assumption of an infinite cladding, and allows the investigation of arbitrary index profiles.

Regarding the structure of the thesis, chapter 1 starts with a detailed presentation of the RTL technique and its application on cylindrical core optical fibers. Beginning with a mathematical analysis based on Maxwell's equations, the presentation serves as a demonstration of the RTL technique as the key toolset that will be used later in the thesis to describe propagation in elliptical fibers. In the same chapter, a basic definition of birefringence is also given for cylindrical core fibers. Chapter 2 presents the existing literature related to elliptical waveguides and elliptical fibers in particular. It continues with the presentation of the prevailing mathematical analysis for the estimation of mode propagation constant β and provides the related formulas, focusing on Yeh's approach and Dyott's valuable research. Further on, birefringence is defined and the major techniques are described towards its estimation. This chapter also describes the elliptical fibers' distinct property of retaining polarization as well as their potential applications. In chapter 3, a fundamental mathematical analysis is provided, applying Maxwell's equations on elliptical coordinates before proceeding with the RTL technique. The analysis involves the appearance of harmonics which are included in the RTL method, hence the solutions provided, all include different numbers of harmonics. The mode propagation constant β is calculated and β-V diagrams are plotted. Comparisons are also presented of results with different numbers of harmonics included. In chapter 4, the RTL method is applied over a mathematical analysis that follows a different approach, utilizing conformal mapping to obtain values of propagation properties. This chapter aims to provide basic tools for the study of D fibers that combine characteristics of both eccentric cores and elliptical cores. Chapter 5 provides yet another method for studying elliptical fibers, following a top-down approach. The chapter defines unconventional fibers as a generic

category of fibers with angular asymmetry and develops a method that can be used in various specific cases including elliptical and holey fibers. The method omits the use of harmonics and achieves significant accuracy in calculating β. The final chapter, chapter 6, describes the advantages and contributions of the current thesis in the study of elliptical fibers and presents suggestions for future research.

ΠΕΡΙΛΗΨΗ

ΜΕΛΕΤΗ ΔΙΑΔΟΣΗΣ ΗΜ ΚΥΜΑΤΩΝ ΣΕ ΟΠΤΙΚΕΣ ΙΝΕΣ ΕΛΛΕΙΠΤΙΚΟΥ ΠΥΡΗΝΑ

Ευριπίδης Γεωργάντζος

Πανεπιστήμιο Πελοποννήσου

1. Εισαγωγή

Η ελλειπτικές οπτικές ίνες αρχικά μελετήθηκαν στο πλαίσιο καθορισμού των επιπτώσεων μεταβολών στη γεωμετρία του πυρήνα της κυλινδρικής οπτικής ίνας που χρησιμοποιείται ως μέσω μεταφοράς πληροφορίας στις σύγχρονες τηλεπικοινωνίες. Ωστόσο, χάρη στις ξεχωριστές τους ιδιότητες, οι ελλειπτικές ίνες σήμερα χρησιμοποιούνται σε μια πληθώρα εφαρμογών. Η διάδοση ηλεκτρομαγνητικών κυμάτων σε οπτικές ίνες με πυρήνα ελλειπτικής διατομής έχει συχνά αποτελέσει αντικείμενο μελέτης. Αναφορά σε κυματοδηγούς ελλειπτικής διατομής γενικά, είχε γίνει αρχικά σε μελέτη των ΗΜ κυμάτων μέσα σε ελλειπτικούς μεταλλικούς σωλήνες, σε έρευνα του L.J. Chu, όμως η πρώτη φορά που δώθηκε λύση στο πρόβλημα της διάδοσης ,ήταν από τους Lyubimov κ.α. Ειδικότερα η περίπτωση της ελλειπτικής οπτικής ίνας ερευνήθηκε αρχικά ως προβληματική περίπτωση παραμόρφωσης της κυλινδρικής ίνας από τους Dyott και Stern και από τον Schlosser. Οι έρευνες κατέληξαν στο συμπέρασμα ότι η χρήση μεγαλύτερου βαθμού ελλειπτικότητας, σε συνδυασμό με αρκούντως ευρεία διαφορά των δεικτών διάθλασης, οδηγεί σε διαχωρισμό των σταθερών διάδοσης των βασικών τρόπων διάδοσης και επιτρέπει στις ίνες να διατηρούν την πόλωση για μεγαλύτερες αποστάσεις. Η ιδιότητα της πόλωσης αποτελεί σημαντικό στοιχείο για τα ιντερφερόμετρα. Οι ίνες που έχουν τη δυνατότητα να διατηρούν πόλωση χρησιμοποιούνταν εξ αρχής στα οπτικά ιντερφερόμετρα, όμως η μέθοδος που εφαρμόζονταν για το διαχωρισμό των οπτικών διαδρομών μέσα στην ίνα, βασιζόταν στην αποσύνδεση των δεικτών διάθλασης εφαρμόζοντας πίεση. Σε αντίθεση με την προαναφερθείσα μέθοδο, η χρήση ελλειπτικών ινών για το διαχωρισμό του

θεμελιώδους τρόπου διάδοσης σε δυο ξεχωριστούς, ορθογώνια πολωμένους ρυθμούς έχει σημαντικά πλεονεκτήματα:

- Οι ελλειπτικές ίνες παρουσιάζουν μικρότερη περιπλοκότητα στην κατασκευή
- Με την αποφυγή εφαρμογής πίεσης, μειώνεται η επακόλουθη ευαισθησία της ίνας στην περαιτέρω πίεση και τη θερμοκρασία.
- Οι υψηλότεροι ρυθμοί διάδοσης στις ελλειπτικές ίνες είναι πιο σταθεροί αζιμουθιακά σε σχέση με τις ίνες κυλινδρικής διατομής, διευκολύνοντας κατ αυτό τον τρόπο την κατασκευή αισθητήρων ίνας με περισσότερους ρυθμούς.

Χάρη στις ξεχωριστές τους ιδιότητες οι ελλειπτικές ίνες χρησιμοποιούνται σε ένα εύρος εφαρμογών που περιλαμβάνει αισθητήρες, ίνες ενισχυμένες με σπάνιες γαίες, ενισχυτές καθώς και στις τηλεπικοινωνίες ως μέσον εξουδετέρωσης της καθυστέρησης κυματοομάδας.

Μεταξύ των προσπαθειών που έχουν γίνει για την έρευνα των ελλειπτικών κυματοδηγών και τον καθορισμό των βασικών ιδιοτήτων της διάδοσης ΗΜ κύματος στο εσωτερικό τους, ξεχωρίζει η έρευνα του Yeh η οποία έθεσε τις μαθηματικές βάσεις για τη σχετική ανάλυση. Η ανάλυση του Yeh κάνει χρήση των εξισώσεων Mathieu και καταλήγει στον καθορισμό των βασικών εξισώσεων μετάδοσης και τον υπολογισμό της σταθεράς διάδοσης, λαμβάνοντας υπόψη κάποιες παραδοχές σχετικά με το εύρος της διαφοράς των δεικτών διάθλασης και το βαθμό ελλειπτικότητας του πυρήνα. Τόσο η μέθοδος με χρήση εξισώσεων Mathieu όσο και οι μεταγενέστερες μέθοδοι που βασίστηκαν σε αυτή, αναγκαστικά προϋποθέτουν την επίλυση μακροσκελών και περίπλοκων σειρών μαθηματικών σχέσεων. Επίσης οι λύσεις στις οποίες καταλήγουν, περιορίζονται σε συγκεκριμένες περιπτώσεις ελλειπτικής ίνας. Για παράδειγμα η ανάλυση του Yeh αφορά σε ίνα βαθμωτού δείκτη διάθλασης (step index), όπου μάλιστα η επένδυση γύρω από τον πυρήνα επεκτείνεται στο άπειρο.

Σκοπός της παρούσας διδακτορικής διατριβής είναι η διαμόρφωση μιας μεθόδου που θα στηρίζεται περισσότερο σε σύχρονα υπολογιστικά μέσα, χωρίς να υστερεί σε ακρίβεια σε σύγκριση με τις αναλυτικές μεθόδους, επεκτείνοντας παράλληλα το εύρος των περιπτώσεων για τις οποίες επιτυγχάνεται λύση.

2. Το περίγραμμα της τρέχουσας ερευνητικής εργασίας

Στο πλαίσιο αυτής της ερευνητικής εργασίας αναπτύχθηκαν νέες αποτελεσματικές μέθοδοι για την μελέτη ελλειπτικών ινών και τον ακριβή καθορισμό σημαντικών παραγόντων διάδοσης. Τα αντικείμενα της έρευνας μπορούν να περιγραφούν μέσα από τις παρακάτω επιμέρους ενότητες:

- Κατά την αρχική προσέγγιση προς τη δημιουργία μιας καινοτόμου μεθόδου για την περιγραφή της ελλειπτικής ίνας, έγινε μια μαθηματική ανάλυση με εφαρμογή των κυματικών εξισώσεων του Maxwell σε επίπεδο ελλειπτικών συντεταγμένων. Η ανάλυση κατέληξε στις βασικές σχέσεις που διέπουν τη διάδοση ΗΜ κύματος μέσα σε κυματοδηγό ελλειπτικής διατομής, για μονούς και ζυγούς ρυθμούς μετάδοσης. Χαρακτηριστικό στοιχείο των τελικών εξισώσεων, είναι η εμφάνιση άπειρων πεπλεγμένων αρμονικών μειούμενης βαρύτητας. Ο υπολογισμός μέσα από τις σχέσεις, της σταθεράς διάδοσης β προϋποθέτει τη χρήση προκαθορισμένου αριθμού αρμονικών: 0, 1, 2 … 5 κ.ο.κ. Η αποτελεσματικότητα της μεθόδου εξακριβώθηκε μέσα από τη σύγκριση τιμών του β υπολογισμένων με την παρούσα μεθοδο, με αντίστοιχες τιμές υπολογισμένες με τη αναλυτική μέθοδο με χρήση εξισώσεων Mathieu. Επιπρόσθετα, για να μελετηθεί η επίδραση του αριθμού των αρμονικών στην ακρίβεια της μεθόδου, η τιμή του β υπολογίστηκε διαδοχικά για τις περιπτώσεις μη χρήσης αρμονικών, και ορισμένων αριθμών αυτών. Βάσει των αποτελεσμάτων εξήχθη το συμπέρασμα ότι η χρήση περισσότερων αρμονικών βελτιώνει την ακρίβεια της μεθόδου. Ωστόσο ενώ η διαφορά στην ακρίβεια μεταξύ καμμίας και μίας αρμονικής είναι αξιόλογη, όσο αυξάνεται ο αριθμός των αρμονικών, τόσο η διαφορά αυτή μειώνεται. Έτσι η χρήση άνω των 5 αρμονικών δεν έχει παρα ελάχιστη διαφορά στην ακρίβεια των αποτελεσμάτων. Άλλο ένα ενδιαφέρον συμπέρασμα είναι οτι όσο αυξάνεται ο βαθμός ελλειπτικότητας του πυρήνα, τόσο αυξάνεται ο αριθμός των απαιτούμενων αρμονικών για την επίτευξη μεγαλύτερης ακρίβειας.
- Η μέθοδος που αναπτύχθηκε με την πρώτη προσέγγιση, χρησιμοποιήθηκε επίσης για τον υπολογισμό της διπλοθλαστικότητας (birefringence). Η διπλοθλαστικότητα είναι μια σημαντική ιδιότητα, που εμφανίζεται πιο έντονα στις ελλειπτικές ίνες, χάρη στην οποία δύνανται να διατηρούν την πόλωση.

Ορίζεται ως το φαινόμενο κατά το οποίο όταν ένα ΗΜ κύμα διαδίδεται σε έναν κυματοδηγό ελλειπτικής διατομής, οι σταθερές διάδοσης των ρυθμών ${}_0HE_{11}$ και ${}_eHE_{11}$ εμφανίζονται αποσυνδεδεμένες μεταξύ τους. Η τιμή της διπλοθλαστικότητας δίδεται ως η διαφορά μεταξύ των κανονικοποιημένων σταθερών διάδοσης $\Delta\bar{\beta} = {}_0\bar{\beta} - {}_e\bar{\beta}$. Έχοντας λοιπόν ήδη υπολογίσει τις σταθερές διάδοσης και τα αντίστοιχα β-V διαγράμματα ο υπολογισμός της διπλοθλαστικότητας για διάφορες τιμές κανονικοποιημένης συχνότητας V ήταν εύκολος χάρη στην απλότητα της μεθόδου και της επεκτασιμότητάς της. Με αρκετή ευκολία αναπτύχθηκαν προγράμματα για τη σύγκριση της διπλοθλαστικότητας για διαφορετικούς βαθμούς ελλειπτικότητας αλλά και τη σύγκριση μεταξύ διαφορετικών προφίλ δεικτών διάθλασης.

- Στην παρούσα διατριβή παρουσιάζεται μια επιπλέον μέθοδος για τον υπολογισμό της σταθεράς β, εφαρμόζοντας τις εξισώσεις του Maxwell σε κυλινδρικές συντεταγμένες, με χρήση σύμμορφης απεικόνισης (conformal mapping). Απαλείφοντας τις προκύπτουσες αρμονικές, η μαθηματική ανάλυση καταλήγει στις σχέσεις που περιγράφουν γραμμή μετάφοράς, ισοδύναμων κυκλωμάτων. Η μέθοδος αυτή, αν και αρχικά περιγράφει οπτικές ίνες με έκκεντρο πυρήνα, μπορεί να χρησιμοποιηθεί για τον ακριβή υπολογισμό της σταθεράς β, και σε ελλειπτικές ίνες. Επιπλέον αποτελεί ιδανικό εργαλείο για τη μελέτη οπτικών ινών της κατηγορίας D fiber, που συνδυάζουν ελλειπτικό πυρήνα τοποθετημένο έκκεντρα σε σχέση με το περίβλημα και που είναι χρήσιμες σε πληθώρα εφαρμογών, οπτοηλεκτρονικών συσκευών κ.α.
- Τέλος, παρουσιάζεται μια τρίτη προσέγγιση για τη μελέτη της ελλειπτικής ίνας, η οποία ξεκινά περιγράφοντας τη γενικότερη περίπτωση οπτικών ινών που εμφανίζουν γωνιακή ασυμμετρία και καταλήγει μεταξύ άλλων και στην περίπτωση της ελλειπτικής ίνας. Η γενικότερη περίπτωση οπτικών ινών καλείται μη-συμβατική ίνα και χαρακτηρίζεται από δείκτη διάθλασης του οποίου η τιμή είναι συνάρτηση τόσο της ακτίνας r (απόσταση από τον άξονα z), όσο κι από τη γωνία φ που διαγράφεται στο επίπεδο που είναι κάθετο στον άξονα z, n(r,φ). Κατ' αυτό τον τρόπο αναπτύχθηκε μια νέα μέθοδος η οποία μπορεί με ακρίβεια να υπολογίσει την σταθερά β και την διπλοθλαστικότητα, όχι μόνο σε ελλειπτικές ίνες αλλά και σε ίνες διαφόρων σχημάτων διατομής του πυρήνα, όπως ορθογώνιου ή και διάτριτου πυρήνα (PCFs).

3. Η δομή της διδακτορικής διατριβής

Η διδακτορική αυτή διατριβή ερευνά τη διάδοση ΗΜ κύματος σε οπτικές ίνες με πυρήνα ελλειπτικής διατομής, με στόχο την ανάπτυξη μιας νέας μεθόδου για τον υπολογισμό βασικών ιδιοτήτων της διάδοσης. Στο πρώτο κεφάλαιο γίνεται μια λεπτομερής περιγραφή της τεχνικής γραμμών μεταφοράς σε συντονισμό (RTL), που αποτελεί και το βασικότερο εργαλείο στην ανάπτυξη των μεθόδων αυτής της διατριβής. Στο πλαίσιο της παρουσίασης της τεχνικής, γίνεται εφαρμογή της σε οπτικές ίνες κυλινδρικού πυρήνα. Έπειτα υπολογίζεται η μεταφορά διάδοσης β αλλά και η διπλοθλαστικότητα. Στο κεφάλαιο 2 γίνεται αναφορά στην ιστορία της σχετικής έρευνας και τις πρώτες προσπάθειες μαθηματικής περιγραφής των βασικών σχέσεων της διάδοσης, γενικά σε ελλειπτικούς κυματοδηγούς. Ειδική αναφορά γίνεται στην ανάλυση του Yeh, που αποτέλεσε σημαντική βάση για τις μετέπειτα μελέτες. Αναφορά γίνεται επίσης και στην έρευνα του Dyott, ειδικότερα στη συνεισφορά του στη μελέτη της διατήρησης της πόλωσης που παρατηρείται στις ίνες ελλειπτικού πυρήνα. Επιπρόσθετα, δίνεται ο ορισμός της διπλοθλαστικότητας και αναφέρονται οι κυρίαρχες προσπάθειες υπολογισμού της. Στο τέλος του $2^{ου}$ κεφαλαίου αναφέρονται οι σημαντικότερες εφαρμογές της ελλειπτικής ίνας. Στο κεφάλαιο 3 παρουσιάζεται η πιο ακριβής προσέγγιση αυτής της διατριβής για τον υπολογισμό της σταθεράς β και της διπλοθλαστικότητας σε ελλειπτικές ίνες. Το κεφάλαιο αφού ξεκινάει με την εφαρμογή των εξισώσεων Maxwell σε ελλειπτικές συντεταγμένες, παρουσιάζει τις σχέσεις διάδοσης μονών και ζυγών ρυθμών, με παράλληλη εμφάνιση αρμονικών. Στη συνέχεια γίνεται μελέτη της ακρίβειας της μεθόδου, υπολογίζοντας τη σταθερά διάδοσης για διαφορετικούς αριθμούς συμπεριλαμβανόμενων αρμονικών. Οι τιμές που προκύπτουν συγκρίνονται μεταξύ τους αλλά και με τις τιμές που προέκυψαν μέσω της αναλυτικές μεθόδου με χρήση εξισώσεων Mathieu. Επιπρόσθετα υπολογίζονται οι τιμές της διπλοθλαστικότητας και παρουσιάζεται μελέτη της επίδρασης του βαθμού ελλειπτικότητας στην ακρίβεια των αποτελεσμάτων. Το κεφάλαιο 4 παρουσιάζει μια διαφορετική προσέγγιση στη μελέτη της ελλειπτικής ίνας, ξεκινώντας με την γενική περιγραφή οπτικών ινών με έκκεντρο πυρήνα. Η μαθηματική ανάλυση που ακολουθεί χρησιμοποιεί τη μέθοδο conformal mapping και οι τελικές σχέσεις οδηγούν περιγράφουν ισοδύναμα κυκλώματα. Ακολουθεί εφαρμογή της τεχνικής RTL και παρουσιάζεται ο τελικός αλγόριθμος. Η μέθοδος μπορεί να χρησιμοποιηθεί μελλοντικά για την περιγραφή της οπτικής ίνας D fiber. Στο κεφάλαιο 5 παρουσιάζεται η τρίτη

προσέγγιση στο πλαίσιο αυτής τη διατριβής, για τη μελέτη της ελλειπτικής ίνας. Σε αυτή την προσέγγιση περιγράφονται οπτικές ίνες που παρουσιάζουν γωνιακή ασυμμετρία. Με χρήση των εξισώσεων Maxwell σε κυλινδρικές συντεταγμένες και κατάλληλη εφαρμογή της τεχνικής των γραμμών μεταφοράς, αναπτύσσεται ένας νέος αλγόριθμος για τον υπολογισμό της σταθεράς β. Ο αλγόριθμος εμφανίζει αξιοσημείωτη ακρίβεια και δύναται να παρέχει αποτελέσματα για ελλειπτικές ίνες χωρίς την περιπλοκότητα της χρήσης αρμονικών. Η μέθοδος αυτή μπορεί να χρησιμοποιηθεί σαν εργαλείο για περαιτέρω μελέτη οπτικών ινών με οπές στον πυρήνα, γνωστές ως PCF fibers. Στο κεφάλαιο 6 παρουσιάζεται η συνεισφορά της παρούσας έρευνας στη μελέτη της διάδοσης σε ελλειτπικές ίνες. Επίσης παρέχονται προτάσεις για μελλοντική έρευνα που μπορεί να βασιστεί στις μεθόδους που αναπτύχθηκαν στο πλαίσιο αυτής της διατριβής.

DEDICATION

This thesis is dedicated to

~ My Wife, Mary ~

For her love, her support and patience

and

to my parents, Ioannis and Penelope

For their valuable support

PUBLICATIONS RESULTING FROM THESIS

Journals

1. Boucouvalas, Anthony C., Euripides Georgantzos, et al. "Resonant transmission line method for unconventional fibers." Applied Sciences 9.2 (2019): 270.

2. Boucouvalas, Anthony C., Christos Papageorgiou, and Euripides Georgantzos. "Elliptical fibre dielectric waveguides: a transverse transmission line analysis." IET Optoelectronics (2019).

International Conference Presentations

3. Georgantzos, E., C. Papageorgiou, and A. C. Boucouvalas. "A transmission line model for propagation in elliptical core optical fibers." AIP Conference Proceedings. Vol. 1702. No. 1. AIP Publishing LLC, 2015.

4. Georgantzos, E., and A. C. Boucouvalas. "Transmission line resonance technique for eccentric core optical fibers." AIP Conference Proceedings. Vol. 1790. No. 1. AIP Publishing LLC, 2016.

5. Georgantzos, E., Anthony C. Boucouvalas, and C. D. Papageorgiou. "Transmission line and resonance technique in cylindrical fibers of circular asymmetry." 2016 International Conference on Telecommunications and Multimedia (TEMU). IEEE, 2016.

6. Papageorgiou, Christos & Georgantzos, Euripides & Raptis, Theophanes & Boucouvalas, Anthony, *Resonant Transmission Line Modeling of Holey Photonic Crystal Fibers*, INASE 2017, Athens, Greece (2017)

ACKNOWLEDGEMENTS

The research behind the current thesis is the result of a supported effort. It would be impossible to complete without the support of individuals whose contribution I would like to acknowledge in this section.

At first, I would like to express my gratitude towards my supervisor, Professor Anthony Boucouvalas, for his unlimited guidance, patience, and persistence to support me when needed.

Furthermore, I wish to thank Dr Christos Papageorgiou for his substantial contribution and for providing valuable knowledge on the subject of transverse resonance.

I would also like to express my gratitude towards the Department of Informatics and Telecommunications of the University of Peloponnese for providing me with the basic knowledge and the necessary tools to carry out my research and complete my PhD. As a former student of the Department I shall never forget some of the most capable and outstanding tutors and personnel that I have had the honor to attend.

CONTENTS

LIST OF FIGURES

LIST OF TABLES

GLOSSARY OF SYMBOLS AND ABBREVIATIONS

c	velocity of light in vacuum
J	Bessel function
K	modified Bessel function
l	azimuthal mode number
V	the normalized frequency
β	wave propagation constant
Δn	relative refractive index difference between the core and cladding
η	azimuth coordinate that describes a set of hyperbolae, orthogonal to the ellipses
z	coordinate corresponding to the axis, parallel to the cylinder, to the direction of propagation
ξ	radial coordinate that describes a set of confocal ellipses
ε	dielectric constant
ε_1	dielectric constant in the core where $\xi < \xi_0$
ε_2	dielectric constant in the cladding where $\xi > \xi_0$
λ	optical wavelength
λ_c	cut-off wavelength for single mode fibre
λ_0	free-space wavelength

$\boldsymbol{\mu}$	**relative permeability (μ_r) , permeability of free space (μ_o)**
$\boldsymbol{\omega}$	**angular frequency**
LP	**linearly polarized (mode)**
TE	**transverse electric**
TM	**transverse magnetic**
TL	**transmission line**
T-Circuit	**transmission line circuit**
PCF	**Photonic-crystal fiber**
UOF	**unconventional optical fibers**
COF	**conventional optical fibers**

CHAPTER 1

Introduction: Fiber Optics and Resonant Transmission Line (RTL) theory

1.1. Optical fibers in communications and other applications

The use of optical fibers for the transmission of information has played a major role in the evolution of modern telecommunications. In order to better describe the potential of modern communication systems one can deploy the product of bit rate with the distance between the repeaters (*BL*) [1]; by 1970 the BL value of non-optical communications had reached approximately 100 (Mb/s)*Km, unable to go beyond [2]. Therefore, as the need for faster and broader communication increased, despite the advances in design and implementation, electrical systems reached their limits [3].

In the second half of the 20th century it became prominent that the use of light as signal carrier would provide the BL product the necessary boost to carry communications to a higher level. The advent of laser and optical fibers provided the required light source and transmission medium for a complete optical communications system. Since their initial implementation optical communication systems have been continuously evolving and increasing the BL product.

The understanding of structural and physical properties of optical fibers led to innovations that surpassed limitations for consecutive generations of light wave systems [2]. The introduction of single mode fibers overcame the 100 Mb/s rate limitation due to dispersion in multimode fibers that were primarily used until 1980s. Dispersion limitations in single mode fibers were dealt with anew with the use of dispersion-shifted fibers [3]. Later on, around 1990, the incorporation of fiber amplifiers in optical systems, further increased the repeater spacing; especially, erbium-doped amplifiers helped compensate fiber losses in WDM systems [1], while the application of revolutionary techniques in transmission and system configuration lead to the implementation of trans-continental submarine optical systems that connect modern civilization (fig. 1.1).

Despite the significant role of optical fibers as a carrier in the transmission of information, the spectrum of their applications is not limited to telecommunications. Optical fibers, depending on their physical properties, are used in a wide range of applications including medicine, defense systems and industrial uses [3]. The elliptical

fiber is a special type of optical fiber, whose distinct geometry renders it useful for many applications, including optical gyroscopes, higher-order sensors, D-fiber coupling via acoustic waves and the readjustment of dispersion in communication fibers.

The main objective of the current thesis, is the study of EM wave propagation in elliptical fibers using an innovative approach, improved in relation to existing analytical methods, that utilizes the computational method of Transmission Lines. However, before proceeding with the description of the new, alternative method, it is necessary to have a solid grasp of the basic theory of EM propagation in optical fibers in general, and to familiarize with the Transmission Line theory, that will be used as the basic tool in the current approach. For that reason, this chapter focuses on the analysis of cylindrical optical fibers and the use of Resonant Transmission line theory for the estimation of key properties of EM wave propagation within them.

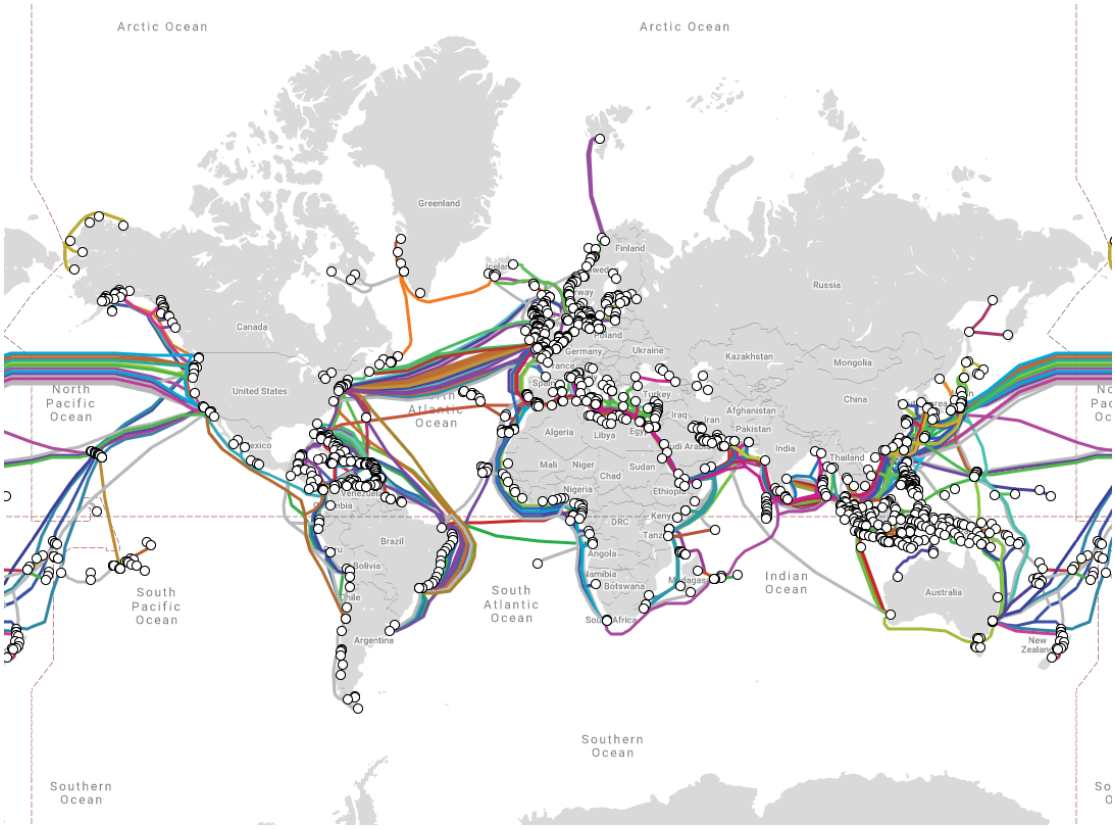

Figure 1-1 International undersea network of fiber-optic communication systems last updated on May 18 2020 **[https://www.submarinecablemap.com/#]**

1.2. Physical aspects of optical fibers

The fibers that will be dealt within the present work are composed of either a central core surrounded by cladding with two different dielectric constants, or by a periodic lattice making a photonic crystal. A particular class of graded dielectric index can be achieved either through successive layering from material of different optical density or with the use of a hexagonal lattice of smaller diameter boring cylindrical holes surrounding the core in which case they are referred as holey or, photonic crystal fibers. We first concentrate on the first case which is simpler.

A more rigorous description can be given with the aid of a simple core-cladding model where n_{in} and n_{out} are the core and cladding dielectric indices respectively. From Snell's law, the condition $n_{in} > n_{out}$ guarantees the total reflection on the cladding's surface for any light ray travelling inside the core. For a standard description based on the homogeneous wave equation similar to waveguides [4] we have a separation of transverse and longitudinal components as $\nabla = \nabla_{\perp} + \hat{\boldsymbol{z}}\frac{\partial}{\partial z}$ which naturally leads to the separation of the propagating part of any mode when written in separable coordinates as $exp(-\gamma z)$ where $\gamma = \alpha + j\beta$ is a generic propagation coefficient with α and β the corresponding attenuation and phase variation coefficients respectively, such that the wave operator can be reduced to the equivalent Helmholtz operator $\nabla^2 = \nabla_{\perp}^2 + \gamma^2$ with the remaining part concerning the mode profile in the fiber's cross section.

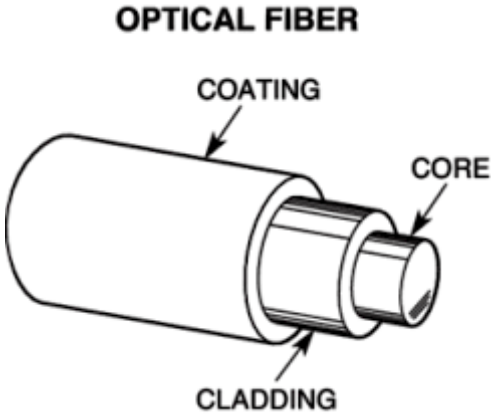

Figure 1-2 3-D representation of a cylindrical core fiber and its layers
[**https://www.newport.com/t/fiber-optic-basics**]

For the simple fiber model with translational invariance (no attenuation), the factor $exp(-j\beta z)$ is common to the core and the cladding while for a free space wavelength taken as λ with a corresponding wavenumber $k = 2\pi/\lambda$ we get the associated wave vector norms $n_{in}k$ and $n_{out}k$ in the core and the cladding respectively. The condition for a beam getting trapped inside the core can then be given as

$$n_{in} < {}^{\beta}/_{k_0} < n_{out} \tag{1.1}$$

A Perpendicular Wavenumber is often used for any local value of the refractive index n defined as

$$k_{\perp}^2 + \beta^2 = (n_{out}k_0)^2 \tag{1.2}$$

The definition leads to a real $k_{\perp}$ in the region where $\beta < \mathrm{nk}_0$ and imaginary everywhere else.

Since, for an ideal fiber the fields across any distance $\delta z = z_2 - z_1$ must differ only by a phasor $exp(-j\beta\delta z)$ we conclude that any values of β and the associated transverse field must correspond to the eigenvalues and eigenvectors of the corresponding wave operator. Hence we are led to a resonance condition naturally associated with the (classical) quantization of the number of allowed modes. These become a countable set inside the interval $n_{in}k_0 < \beta < n_{out}k_0$. We shall refer to this set, as the set of Guided Modes.

There will also be an unaccountable set of other solutions of the wave equation outside the total reflection range which can still propagate in the cladding which we shall call, the Radiative Modes. The number of guided modes is characterized by a specific index [5] given as

$$v = k_0 r \sqrt{n_{in}^2 - n_{out}^2} \tag{1.3}$$

There is a specific wavelength defined by the condition v < 2.405 for which the number of allowed modes falls to one, in which case we speak of a single mode fiber running on the Fundamental Mode. This is achieved in practice by a small difference of the two refractive indices and/or a small ratio of core radius to wavelength. On the

other hand, any fiber can become multi-mode for some sufficiently small wavelengths but there will always be a fundamental mode independently of the magnitude of the v parameter.

1.3. Electromagnetic description of optical fibers

Following standard EM theory [6], [7], [8], we consider the case of source-less Maxwell's equations (absent currents and charges) with linear constitutive relations for the associated macroscopic magnetic and electric fields $\mu \boldsymbol{H} = \boldsymbol{B}$ and $\boldsymbol{D} = \varepsilon \mathbf{E}$ respectively, which take the form

$$\begin{cases} \nabla \cdot \boldsymbol{E} = \nabla \cdot \boldsymbol{B} = 0 \\ \nabla \times \boldsymbol{E} = -\frac{\partial}{\partial t}\boldsymbol{B} \\ \nabla \times \boldsymbol{B} = \varepsilon\mu\varepsilon_0\mu_0 \frac{\partial}{\partial t}\boldsymbol{E} \end{cases} \tag{1.4}$$

A simple, monochromatic frequency dependence will be also assumed in what follows such that all time derivatives result in $\partial_t \to -j\omega$. Under these assumptions, the equations for both the electric and magnetic field reduce to a compact Helmholtz operator of the form

$$(\nabla^2 + k^2)\begin{Bmatrix} \boldsymbol{E} \\ \boldsymbol{B} \end{Bmatrix} = 0 \tag{1.5}$$

where $k = \omega/c = \omega\varepsilon\mu$. Using the notation *n* for the refractive index we may also write $c^{-2} = n^2\varepsilon_0\mu_0 = (n/c_0)^2$ to obtain $k^2 = (nk_0)^2$. Using also the previously introduced separation of transverse and longitudinal (axial) parts we end up with the equivalent reduced Helmholtz operator

$$\left(\nabla_\perp{}^2 + k_\beta^2\right)\begin{Bmatrix} \boldsymbol{E} \\ \boldsymbol{B} \end{Bmatrix} = 0 \tag{1.6}$$

where now $k^2 = n^2k_0^2 + \beta^2$, and the expression of the transverse derivative in cylindrical coordinates becomes

$$\nabla_\perp = \hat{\boldsymbol{r}}\frac{\partial}{\partial r} + \hat{\theta}\frac{1}{r}\frac{\partial}{\partial \theta} \Rightarrow \nabla_\perp^2 = \frac{1}{r}\frac{\partial^2}{\partial r^2} + \frac{1}{r^2}\frac{\partial^2}{\partial \theta^2}$$

Separation of variables for the transverse fields is given as

$$\begin{Bmatrix} \boldsymbol{E} \\ \boldsymbol{B} \end{Bmatrix} = \begin{Bmatrix} E_\perp \\ B_\perp \end{Bmatrix} e^{j(\beta kz - \omega t)}$$

which leads to the equations

$$\left(\frac{1}{r}\frac{\partial^2}{\partial r^2}+\frac{1}{r^2}\frac{\partial^2}{\partial \theta^2}+k^2\right)\begin{Bmatrix}E_\perp\\B_\perp\end{Bmatrix}=0 \tag{1.7}$$

Solutions of the last equations give rise in general to both *Transverse Electric* (TE) and, *Transverse Magnetic* (TM) waves as well as their linear combinations also called *Hybrid modes* (HE). A general procedure for obtaining those expresses first all transverse parts of the fields as functions of the axial parts in terms of the so called, Hertzian potentials [9] which only demands the solutions of a scalar Helmholtz operator.

Such a general set of solutions for the case of graded dielectrics with purely radial dependence had already been prescribed in terms of linear combinations of modified Bessel functions. For the matching conditions between layers, a determinantal equation had to be solved containing the linear terminal conditions between layers. There is often a need for efficient numerical methods starting directly from the expressions of the original Maxwell's equations (1.4-6) in cylindrical coordinates. Methods used in the past include the Wentzel-Kramers-Brillouin (WKB) approximation, the Rayleigh-Ritz method, the series-expansion method and the Finite Elements method while a less complex but powerful method of *Transverse Resonance* shall be fully explained in later chapters.

For uniform core fibers, the full expression of Maxwell equations in cylindrical coordinates leads to the set of both 1st order equations

$$\begin{cases}\beta\frac{\partial}{\partial r}E_z+\frac{\omega\mu}{r}\frac{\partial}{\partial\theta}H_z=j\beta_\perp^2E_r\\ \frac{\beta}{r}\frac{\partial}{\partial r}E_z-\omega\mu\frac{\partial}{\partial r}H_z=j\beta_\perp^2E_\theta\\ \beta\frac{\partial}{\partial r}H_z-\frac{\omega\varepsilon}{r}\frac{\partial}{\partial\theta}E_z=j\beta_\perp^2H_r\\ \frac{\beta}{r}\frac{\partial}{\partial\theta}H_z+\omega\varepsilon\frac{\partial}{\partial r}E_z=j\beta_\perp^2H_r\end{cases} \tag{1.8}$$

as well as 2nd order ones

$$\left(\frac{\partial^2}{\partial r^2}+\frac{1}{r}\frac{\partial}{\partial r}+\frac{1}{r^2}\frac{\partial^2}{\partial\theta^2}+\beta_\perp^2\right)\begin{Bmatrix}E_z\\H_z\end{Bmatrix}=0 \tag{1.9}$$

For non-uniform core fibers, in cases of azimuthal symmetry with only a radial dependence of the refractive index profile *n(r)* we can extract the angular dependence via a substitution

$$\begin{Bmatrix} E_\perp \\ B_\perp \end{Bmatrix} \rightarrow \begin{Bmatrix} e(r) \\ b(r) \end{Bmatrix} e^{-\mathrm{j}l\theta}$$

From the last equations we end up with a standard Bessel ordinary differential equation of the general form

$$u'' + u'/r + [k^2(n^2(r) - \beta^2) - (l/r)^2]u = 0 \qquad (1.10)$$

After providing a maximal value for the refractive index as $n_{\max}$ the following substitutions can take place $m = k^2(n_0^2 - \beta^2)$, $q(r) = k^2(n_0^2 - n^2(r))$; these substitutions, together with the redefinition of the unknown scalar as $w(r) = \sqrt{r}u(r)$ lead to the self-adjoint eigenvalue problem

$$w'' + [m^2 - q(r) - (l^2 - 1/4)/r^2]w = 0 \qquad (1.11)$$

A set of general solutions for eigenvalues in $0 < m < d^2$ can then be given as linear combinations of two linearly independent functions given in terms of the modified Bessel functions [10]

$$w^1(r) = \begin{Bmatrix} K_l(r\sqrt{d^2 - l}) \\ I_l(r\sqrt{d^2 - l}) \end{Bmatrix}, \; l < d^2 \qquad (1.12)$$

where $d = k\sqrt{n_0^2 - n_{out}}$ and

$$w^2(r) = \begin{Bmatrix} J_l(r\sqrt{d^2 - l}) \\ Y_l(r\sqrt{d^2 - l}) \end{Bmatrix}, \; l > d^2 \qquad (1.13)$$

the pair of the standard Bessel functions of the 1st and 2nd kind respectively. The upper index represents modes inside the core and the cladding respectively.

From the longitudinal components we can then compute the transverse fields via (1.8) and apply the necessary boundary conditions which require from the tangential components of both the electric and the magnetic fields to be continuous along the core-cladding boundary. This gives then rise to the *characteristic mode equation*. Since the tangential modes involve only the *z* and *φ* components we have

$$E_\theta^1\big|_{r=R} = E_\theta^1\big|_{r=\alpha},\ E_z^1|_{r=R} = E_z^1|_{r=\alpha}$$
$$H_\theta^1\big|_{r=\alpha} = H_\theta^1\big|_{r=\alpha},\ H_z^1|_{r=\alpha} = H_z^1|_{r=\alpha}$$

The above will result in four equations over four constants plus the mode phase constant β of which the solution results in a characteristic equation of the form

$$\left[\frac{J_m'(pa)}{pJ_m(pa)} + \frac{K_m'(qa)}{aK_m(qa)}\right]\left[\frac{\beta_1^2 J_m'(pa)}{pJ_m(pa)} + \frac{\beta_2^2 K_m'(qa)}{aK_m(qa)}\right] = \frac{\beta^2 v}{\alpha}(p^{-2} + q^{-2})^2 \qquad (1.14)$$

The remaining two unknown constants p and q can be eliminated with the aid of the auxiliary relations

$$\beta^2 = \omega^2 n_1 - p^2 = \omega^2 n_2 + q^2 \qquad (1.15)$$

Combined use of (1.14) and (1.15) allows determining the unknown phase constant β. Due to the transcendental character of the (1.14), only numerical methods allow a complete solution in which the resulting multiple branches prescribe different modes for any value of v and any core radius.

1.4. Computational photonics

Since nowadays computers allow very fast convergence, simulation has become a popular and efficient tool for engineering new solutions in the area of optical fibers and photonics in general. Provided there is good knowledge of material properties and the exactness and scale invariance of Maxwell's equations, numerical predictions are in very close proximity to actual laboratory measurements. Electromagnetics simulation can be broadly separated in the following main classes. We generally distinguish between "*Time-Domain*" solvers attempting to simulate propagation of both electric and magnetic fields given an initial source distribution, and "*Frequency-Domain*" solvers. The latter can be further characterized as either eigen-solvers for finding dispersion relations $\omega(\boldsymbol{k})$ via some eigenvalue condition due to basis function expansion, and general solvers for the evolution of a harmonic source $\boldsymbol{J}(\boldsymbol{x})\exp(j\omega t)$ again via reduction to a linear algebraic equation.

Methods used to approximate solutions inside complicated spatial structures require discretization of the spatial and also, temporal domain if propagation is to be studied. Such methods can be classified according to the discretization method used. These include

1. *"Finite-Differences"*(FD) or *"Finite-Difference-Time Domain"*(FDTD) methods, where derivatives are approximated as $Df(u) \approx (f_{n+1} - f_n)/(2\delta u)$.

2. "*Finite Elements*" where some form of usually triangular or tetrahedral mesh is projected on the surface and polynomial interpolation of relatively low order is used over them for the unknown functions over each element.

3. "*Spectral Methods*" representing unknowns as a series expansion, the simplest one being that of a plane wave expansion resulting in Fourier series or other appropriate bases adapted to non-periodic boundary conditions.

4. "Boundary-Elements" which avoids discretization apart from the boundaries between inhomogeneities while the interiors are approximated analytically. These methods include the "Multipole" approach as well as "Coupled Wave" or "Transfer Matrix" approaches which propagate the information through separate uniform regions.

The last case is the closest possible to the approach presented in the current thesis for the study of EM propagation in elliptical core fibers.

1.5. The resonant transmission line (RTL) method

An alternative numerical method for multilayered dielectrics was already in use in the middle of the previous century, based on appropriate discretizations of the partial differential extension of the telegrapher's equation. In such a method, one generally exchanges Maxwell's equations with an infinity of ordinary differential equations [11]-[14], using an analogy between electric and magnetic field components and their voltage and current equivalents. This is justified in terms of capacitive and inductive parts of a reactive field where the first are linked with electric field components via associated voltage elements and their associated admittances as well as magnetic ones via their respective inductances and their current elements. It then becomes possible to effectively describe a succession of dielectric variations via appropriate matching conditions between successive admittances and inductances. In early uses of such models, TM and TE modes corresponded to a sequence of successive admittances (*E-Line*) and successive impedances (*H-Line*) respectively, while hybrid modes required

an additional inductive coupling given as an abstract transformer matching lines between successive angular sectors. Successive applications of the appropriate boundary conditions between layers for the electric and magnetic field components lead to some linear algebraic systems from which the field variation across the material could be obtained.

An essential step of progress towards further simplification and one of the first direct solvers for optical fibers appeared in 1982 with two papers of Papageorgiou and Boucouvalas [15], [16], where the *Transverse Resonance* condition for the successive impedances was successfully adapted and applied in a recursive formula using Continued Fraction Expansion giving rise to a much more direct and fast numerical method. In later work it was shown how to associate this method with any eigenvalue problem in the so called, Sturm-Liouville class [17] and even for inverse problems [18].

A radial index profile is assumed for simplicity at first, while the study of more complex profiles will be presented in later chapters. A variable separation is adopted and a finite discretization is assumed for both the core and cladding in a radial succession of thin circular layers in which case each field component may be written as

$$\begin{Bmatrix} \boldsymbol{e}_i(r,\theta,z,t) \\ \boldsymbol{b}_i(r,\theta,z,t) \end{Bmatrix} = \begin{Bmatrix} E_i(r) \\ H_i(r) \end{Bmatrix} e^{-j(\omega t + l\theta + \beta z)}$$

In the above relation, l is taken as the azimuthal number and β as the propagation constant. The presence of a conductivity σ is also assumed with electric and magnetic constants being denoted as usual via ε and μ, respectively. Using the auxiliary notations $\beta_- = \omega\varepsilon - j\sigma$ and $\beta_+ = \sigma + j\omega\varepsilon$ together with $\gamma^2 = \beta^2 - \mu\omega\beta_- + (l/r)^2$, the resulting Maxwell equations for each layer have been obtained in [15] as

$$\begin{cases} \beta r E_\theta - l E_z = \omega\mu r H_r \\ l H_z - \beta r H_\theta = \beta_- r E_r \\ \frac{\partial}{\partial r}(\omega\mu r H_r) = -j\omega\mu(l H_\theta + \beta r H_z) \\ \frac{\partial}{\partial r}(\beta_- r H_r) = -\beta_+(l E_\theta + \beta r E_z) \\ \frac{\partial}{\partial r}(l H_\theta + \beta r H_z) = j\gamma r^2 H_r + \beta H_z - (l/r) H_\theta \\ \frac{\partial}{\partial r}(l E_\theta + \beta r E_z) = -\gamma^2 \left(\frac{\beta_-}{\beta_+}\right) r E_r + \beta E_z - (l/r) E_\theta \end{cases} \tag{1.16}$$

It is then possible to put them in a direct correspondence with the equations for an equivalent local pair of coupled transmission lines using the redefinitions of a pair of electric and magnetic voltages and currents given as

$$V_{\pm} = \frac{1}{\sqrt{n}}\left(\frac{lH_{\theta}+\beta rH_z}{jF} \pm \frac{lE_{\theta}+\beta rE_z}{F}\right) \tag{1.17}$$

$$I_{\pm} = \frac{1}{\sqrt{n}}\left(\frac{\omega\mu rH_r}{jZ_0} \pm \beta_{-} rE_r\right) \tag{1.18}$$

where Z_0 the vacuum impedance (120π) and $F = \beta^2 + (l/r)^2$. For the case of a fiber with zero conductivity σ, $\mu = \mu_0$ and $\varepsilon = \varepsilon_0 n^2$. This reduces the original system in the form

$$\begin{cases} \frac{\partial}{\partial r} V_{+} = -\delta_{+} I_{+} \\ \frac{\partial}{\partial r} I_{+} = -j\omega\varepsilon_0 n F V_{+} \end{cases} \tag{1.19}$$

$$\begin{cases} \frac{\partial}{\partial r} V_{-} = -\delta_{-} I_{-} \\ \frac{\partial}{\partial r} I_{-} = -j\omega\varepsilon_0 n F V_{-} \end{cases} \tag{1.20}$$

where

$$\begin{cases} \delta_{\pm} = \frac{\gamma^2}{j\omega\varepsilon_0 nF} \pm jM \\ M = \frac{2\beta l Z_0}{rF^2} \end{cases} \tag{1.21}$$

The above system describes a pair of coupled transmission lines with M the mutual reactance, constant specific impedance per unit length $j\varepsilon_0 nF = jnk_0 F/Z_0$ and two different propagation constants given as

$$\gamma_{\pm}^2 = \beta^2 - (nk_0)^2 \mp 2nk_0 \frac{\beta l}{(\beta r)^2 + l^2} + \left(\frac{l}{r}\right)^2 \tag{1.22}$$

where $k_0 = 2\pi/\lambda_0$ is the free space propagation constant. We can then introduce a cutoff limit for the wavelengths allowed as a new $k_c = 2\pi/\lambda_c$ for which $\beta = n_2 k_c$ such that eq. (1.22) becomes

$$\gamma_{c\pm}^2 = \beta^2 - (n_2 k_c)^2 \mp 2n \frac{n_2 k_c^2 l}{(n_2 k_c r)^2 + l^2} + \left(\frac{l}{r}\right)^2 \tag{1.23}$$

The characteristic impedances are then given by $Z_{c\pm} = \frac{\gamma_\pm}{j\omega_0\varepsilon_0 nF}$. The fundamental TE and TM modes can be found for the $l = 0$ case from the simplified pair of transmission lines with the same constant propagation factor $\gamma_c = (n_2^2 - n^2)k_c^2$ and $F_c = (l/r)^2 + (n_2 k_c)^2$ but different characteristic impedances $Z_M = \frac{\gamma_c}{j\omega_c\varepsilon_0 nF_c}$ and $Z_E = \frac{Z_M}{n^2}$. From the solutions of the generic telegrapher's equation [19] for the transmission function one obtains the equivalent terminal impedances as

$$\begin{cases} Z_B = Z\,tanh(\gamma_c \delta r/2) \\ Z_p = \frac{Z}{sinh(\gamma_c \delta r/2)} \end{cases} \tag{1.24}$$

An equivalent 4-port T-circuit for this model is shown in fig. 1.3

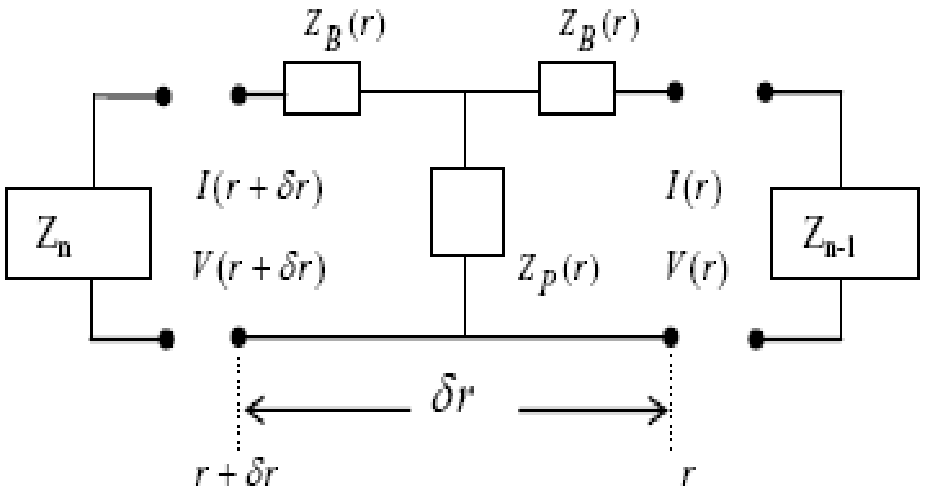

Figure 1-3 T-circuit equivalent for an optical fiber cylindrical thin layer [29].

Next, the limiting case may be considered, of δr << 1 for which one has the approximations

$$\begin{cases} Z_B = (\delta r k_c)^2 \gamma_c' Z_p'/2 \\ Z_p = \frac{Z_0}{\delta r k_c^2 n(n_2^2 + (l/rk_c)^2)} \end{cases} \tag{1.25}$$

where now

$$\gamma_c' = n_2^2 - n^2 + \frac{l}{(rk_c)^2} \pm \frac{2nn_2 l}{l^2 + (rnk_c)^2} \tag{1.26}$$

The original characteristic impedances have the corresponding limits

$$\begin{cases} For\ l \neq 0,\ r = 0,\ Z_0 = \frac{1}{j\omega_c \varepsilon_0 n|l|},\ r \to \infty,\ Z_\infty = 0 \\ For\ \ l = 0,\ r = 0,\ Z_M = Z_E \to \infty,\ r \to \infty,\ Z_M = Z_E = 0 \end{cases} \quad (1.27)$$

With the above definitions, the cutoff behavior of any homogeneous dielectric layer of width δ can be approximated with the use of two equivalent, independent T-circuits.

A long series of such layers constituting the cross section of a radially inhomogeneous fiber can then be approximated with the synthesis of a series of such cutoff circuits in tandem. Complete solution of the problem then can be given with two such series with total impedances Z_{in} and Z_{out}, the first starting from a large radius towards the core-cladding boundary and the second from $r = 0$ to the same boundary respectively. The transverse resonance condition is then directly given from the roots of

$$Z_{in} + Z_{out} = 0 \quad (1.28)$$

The respective values for the total impedances can be found from the general theory of network synthesis which has been described by a well-known set of theorems due to Thevenin, Norton and Foster [20], and it is guaranteed that any such series will have a total impedance given as a continued fraction expansion of the form

$$Z_{\{in,out\}} = Z_b(a \pm 1) + \Big(Z_p(a \pm 1) + (Z_B(a \pm 1) + Z_B(a \pm 2) + \ldots (Z_N + Z_B(N - 1))^{-1})^1\Big)^{-1} \quad (1.29)$$

where Z_{N}, is the characteristic impedance at infinity for the positive sign or at 0 for the negative sign and *a* the core-cladding interface. The advantage of this method is the very low programming complexity of which the efficiency depends solely on the particular root finding algorithm to be used. Application of the above prescribed algorithm gives a series of roots and poles with the roots corresponding to the set of eigenvalues for the fundamental and higher modes. A method for the computation of the E fields for each mode is given in the later chapters.

1.6. Accuracy of the estimated roots

In the Transmission-Line technique the fiber is divided into concentric layers, each represented by a T-circuit. The allocation of the circuits is vital for the program's accuracy and dependent on the distance *r* of each layer from the fiber's center. That distance is determined within the algorithm by two parameters, '*w*' and '*N*' where, '*w*'

expresses a constant $\delta r/r$ ratio denoting the analogy between distance r and thickness of each layer. The 'N' parameter on the other hand expresses the number of layers that make up the required distances from the core center. The resonance frequency of the cascade of the series of equivalent electric circuits for a fixed wavelength represents the mode propagation constants β of the related waveguide with certain refractive index profile.

In order to determine the accuracy of the technique the mode propagation constants have been calculated via the Bessel functions; moreover any results from the T-Line technique are compared to the Bessel results. After thorough experimentation with the 'w' and 'N' parameters it appears that beyond certain values, the accuracy of the algorithm's estimations deteriorates rapidly. Specifically, existing algorithms calculating the mode propagation constant have been altered in order to correlate the change in the 'w' and 'N' parameters, with a varying error on the results. In an effort to "fine tune" the current technique, a considerable part of the initial research was dedicated to estimating an optimal combination of these two parameters and optimizing the accuracy of the solutions reached by the method.

Every time the algorithm is run (to calculate the mode propagation constants) it reaches a predefined distance inside (towards the core center) and outside the core-cladding interface. The outer distance is related to the inner distance in a way that, the further we reach externally, the closer we get to the fiber core. The 'w' and 'N' parameters play a significant role in the calculation of the distance and are closely connected to one another. That means that we cannot change one without changing the other in order to reach a predefined distance. The exact connection between the two can be described as follows: we mentioned earlier that the algorithm has to reach a predefined distance which is shown as a ratio of the outer distance over the core radius let there be $r_N = ar_1$ whereas r_1 is the core radius and r_N the outer distance after N steps. Using the definitions

$$r_{out} = r + \frac{\Delta r}{2}, r_{in} = r - \frac{\Delta r}{2}, r_{out} - r_{in} = \Delta r, r = \frac{r_{out} + r_{in}}{2}, \frac{\Delta r}{r} = w$$

we get by substitution $r_{in}\left(1+\frac{w}{2}\right)=r_{out}(1-\frac{w}{2})$ and $\frac{r_{out}}{r_{in}}=\frac{1+\frac{w}{2}}{1-\frac{w}{2}}=\xi$ whereas $\frac{r_2}{r_1}=\xi$, $\frac{r_3}{r_2}=\xi$, $\frac{r_4}{r_3}=\xi,\ldots,\frac{r_N}{r_{N-1}}=\xi$. By sidewise multiplication we obtain $\frac{r_N}{r_1}=\xi^{N-1}$ and finally

$$N=1+\frac{\log(\frac{r_N}{r_1})}{\log(\xi)} \qquad (1.30)$$

We must predetermine a safe R_N/r1=a ratio to make sure that the algorithm will reach a distance covering the most of the electromagnetic field around and into the fiber core. In order to evaluate the accuracy of the resonance technique, Bessel functions have been used as a point of reference for the estimation of mode propagation constants and the results were then compared to those from the resonance technique. Since the Bessel functions were used as a measure of accuracy, it was important to retain the eigenvalue equations in their original analytical form as given in (1.29).

Firstly, the transverse resonance method of (1.28) was iterated for both the core and the cladding for a step index profile with relative difference $\delta n/n$ ~0.05 and for a varying number of layers, and the differences in the propagation factor values were plotted as shown in figure 1.4. Secondly, the fundamental modes for the same profile were also computed with the aid of the transfer matrix technique given the correct number of eigenvalues for a number of 200 steps and the difference from the accurate form as given via Bessel functions was also plotted as shown in figure 1.5. As is evident these get saturated for V > 3.5. It can be safely concluded that a $N \geq 200$ number of layers is sufficient to produce a level of accuracy with error $< 10^{-5}$.

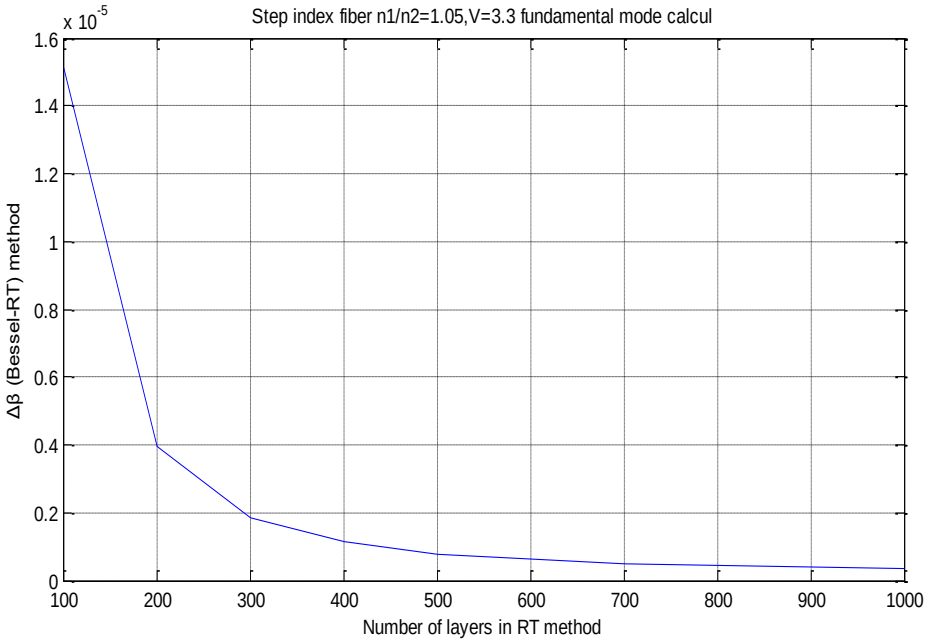

Figure 1-4 Error in the propagation factor estimates between transverse resonance method and analytical solutions with number of layers.

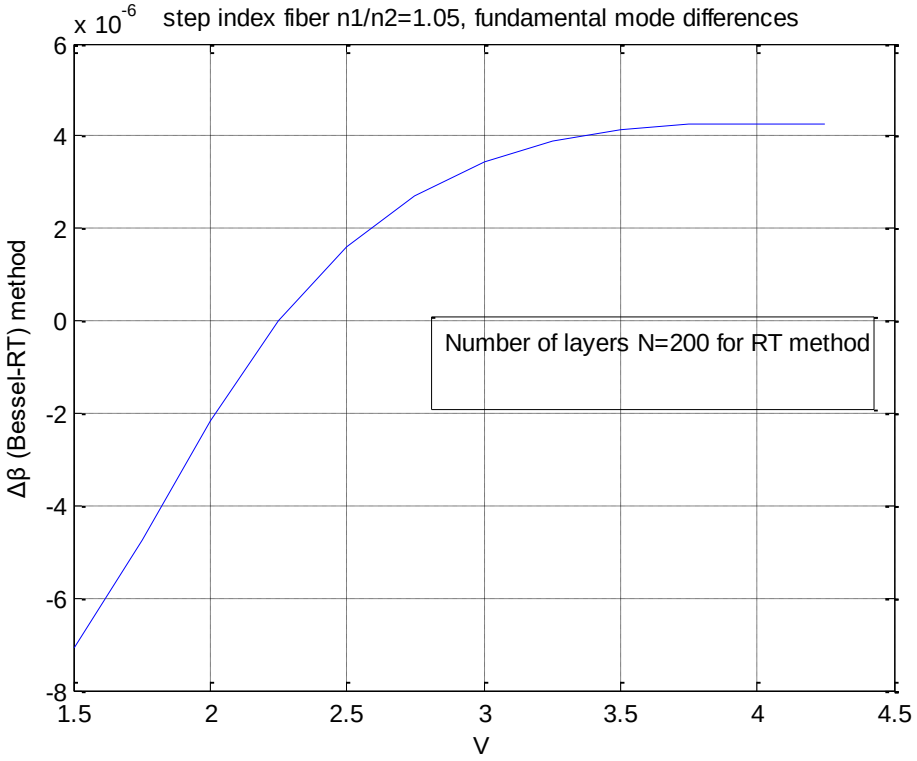

Figure 1-5 Differences of RT method from analytical expressions for N = 200 and varying V parameter.

The importance of the presented accuracy analysis lays in the provision of optimal parameters for the estimation of mode propagation constants, not merely for step index profiles but also for more complicated profiles including graded-index, triangular and parabolic among others.

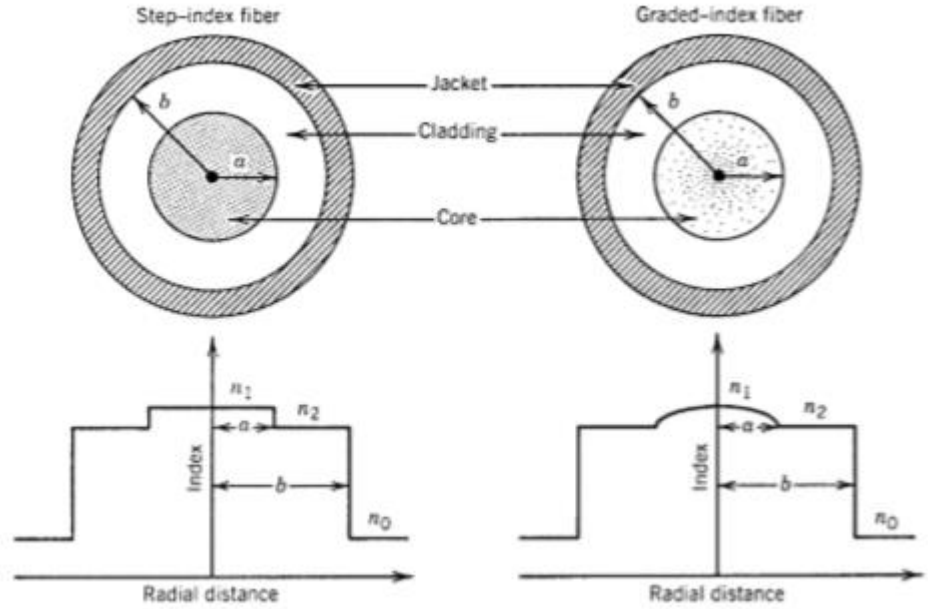

Figure 1-6 Cylindrical fiber cross sections and their corresponding index profiles [3]

1.7. RTL method for the precise analysis of a cylindrical fiber including the birefringence effect

A more recent analysis of the same problem examined in section *1.3* was based on a partial Fourier transform of the reduced Maxwell equations [21] which we present in this section as it will be useful in the study of the unconventional fibers in following chapters.

The basis for the application of the previously introduced RTL method is the radial discretization of all cylindrical fibers via a separation into a succession of thin cylindrical layers, each one with its own constant refractive index *n*. These layers can be made to extend outside of the cladding in order to take into consideration the effect of the surrounding air (n = 1). Each thin cylindrical layer could have thickness δr proportional to each average radius r which means that given discrete steps as $\delta r = r_2 - r_1$ with $r = \frac{r_1 + r_2}{2}$ one obtains

$$\frac{r_2-r_1}{r_2+r_1} = \frac{c}{2} => \begin{cases} \frac{1+c/2}{1-c/2} r_1 = r_2\ (out) \\ \frac{1-c/2}{1+c/2} r_2 = r_1 (in) \end{cases} \quad (1.31)$$

For any such circular cylindrical layer Maxwell equations (for a constant wavelength, i.e., constant frequency "ω") can be written in their standard form as

$$\begin{cases} \nabla X\vec{E} = -j\omega\mu_0\vec{H} \\ \nabla X\vec{H} = j\omega\varepsilon_0 n^2(r)\vec{E} \end{cases} \quad (1.32)$$

Taking into consideration the relations $\omega\mu_0 = k_0 z_0$ and $\omega\varepsilon_0 = \frac{k_0}{z_0}$ where $k_0 = \frac{\omega}{c}, z_0 = 120\pi$ and replacing $z_0\vec{H}$ with $\vec{H}$ in order $\vec{E}$ and $\vec{H}$ to have the same units (V/m), Maxwell equations become then

$$\begin{cases} \nabla X\vec{E} = -jk_0\vec{H} \\ \nabla X\vec{H} = jk_0 n^2(r)\vec{E} \end{cases} \quad (1.33)$$

In circular cylindrical geometry of coordinates (r, φ, z) the following set of three partial differential equations can be derived by the first vector Maxwell equation as

$$\begin{cases} \frac{1}{r}\frac{\partial E_z}{\partial\varphi} - \frac{\partial E_\varphi}{\partial z} = -jk_0 H_r \\ \frac{\partial E_r}{\partial z} - \frac{\partial E_z}{\partial r} = -jk_0 H_\varphi \\ \frac{1}{r}\frac{\partial(rE_\varphi)}{\partial r} - \frac{1}{r}\frac{\partial E_r}{\partial\varphi} = -jk_0 H_z \end{cases} \quad (1.34)$$

Applying a Fourier Transform along "z" and "φ" with wave numbers "β" and "l", where l is integer (because along "φ" we have Fourier series of period 2π), the set (1.34) becomes:

$$\begin{cases} \frac{jl}{r}\overline{E_z} - j\beta\overline{E_\varphi} = -jk_0\overline{H_r} \\ j\beta\overline{E_r} - \frac{\partial\overline{E_z}}{\partial r} = -jk_0\overline{H_\varphi} \\ \frac{1}{r}\frac{\partial(r\overline{E_\varphi})}{\partial r} - \frac{jl}{r}\overline{E_r} = -jk_0\overline{H_z} \end{cases} \quad (1.35)$$

In (1.35) we use new variables $\overline{E_r}, \overline{E_\varphi}, \overline{E_z}, \overline{H_r}, \overline{H_\varphi}, \overline{H_z}$ to denote the Fourier Transforms of the respective electromagnetic field components. Furthermore, replacing β and r by their reduced variables according to the following relations:

$$\begin{cases} \dfrac{\beta}{k_0} = > \beta \\ r k_0 = > r \end{cases}$$

then (1.35) takes the form

$$\begin{cases} \frac{jl}{r}\overline{E_z} - j\beta\overline{E_\varphi} = -j\overline{H_r} \\ j\beta\overline{E_r} - \frac{\partial\overline{E_z}}{\partial r} = -j\overline{H_\varphi} \\ \frac{1}{r}\frac{\partial(r\overline{E_\varphi})}{\partial r} - \frac{jl}{r}\overline{E_r} = -j\overline{H_z} \end{cases} \tag{1.36}$$

Following a similar approach, the second Maxwell vector equation (1.33) can be written in the form

$$\begin{cases} \frac{jl}{r}\overline{H_z} - j\beta\overline{H_\varphi} = jn^2(r)\overline{E_r} \\ j\beta\overline{H_r} - \frac{\partial\overline{H_z}}{\partial r} = jn^2(r)\overline{E_\varphi} \\ \frac{1}{r}\frac{\partial(r\overline{H_\varphi})}{\partial r} - \frac{jl}{r}\overline{H_r} = jn^2(r)\overline{E_z} \end{cases} \tag{1.37}$$

Furthermore, following a cumbersome analysis as shown in Appendix A, it is possible to prove that the system of Equations (1.36) and (1.37) can be transformed in a set of four differential equations (1.38), relating the equivalent "voltage' and "current" functions V_M, I_M, V_E, I_E defined as follows:

$$V_M = \frac{l\overline{H_\varphi} + \beta r\overline{H_z}}{jF}$$

$$I_M = \frac{r\overline{H_r}}{j} = \frac{\beta r\overline{E_\varphi} - l\overline{E_z}}{j}$$

$$V_E = \frac{l\overline{E_\varphi} + \beta r\overline{E_z}}{F}$$

$$I_E = n^2 r\overline{E_r} = l\overline{H_z} - \beta r\overline{H_\varphi}$$

where we use the notation $F = \frac{(\beta r)^2 + l^2}{r}$

$$\begin{cases} \frac{\partial V_M}{\partial r} = -\frac{\gamma^2}{jF} I_M - jMI_E \\ \frac{\partial I_M}{\partial r} = -jFV_M \\ \frac{\partial V_E}{\partial r} = -\frac{\gamma^2}{jn^2F} I_E - jMI_M \\ \frac{\partial I_E}{\partial r} = -jn^2FV_E \end{cases} \tag{1.38}$$

In (1.38) we introduced the total propagation factor $\gamma^2 = \frac{l^2}{r^2} + \beta^2 - n^2$ and the auxiliary function $M = \frac{2l\beta}{[(\beta r)^2 + l^2]F}$.

At this point it is noticed that V_M, I_M, V_E, I_E are continuous functions at the boundaries because the tangential components of electric and magnetic fields $\overrightarrow{H_\varphi}\ \overrightarrow{H_z}$ and $\overrightarrow{E_\varphi}\ \overrightarrow{E_z}$ on the cylindrical surface are continuous functions passing the boundaries of the cylindrical layer. Using the previous relations, the Fourier Transforms of the electromagnetic field components along (r,l,β) can be expressed as functions of their equivalent "voltages" and "currents" functions with the auxiliary relations

$$\overline{H_r} = {jI_M}/{r}\,, \overline{E_r} = \frac{I_E}{n^2 r}$$

$$\overline{H_\varphi} = jlV_M/r - \frac{\beta}{F} I_E$$

$$\overline{E_\varphi} = lV_E/r + j\frac{\beta}{F} I_M$$

$$\overline{H_z} = \frac{l}{Fr} I_E + j\beta V_M$$

$$\overline{E_z} = -j\frac{l}{Fr} I_M + \beta V_E$$

It becomes evident by inspection that the final equation (1.38) represents two coupled electric transmission lines.

1.8. Decoupling the Transmission Line Equations

The prescribed set of equations (1.38) constitutes a homogeneous set of ordinary differential equations of r . Moreover all the vectors $[V_M, I_M, V_E, I_E]$ can be turned into exponential functions of r given by $V_M = V_M e^{\xi r}, I_M = I_M e^{\xi r}, V_E = V_E e^{\xi r}, I_E = I_E e^{\xi r}$, where V_M, I_M, V_E, I_E are constants, i.e., not functions of r. Thus, the system (1.38) can be transformed in an algebraic set of the following four equations

$$\begin{cases} \xi V_M = -\frac{\gamma^2}{jF} I_M - jM I_E \\ \xi I_M = -jF V_M \\ \xi V_E = -\frac{\gamma^2}{jn^2F} I_E - jM I_M \\ \xi I_E = -jn^2 F V_E \end{cases} \tag{1.39}$$

Replacing $I_M = -\frac{jF}{\xi} V_M$, $I_E = -\frac{jn^2F}{\xi} V_E$, we obtain a set of two homogeneous equations

$$\begin{cases} \xi V_M = \frac{\gamma^2}{\xi} V_M - M\frac{n^2F}{\xi} V_E \\ \xi V_E = \frac{\gamma^2}{n^2\xi} V_E - M\frac{F}{\xi} V_M \end{cases} \text{ or } \begin{cases} \xi^2 V_M = \gamma^2 V_M - n^2 MF V_E \\ \xi^2 V_E = \gamma^2 V_E - MF \end{cases}$$

This then leads to the eigenvalue equations

$$\begin{cases} (\xi^2 - \gamma^2) V_M + n^2 MF V_E = 0 \\ MF V_M + (\xi^2 - \gamma^2) V_E = 0 \end{cases}$$

From the standard form of the eigenvalue problem we obtain through the determinant differential equations as follows

$$(\xi^2 - \gamma^2)^2 - n^2 M^2 F^2 = 0, \text{ or } \xi^2 = \gamma^2 \pm nMF \tag{1.40}$$

Hence the system has two eigenvalues and two mutually excluded or "normal" eigenvectors. The eigenvectors will be found by replacing ξ^2 by its value. Thus, for $\xi^2 = \gamma^2 - nMF$ it follows that $n^2 MF V_E - nMF V_M = 0 => V_M = nV_E$ and the eigenvector is $V_S = V_M + nV_E$. For $\xi^2 = \gamma^2 + nMF$ it follows that $V_M = -nV_E$ and the eigenvector becomes $V_d = V_M - nV_E$. Their respective "current" eigenvectors

are related as $\frac{I_M}{I_E} = \frac{V_M}{n^2 V_E} = \frac{1}{n}$, thus $I_M = \frac{I_E}{n}$ and $I_s = I_M + \frac{I_E}{n}$, $I_d = I_M - \frac{I_E}{n}$. Since the auxiliary *M* function has the sign of *l*, the set (V_s, I_s), for $l = -l$ becomes equal to the set (V_d, I_d). Thus, we can consider as a unique solution for the set (V_s, I_s) and for integer 'l 'that varies from $-\infty \; to \; +\infty$, and of course for $\xi^2 = \gamma^2 - nMF$:

$$\begin{cases} \frac{\partial V_s}{\partial r} = -\frac{\xi^2}{jF} I_s \\ \frac{\partial I_s}{\partial r} = -jF I_s \end{cases} \tag{1.41}$$

Furthermore, V_s, I_s should be continuous functions at their boundaries although *n*(*r*) varies from layer to layer. This is achieved via the adjustment $V_s = V_M + nV_E = 2V_M$ and $I_s = I_M + \frac{I_E}{n} = 2I_M$, which are continuous functions of *r* by definition.

$$\begin{cases} \frac{\partial V_M}{\partial r} = -\frac{\xi^2}{jF} I_M \\ \frac{\partial I_M}{\partial r} = -jF I_M \end{cases} \tag{1.42}$$

Another option for achieving continuity is to consider the functions $V_{ss} = \frac{V_M}{n} + V_E$ and $I_{ss} = nI_M + I_E$. In this case, $V_{ss} = 2V_E$ and $I_{ss} = 2I_E$ are also continuous, leading to:

$$\begin{cases} \frac{\partial V_E}{\partial r} = -\frac{\xi^2}{jn^2 F} I_E \\ \frac{\partial I_E}{\partial r} = -jF n^2 I_E \end{cases} \tag{1.43}$$

Thus, the set of two coupled transmission lines (1.39) is equivalent to two independent transmission lines (1.42) and (1.43).

The two waves represented by the equations of transmission lines (1.42) and (1.43), are geometrically normal because the first is related to the magnetic field and the second to the electric field that are geometrically normal for transmitted EM waves. This property is an inherent property of EM modes in optical fibers related to birefringence phenomena. However, the β respective values, for any mode, are always found to be very close and can be considered as practically equal.

1.9. Equivalent Circuits for Cylindrical Layers, Boundary Conditions, and Birefringence

Taking into consideration the transmission line theory, it can be proved that each layer of infinitesimal thickness δr is equivalent to a T-circuit as the one shown in Figure 1.7

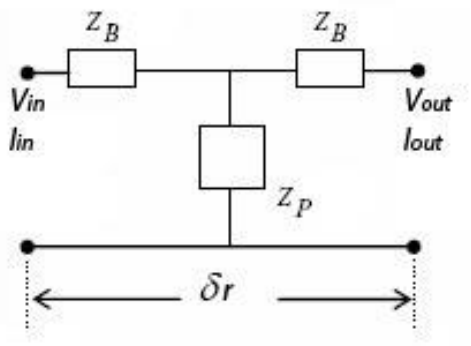

Figure 1-7 The equivalent quadrupole for each cylindrical sector [29].

$$\begin{cases} Z_B = \dfrac{\xi}{jF}\tanh\left[{}^{(\xi\delta r)}/_{2}\right] \\ Z_p = \dfrac{\xi}{jF\sinh(\xi\delta r)} \end{cases}$$

For $\xi\delta r \ll 1$ the impedances can be approximated by the equivalent relations

$$\begin{cases} Z_B = \dfrac{\xi^2\left({}^{\delta r}/_{2}\right)}{jF} \\ Z_p = \dfrac{1}{jF\delta r} \end{cases} \tag{1.44}$$

If $\xi^2 > 0$, both Z_B, Z_p are "capacitive" reactances. For $\xi^2 < 0$ however, Z_B becomes "inductive" reactance. For (V_E, I_E) the approximate respective impedances of the T-circuit are given as

$$\begin{cases} Z'_B = \dfrac{\xi^2\left({}^{\delta r}/_{2}\right)}{jn^2F} \\ Z'_p = \dfrac{1}{jn^2F\delta r} \end{cases} \tag{1.45}$$

As previously stated, the functions (V_M, I_M) of each layer are continuous at the cylindrical boundaries of the layer, thus if we divide the fiber (including a sufficient number of air layers) in successive thin layers and replace them by their equivalent T-circuits, an overall lossless transmission line is formed with only reactive elements. For given "*l*", the "β" values that lead to the resonance of the overall transmission line are the eigenvalues of the whole optical fiber.

When a transmission line is in resonance, at any arbitrary point r_0 of the line, the sum of reactive impedances arising from the successive T-circuits on the left and right sides of r_0 should be equal to zero, thus the equation giving the eigenvalues of the transmission line is the following:

$$\dot{Z}_{L.r_0} + \dot{Z}_{R.r_0} = 0 \qquad (1.46)$$

Equation (1.46) provides the eigenvalues "β" for a given "*l*", where $\dot{Z}_{L.r_0}$, $\dot{Z}_{R.r_0}$ are the overall reactive impedances of successive T-circuits on the left and right of r_0, using equations (1.44) or (1.45). The value of r_0 is usually given by the core radius. For the same "l" the equations (1.44) and (1.45) give usually slightly different values of *'β'*. This phenomenon is called "Birefringence". For circular step index fibers, the birefringence is negligible; however, for elliptic fibers and fibers of any other non-circular cores, the birefringence phenomenon could be not negligible.

In order to calculate the overall reactive impedances on the left and right of r_0 one should find the impedances for $r \to 0$ and for $r \to \infty$. As we proceed to 0 or to ∞, the remaining piece of transmission line becomes "homogeneous", i.e., its overall reactive impedance is equal to its characteristic impedance given by $Z = \frac{\xi}{jF} \left(or \frac{\xi}{jn^2F}\right)$. Then we must have

$r \to \infty: F \to \beta^2 r, MF \to 0, \xi \to \sqrt{\beta^2 - n^2} \rightarrow Z_{r\to\infty} = 0$

$r \to 0: F \to \frac{l^2}{r} \rightarrow$

Taking into consideration that $E_r \rightarrow 0$, the equation $\nabla X\vec{E} = -j\vec{H}$ is giving

$$2\pi r E_{\varphi(0)} = -j\pi r^2 H_{z(0)} \qquad (1.47)$$

For TE modes the analysis proceeds as follows:

$$E_{\varphi(0)} = -j\frac{r}{2}H_{z(0)} \tag{1.48}$$

$$\frac{I_M}{F} = -j\frac{r}{2}V_M \Rightarrow \frac{V_M}{I_M} = -\frac{2j}{rF_{(r=0)}} \tag{1.49}$$

Where

$$rF = (\beta r)^2 + l^2 \tag{1.50}$$

For $r = 0$ (1.49) becomes

$$\frac{V_M}{I_M} = -\frac{2j}{l^2} \Rightarrow Z_{M(r=0)} = -\frac{2j}{l^2} \tag{1.51}$$

In a similar way, for TM modes, it can be proved that

$$Z_{E(r=0)} = -\frac{2j}{n^2 l^2} \tag{1.52}$$

For $l = 0$ $Z_{r\to 0} = \infty$ (open circuit at the center of the equivalent transmission line) It is useful to notice that there is an equivalence between our formulation and the classic formulation modes of optical fibers. In particular, for $l = 0$, the modes (V_M,I_M) are the TE modes, while the modes (V_E,I_E) are the TM modes. For $l > 0$, the modes (V_M,I_M) are the HE modes, while the modes (V_E,I_E) are their HE birefringence modes. For $l < 0$ the modes (V_M,I_M) are the EH modes, while the modes (V_E,I_E) are their EH birefringence modes. For any given l, using the resonance technique the β values of the two birefringence modes can be calculated.

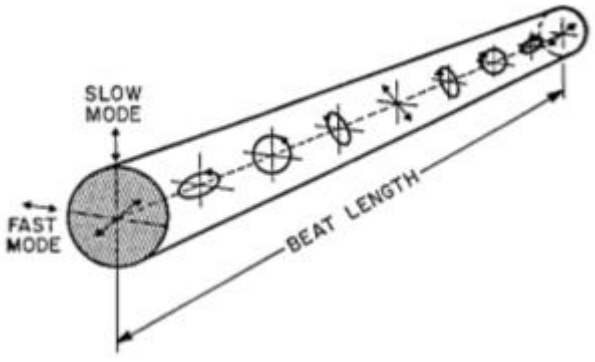

Figure 1-8 Polarization inside a birefringent fiber where the input beam is linearly polarized at 45° related to the slow and fast axis [3]

Let us consider for example a step-index fiber of n_1 = 1.54, n_2 = 1.47, n_1 being the refractive index in the core and n_2 being the refractive index in the cladding. The V_M, V_E, fundamental modes for normalized frequency V = 3.3, can be calculated and their β/k_0 values are respectively 1.518934962534846 and 1.518340184686295, hence their birefringence is equal to 0.0004947 or 0.0391%. The β/k_0 value for the equivalent mode V_{eq} was also calculated and was equal to 1.518638548412019 (that is approximately equal to the mean value of the previous β/k_0 values), while the β/k_0 value calculated conventionally by Bessel functions is equal to 1.518642063686336. These β values are very close differing only by 0.0002315%.

In the following Figure 1.9, the normalized birefringence of the step-index fibers for n_1 = 1.54, n_2 = 1.47, and of n_1 = 1.475, n_2 = 1.47 as functions of V are shown.

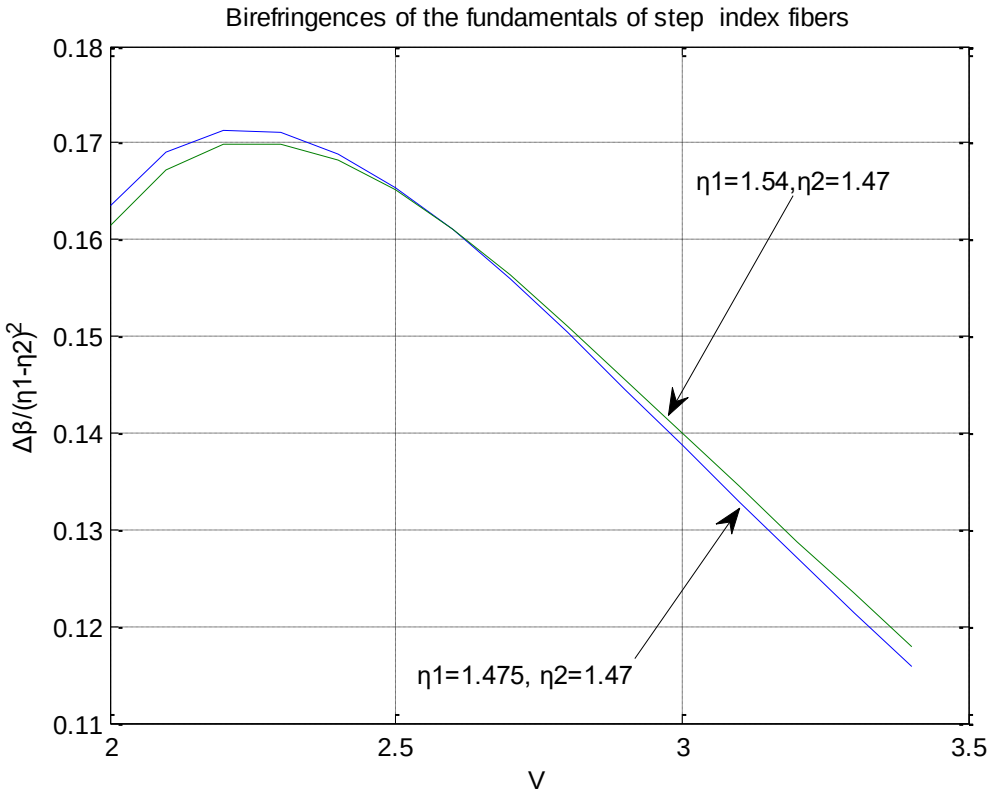

Figure 1-9 Normalized birefringence of two step-index fibers with different refractive indexes as functions of their parameters V.

We notice that for any V, the normalized birefringence is almost proportional to $\Delta n^2 = (n_1 - n_2)^2$, thus the birefringence of step-index fibers of very small Δn is negligible. For instance, for a value of V = 2.4, and Δn = 1.54 − 1.47 = 0.07, the birefringence is

found to be 0.168 × 0.0049 = 0.0008232 or ~0.055% on the average β, while for Δn = 1.475 − 1.47 = 0.005, the birefringence becomes 0.168 × 0.000025 = 0.000042 or ~0.0028% on the average β. The presented RTL method is accurate enough to calculate it.

1.10. Calculating "Voltages" VM, VE and "Currents" IM, IE and Resulting Fields

For any given l, using the resonance technique the β values of the two birefringence modes can be calculated. These β values are practically the same, thus we can consider them as equal or we can consider as the proper value of β the mean value of the two modes. Taking $V_M = 1$ at the center point of the fiber ($r = 0$), the respective value of I_M at the same point can be calculated by the respective terminal impedance. Using the matrix relations between input–output for the equivalent successive T-circuits, the values of V_M and I_M at the rest of the thin cylindrical layers can be calculated. In fact, from the general theory of the telegrapher's equation we know that the inputs and outputs are associated via a transfer matrix as follows

$$\begin{cases} [V_{out} I_{out}] = \begin{pmatrix} \cosh(\xi(r)\cdot\delta r) & Z(r)\cdot\sinh(\xi(r)\cdot\delta r) \\ \sinh(\xi(r)\cdot\delta r)/Z(r) & \cosh(\xi(r)\cdot\delta r) \end{pmatrix} \begin{bmatrix} V_{in} \\ I_{in} \end{bmatrix} \approx \\ \approx \begin{pmatrix} 1 & Z(r)\cdot(\xi(r)\cdot\delta r) \\ (\xi(r)\cdot\delta r)/Z(r) & 1 \end{pmatrix} \begin{bmatrix} V_{in} \\ I_{in} \end{bmatrix} = \\ = \begin{pmatrix} 1 & \xi^2(r)\cdot\delta r/jF(r) \\ jF(r)\cdot\delta r & 1 \end{pmatrix} \begin{bmatrix} V_{in} \\ I_{in} \end{bmatrix} \end{cases} \quad (1.53)$$

In equation (1.47), the characteristic impedance should be taken as $Z(r) = \xi(r)/jF(r)$ to comply with the previous analysis. Using the relations $nV_E = V_M$ and $nI_M = I_E$ the respective values of their birefringence partners can also be calculated for every thin cylindrical layer r_i. Finally, we obtain the actual fields via the relations

$$\begin{cases} \overline{H_r} = {jI_M}/{r}, \overline{E_r} = \frac{I_E}{n^2 r} \\ \overline{H_\varphi} = jlV_M/r - \frac{\beta}{F} I_E \\ \overline{E_\varphi} = lV_E/r + j\frac{\beta}{F} I_M \\ \overline{H_z} = \frac{l}{Fr} I_E + j\beta V_M \\ \overline{E_z} = -j\frac{l}{Fr} I_M + \beta V_E \end{cases} \quad (1.54)$$

The field components $H_\varphi, E_\varphi, H_z, E_z$ are made of two independent parts due to TM and TE fields. Due to birefringence these parts have different mode propagation constants along the z axis. Thus the parts have variating phase differences along z. Moreover, in certain points along z the parts have the same phase and their maximum values are

$$\begin{cases} |\overline{H_r}| = \left|{I_M}/{r}\right|, |\overline{E_r}| = \left|\frac{I_E}{n^2 r}\right| \\ \left|\overline{H_\varphi}\right| = \left|\frac{lV_M}{r}\right| + \left|\frac{\beta}{F} I_E\right| \\ \left|\overline{E_\varphi}\right| = |lV_E/r| + \left|\frac{\beta}{F} I_M\right| \\ |\overline{H_z}| = \left|\frac{l}{Fr} I_E\right| + |\beta V_M| \\ |\overline{E_z}| = \left|\frac{l}{Fr} I_M\right| + |\beta V_E| \end{cases} \quad (1.55)$$

A very useful field component for optical fibers is the value of the overall electric field at any thin cylindrical layer of average radius *r* that can be calculated by the formula:

$$\left|\vec{E}\,(r)\right|^2 = |\bar{E}_r|^2 + |\bar{E}_\phi|^2 + |\bar{E}_z|^2 \quad (1.56)$$

1.11. Calculation of EM Field Components

By the formulae (1.54) we can calculate, for a given β, the EM field components. Taking into consideration that the birefringence is extremely low (e*10^-4), it can be assumed that V_E , I_E, become

$V_E = \frac{V_M}{n}$ and $I_E = nI_M$.

Finally the set of equations (1.54) become:

$$\begin{cases} \overline{H_r} = \frac{j}{r} I_M \,, \overline{E_r} = \frac{I_M}{nr} \\ \overline{H_\varphi} = \frac{jl}{r} V_M - \frac{n\beta}{F} I_M \\ \overline{E_\varphi} = \frac{l}{nr} V_M + j\frac{\beta}{F} I_M \\ \overline{H_z} = \frac{nl}{Fr} I_M + j\beta V_M \\ \overline{E_z} = -\frac{jl}{Fr} I_M + \frac{\beta}{n} V_M \end{cases} \quad (1.57)$$

And the set of equations (1.55) become

$$\begin{cases} |\overline{H_r}| = \left|I_M/r\right|, |\overline{E_r}| = \left|\frac{I_M}{rn}\right| \\ \left|\overline{H_\varphi}\right| = \left|\frac{lV_M}{r}\right| + \left|\frac{n\beta}{F} I_M\right| \\ \left|\overline{E_\varphi}\right| = |lV_M/n/r| + \left|\frac{\beta}{F} I_M\right| \\ |\overline{H_z}| = \left|\frac{nl}{Fr} I_M\right| + |\beta V_M| \\ |\overline{E_z}| = \left|\frac{l}{Fr} I_M\right| + \left|\frac{\beta V_M}{n}\right| \end{cases} \quad (1.58)$$

The set of equations in (1.58) can be used to create programs for the estimation and plotting of the EM field components for a given mode propagation constant, ie for the fundamental mode.

The preceding analysis describes the basis of the methodology used to investigate fundamental propagation characteristics in cylindrical optical fibers. The successful implementation of the method in cylindrical fibers, the gradual refinement of the method through research and the proven accuracy in result estimation have provided a powerful tool for the investigation of additional types of optical fibers; specifically fibers with elliptical core cross-section that constitute the main subject of study in the current thesis. Below follows a brief enumeration of the main topics that are addressed within the scope of our research, presented per chapter.

1.12. Main goal of the present thesis

The main goal of this thesis is the numerical investigation of the propagation characteristics of EM modes inside elliptical optical fibers, using the Transmission Line theory. Chapter 1, serves as a necessary introduction to the EM theory behind the cylindrical fibers and the theory of Transmission Lines. Before applying the Transmission Line theory on elliptical fibers, this chapter presents the application of the theory on cylindrical fibers. The obtained method can be transformed into an algorithm for the estimation of mode propagation constants in cylindrical fibers. A case study is further provided regarding the optimization of the algorithm, aiming to achieve maximum accuracy in the estimation of mode propagation constants. The results of the case study are presented in section 1.6. Chapter 1 also provides a secondary algebraic analysis of EM propagation in cylindrical fibers, focusing on the definition and estimation of birefringence. The analysis concludes with the calculation of EM field components for cylindrical core fibers.

Chapter 2 includes a presentation of existing literature on the issue of EM wave propagation inside elliptical waveguides. Initial approaches to the problem, are mentioned, while the most important studies are presented in more depth. Especially the related researches of C. Yeh and R.B. Dyott are mentioned in detail since they provide the theoretical basis for the problem this thesis seeks to address. Yeh provides the analytical solution for EM wave propagation on a dielectric medium of elliptical cross-section while Dyott uses this solution to further investigate the properties of elliptical fibers. In this chapter, the property of birefringence is also defined with regards to elliptical fibers as well as their distinct ability to retain polarization. Finally, the conclusion is reached related to the elliptical fibers' potential usability and applications.

Chapter 3 contains a basic theoretical analysis of EM wave propagation inside elliptical optical fibers, applying Maxwell's equations in the case elliptical coordinates. It continues with the adaptation of the Resonant Transmission Line method over the subsequent analysis in order to estimate the mode propagation constant β. As the analysis results to the appearance of harmonics which constitute critical components for the calculation of β, the chapter presents several approaches based on harmonics' use cases, to produce the corresponding results. The RTL method is also used for the estimation of the mode propagation constant for cases of arbitrary index profiles. The chapter concludes with the presentation of the estimation of field components for the elliptical fiber.

Chapter 4 deals with the eccentricity problem and eccentric core fibers are defined. Eccentric core fibers are studied as a case that could be used for the analysis of the D-fiber, whose core is of elliptical cross section. After the theoretical analysis involving the adaptation of Maxwell's equations on the fiber's geometry, the RTL method is applied in order to estimate the mode propagation constant β in the case of eccentric fibers. The chapter concludes with result comparison for several cases of eccentricities.

Chapter 5 presents a definition of the generic unconventional fiber and describes a method for the calculation of EM wave propagation properties. A different approach is presented that can be used for the estimation of various cases of ellipticity and/or eccentricity in the fiber core. The method described can be used instead of the harmonics' inclusion method presented in chapter 3 for the study of elliptical core

fibers. Results are further presented calculating the mode propagation constant β and are then compared to corresponding results using the method from chapter 3. Results from the calculation of birefringence using both methods are also compared.

In chapter 6, a review is presented, of the benefits of the described numerical methods compared with the existing theoretical/analytical methods, towards the estimation of key propagation properties for the elliptical fiber. Recommendations are made regarding future studies that could arise based on the described methods. Finally, a list is presented with applications based on elliptical fibers.

2 CHAPTER 2

History and Theory of Elliptical Core Fibers

2.1. Elliptical fibers history and usage

In chapter one we referred to the application of optical fibers as a solution in the ever increasing need to transfer significant amounts of information across higher distances. The success of optical fibers communication systems lays in their effectiveness to achieve minimum loss combined with greater bandwidth while along wider repeater spacing. Throughout the evolution of the optical fibers with circular core, and under the efforts made to optimize their performance, studies were conducted to monitor the effect of alterations from circularity on the bandwidth of the system. One of the cases investigated was that of the elliptical fiber. Ironically, one of the main concerns in studying the elliptical fiber was not related to its properties and potential applications but rather to the effects of ellipticity as a deviation from cylindrical fibers' circular section.

Elliptical waveguides where initially studied in a research related to EM waves propagation inside elliptical metal pipes, by L.J. Chu[22] in "Electromagnetic waves in elliptic hollow pipes of metal.", 1938, but the first attempt to estimate the dispersion relation of an EM wave propagating inside an elliptical cylinder structure was made by Karbowiak [23] in 1954. In order to formulate the wave equation in elliptical coordinates, Karbowiak examined the elliptical cross-section Geubau line and Sommerfeld line. However, the solutions were obtained with boundary conditions matching merely at a single point on the surface, which was insufficient. Therefore the solutions could be treated only as an approximation for the case of low eccentricity. A similar research was presented by Lyubimov, et al. [24] in 1961 providing solutions over the properties of EM wave propagation, based on Mathieu functions. Despite the fact that the pre mentioned studies did not provide generic solutions for the boundary conditions on dielectric waveguides of elliptical cross section, they set the basis of the electromagnetic theoretical analysis, with Mathieu and modified Mathieu functions as the key tools for future research. In that context, C. Yeh [25], managed to utilize and expand the existing theoretical basis and provide updated and effective solutions over

the full boundary problem of a dielectric rod of elliptical cross section, using Mathieu Functions. Among the studies that followed, the specific case of an elliptical optical waveguide was investigated as a problematic malformation in cylindrical fibers by Dyott and Stern [26] and by Schlosser [27]. It was further concluded that using a broad ellipticity and an adequately high difference in the refractive index, leaded to separation of the fundamental modes' propagation constants and allowed fibers to sustain polarization over significant distances [28], [29]. As an important feature in the study of propagation, the mode cutoff frequencies have also been studied [30, 31] and experimentally also in [32]. In the following sections of this chapter, works of Yeh and Dyott will be presented in detail, supporting a comprehensive analysis of the related EM theory.

2.2. Study of EM Wave Propagation Within Dielectric Waveguides of Elliptical Cross-Section - Yeh's analysis

The properties and the characteristics of EM wave propagation within a dielectric rod of elliptical cross-section are associated to its' distinct geometry. The Bessel functions that are used to describe propagation in cylindrical core fibers cannot be used in the case of the elliptical core. C. Yeh was not the first to use Mathieu functions to describe propagation in such a dielectric environment, but he was the first to provide the necessary terms under which boundary conditions can be fulfilled permitting further analysis [33].

In Yeh's analysis the problem is formulated on a properly defined (infinitely long, straight, isotropic and homogeneous) dielectric cylinder of elliptical cross section, situated inside an infinite dielectric medium. The medium's properties are given:

- dielectric constant ε_0
- magnetic permeability μ_0

The properties of the cylinder are also given:

- dielectric constant $\varepsilon_1 > \varepsilon_0$
- magnetic permeability $\mu_1 = \mu_0$

Conductivity in the whole system is considered zero

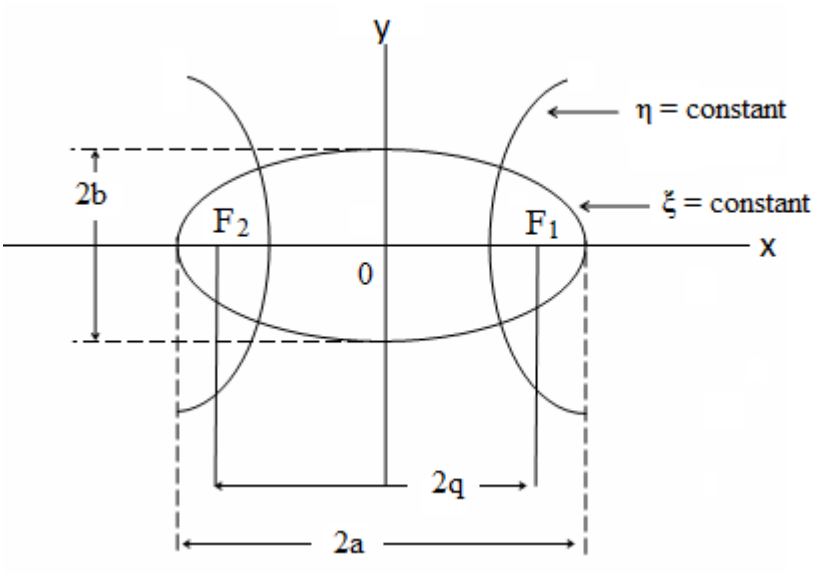

Figure 2-1 Elliptical coordinate system

In accordance to the geometrical nature of the problem, the elliptical cylinder coordinates (fig. 2.1) are introduced as follows:

- ξ is the radial coordinate that describes a set of confocal ellipses
- η is the azimuth coordinate that describes a set of hyperbolae, orthogonal to the ellipses.
- z is the coordinate corresponding to the axis, parallel to the cylinder, to the direction of propagation.
- q is the semifocal length of the ellipse.

In terms of the Cartesian coordinates, the elliptical coordinates are defined as follows:

$$\begin{cases} x = q\cosh\xi\cos\eta \\ y = q\sinh\xi\sin\eta \\ z = z \end{cases} \tag{2.1}$$

The boundary of the core is defined as $\xi = \xi_0$ while the semi-major and semi-minor axes of the core ellipse are defined as $a = q\cosh\xi_0$ and $b = q\sinh\xi_0$ respectively. Eccentricity e is given by

$$e = \left[1 - \left(\frac{b}{a}\right)^2\right]^{\frac{1}{2}} = \frac{1}{\cosh\xi_0} \tag{2.2}$$

Yeh proceeds to solve Maxwell's equations in elliptical cylindrical coordinates. The initial equations in a source-free medium with properties of ε and μ, are given by:

$$\nabla \times \underline{E} = i\omega\mu\underline{H} \tag{2.3.a}$$

$$\nabla \times \underline{H} = -i\omega\varepsilon\underline{E} \tag{2.3.b}$$

$$\nabla \cdot \underline{H} = 0 \tag{2.3.c}$$

$$\nabla \cdot \underline{E} = 0 \tag{2.3.d}$$

With $\underline{E}$ and $\underline{H}$ representing the electric and magnetic field vectors respectively. Using the elliptical coordinates, the field components are obtained:

$$E_\xi = \frac{1}{(k^2-\beta^2)p}\left\{i\beta\frac{\partial E_z}{\partial \xi} + i\omega\mu\frac{\partial H_z}{\partial \eta}\right\} \tag{2.4.a}$$

$$E_\eta = \frac{1}{(k^2-\beta^2)p}\left\{i\beta\frac{\partial E_z}{\partial \eta} + i\omega\mu\frac{\partial H_z}{\partial \xi}\right\} \tag{2.4.b}$$

$$H_\xi = \frac{1}{(k^2-\beta^2)p}\left\{-i\omega\varepsilon\frac{\partial E_z}{\partial \eta} + i\beta\frac{\partial H_z}{\partial \xi}\right\} \tag{2.4.c}$$

$$H_\eta = \frac{1}{(k^2-\beta^2)p}\left\{-i\omega\varepsilon\frac{\partial E_z}{\partial \xi} + i\beta\frac{\partial H_z}{\partial \eta}\right\} \tag{2.4.d}$$

where, $p = q(\sinh^2\xi + \sinh^2\eta)^{1/2}$; while wave equations take the form:

$$\frac{\partial^2 E_z}{\partial \xi^2} + \frac{\partial^2 E_z}{\partial \eta^2} + [q^2(k^2-\beta^2)(\sinh^2\xi + \sin^2\eta)]E_z = 0 \tag{2.5}$$

$$\frac{\partial^2 H_z}{\partial \xi^2} + \frac{\partial^2 H_z}{\partial \eta^2} + [q^2(k^2-\beta^2)(\sinh^2\xi + \sin^2\eta)]H_z = 0 \tag{2.6}$$

Where $k^2 = \omega^2\mu\varepsilon$ and β is the mode propagation constant

Solving only one of the equations (2.5) and (2.6), is sufficient since they are both in the same form. Under the condition of $H_z = 0$ or $E_z = 0$, TM or TE waves result respectively.

2.2.1. Obtaining Solutions for the Wave Equations

Before introducing the Mathieu functions, the wave equation is slightly modified by substituting E_z or H_z with a generic factor Λ, thus leading to the following partial differential equation:

$$\frac{\partial^2 \Lambda}{\partial \xi^2} + \frac{\partial^2 \Lambda}{\partial \eta^2} + [q^2(k^2-\beta^2)(\sinh^2\xi + \sin^2\eta)]\Lambda = 0 \tag{2.7}$$

The solution of (2.7) is obtained by setting

$$\Lambda(\xi,\eta) = R(\xi)\Theta(\eta) \tag{2.8}$$

Incorporating (2.8) in (2.7) and following separation of variables, equation (2.7) can be further split into two ordinary differential equations:

$$\frac{d^2\Theta(\eta)}{d\eta^2} + (c - 2\gamma^2\cos 2\eta)\Theta(\eta) = 0 \tag{2.9}$$

and

$$\frac{d^2R(\xi)}{d\xi^2} + (c - 2\gamma^2\cosh 2\xi)R(\xi) = 0 \tag{2.10}$$

Where c is the separation constant and $\gamma^2 = (k^2 - \beta^2)q^2/4$

The above relations (2.9), (2.10) are the Mathieu and modified Mathieu differential equations respectively and the later is formed from the former through the transformation $\eta = \pm i\xi$. It is noted that in the case of physically acceptable single-valued EM fields, $\Lambda(\xi,\eta)$ must be a periodic function of η, with a period of π or 2π. c is the separation constant and a function of γ^2. When $\gamma^2 \neq 0$, a c value leads to merely a single periodic solution with η being either even or odd.

The periodic solutions of the Mathieu and modified Mathieu differential equations are restricted by the boundary conditions and the characteristics of the regions on either side of the boundary, since in Yeh's analysis, they represent the EM field of an elliptical dielectric cylinder. Region 1 is the area inside the dielectric cylinder where field components are finite. Region 0 is the area outside the dielectric cylinder where field components should approach zero. Consequently, the relations (2.5), (2.6) for each region become:

Inside the cylinder $0 \leq \xi \leq \xi_0$ (region 1)

$$H_{z1}(\xi,\eta,z,t) = \sum_{n=0}^{\infty} A_n Ce_n(\xi,\gamma_1^2)ce_n(\eta,\gamma_1^2)\, e^{-i\omega t}e^{i\beta_1 z} + \sum_{n=1}^{\infty} A'_n Se_n(\xi,\gamma_1^2)se_n(\eta,\gamma_1^2)\, e^{-i\omega t}e^{j\beta_1 z} \tag{2.11}$$

$$E_{z1}(\xi,\eta,z,t) = \sum_{n=0}^{\infty} B'_n Ce_n(\xi,\gamma_1^2)ce_n(\eta,\gamma_1^2)\, e^{-i\omega t}e^{i\beta_1 z} + \sum_{n=1}^{\infty} B_n Se_n(\xi,\gamma_1^2)se_n(\eta,\gamma_1^2)\, e^{-i\omega t}e^{i\beta_1 z} \tag{2.12}$$

Outside the cylinder $\xi_0 \leq \xi \leq \infty$ (region 0)

$$H_{z0}(\xi,\eta,z,t) = \sum_{n=0}^{\infty} L_n Fek_n(\xi,|\gamma_0^2|)ce_n^*(\eta,|\gamma_0^2|)e^{-i\omega t}\, e^{i\beta_0 z} + \sum_{n=1}^{\infty} L_n' Gek_n(\xi,|\gamma_0^2|)se_n^*(\eta,|\gamma_0^2|)e^{-i\omega t}\, e^{i\beta_0 z} \quad (2.13)$$

$$E_{z0}(\xi,\eta,z,t) = \sum_{n=0}^{\infty} P_n' Fek_n(\xi,|\gamma_0^2|)ce_n^*(\eta,|\gamma_0^2|)e^{-i\omega t}\, e^{i\beta_0 z} + \sum_{n=1}^{\infty} P_n Gek_n(\xi,|\gamma_0^2|)se_n^*(\eta,|\gamma_0^2|)e^{-i\omega t}\, e^{i\beta_0 z} \quad (2.14)$$

$A_n, A_n', B_n, B_n', L_n, L_n', P_n, P_n'$ are coefficients associated with the boundary conditions and constitute functions of $n, \omega, \gamma_1^2, |\gamma_0^2|$. These coefficients are also related to the nature of the exciting source and are independent of the coordinates.

$\gamma_1^2, |\gamma_0^2|$ are given by $\gamma_1^2 = (k_1^2 - \beta_1^2)q^2/4$ and $\gamma_0^2 = |(k_0^2 - \beta_0^2)q^2/4|$.

$k_1^2 = \omega^2\mu\varepsilon_1$ and $k_0^2 = \omega^2\mu\varepsilon_0$

ε_1 is the dielectric constant of the cylinder.

ε_0 is the dielectric constant of the surrounding medium.

$\xi = \xi_0$ is the surface of the elliptic cylinder

2.2.2. Simplification of Boundary Conditions with Mathieu Functions

Boundary conditions in EM wave theory provide the necessary relations for solving the wave propagation problem. Solutions must be single valued and finite while satisfying the free of source Maxwell's equations and the boundary conditions. According to the boundary conditions, the tangential components of the electric and magnetic fields are continuous through any surface, which in the current case of elliptical cylindrical coordinates, this translates to the following set of relations:

$$E_{z_1} = E_{z_0} \quad (2.15)$$

$$H_{z_1} = H_{z_0} \quad (2.16)$$

$$E_{\eta_1} = E_{\eta_0} \quad (2.17)$$

$$H_{\eta_1} = H_{\eta_0} \quad (2.18)$$

In order to demonstrate the complexity and the difficulties arising from satisfying the boundary conditions, Yeh proceeds with applying the predefined wave equations (2.12), (2.14) on the first continuity condition $E_{z_1} = E_{z_0}$, in the elliptical cylindrical coordinates.

$$\sum_{n=0}^{\infty} B_n' Ce_n(\xi, \gamma_1^2) ce_n(\eta, \gamma_1^2)\, e^{i\beta_1 z} + \sum_{n=1}^{\infty} B_n Se_n(\xi, \gamma_1^2) se_n(\eta, \gamma_1^2)\, e^{i\beta_1 z}$$
$$= \sum_{n=0}^{\infty} P_r' Fek_r(\xi, |\gamma_0^2|) ce_r^*(\eta, |\gamma_0^2|)\, e^{i\beta_0 z}$$
$$+ \sum_{n=1}^{\infty} P_r Gek_r(\xi, |\gamma_0^2|) se_r^*(\eta, |\gamma_0^2|)\, e^{i\beta_0 z} \tag{2.19}$$

The analysis reaches a point where the equations involved, include an infinite number of arbitrary constants, requiring a corresponding number of linear algebraic relations. Consequently, it is apparent that satisfying the boundary conditions, would require and infinite number of Mathieu functions in order to describe the fields in the areas in either side of the boundary – inside and outside of the cylinder.

In order to overcome the difficulty involved with the analysis, Yeh proposed the assumption that the field configurations in one medium can be expressed by one single term of the Mathieu function, while the field configurations in the other medium could be expressed by an infinite series of Mathieu functions, [34]. The exact method proposed shall be presented analytically later, in the section referring to the calculation of the field components of the principal modes.

2.2.3. Mode classifications for elliptical waveguides

Unlike in circularly symmetrical waves (where the field is a function of the angular coordinates), in the case of the elliptical waveguide, E and M waves must both exist in order for the boundary conditions to be satisfied. In that context, the asymmetrical waves inside an elliptical waveguide are expressed by HE_{mn} and EH_{mn} depending on whether the cross-section field pattern resembles that of an H or a E wave respectively. At this point it should be noted that modes must all be hybrid, in the sense that no pure TE or TM waves can exist inside and elliptical waveguide. Yeh's analysis is further

restricted to the study of principal modes, defined as the modes that, when eccentricity approaches zero, they gradually degenerate to the hybrid HE_{mn}. In their final form, the principal modes' notation will be ${}_eHE_{mn}^{(1,0)}$ and ${}_oHE_{mn}^{(1,0)}$ for even and odd modes respectively. When a mode is even, the axial magnetic and electric fields within, are expressed by an even and odd Mathieu function respectively. Similarly, for an odd mode, the axial magnetic and electric fields within, are expressed by an odd and even Mathieu function respectively [33]. m denotes the order of the Mathieu function representing the single product term, while n denotes the nth root of the characteristic equation. The 0,1 superscripts indicate the region inside or outside, related to, within what region a single product term was used to express the field configuration.

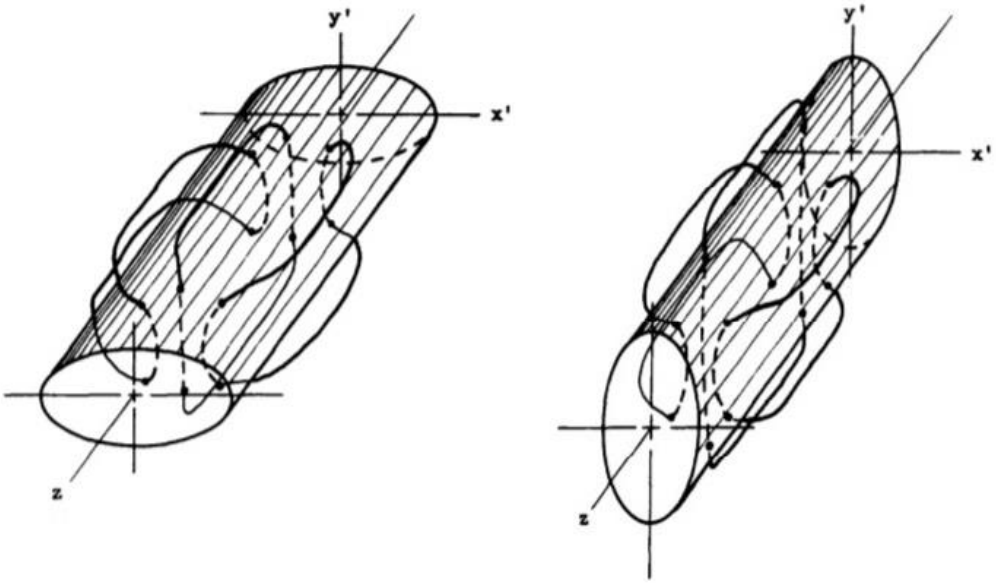

Figure 2-2 Visual representation of even ${}_e\boldsymbol{HE}_{\boldsymbol{11}}^{\boldsymbol{(1)}}$ and odd ${}_o\boldsymbol{HE}_{\boldsymbol{11}}^{\boldsymbol{(1)}}$ modes and the course of the electric lines, left and right respectively [33]

The above visual representation (Figure 2-2) helps understand the geometrical differences between even and odd variations of the fundamental mode in 3 dimensions.

2.2.4. Derivation of principal modes' field components and characteristic equations

Defining the field components and applying the boundary conditions will lead to the necessary characteristic equations for the principal modes which in turn provide the values of the propagation constants. The methods and assumptions required to simplify the problem to a point of feasibility are already presented in Yeh's analysis and are

applied in the following section to obtain the solutions. Initially, Mathieu and modified Mathieu function notations are simplified as follows:

$$Ce_m(\xi) = Ce_m(\xi, \gamma_1^2) \qquad ce_m(\eta) = ce_m(\eta, \gamma_1^2)$$

$$Se_m(\xi) = Se_m(\xi, \gamma_1^2) \qquad se_m(\eta) = se_m(\eta, \gamma_1^2)$$

$$Fek_r(\xi) = Fek_r(\xi, |\gamma_0^2|) \qquad ce_r^*(\eta) = ce_r^*(\eta, |\gamma_0^2|)$$

$$Gek_r(\xi) = Gek_r(\xi, |\gamma_0^2|) \qquad se_r^*(\eta) = se_r^*(\eta, |\gamma_0^2|)$$

The following four types of principal modes are considered, according to the notation described in section 2.2.3:

$${}_eHE_{mn}^{(1)}$$

$${}_eHE_{mn}^{(0)}$$

$${}_oHE_{mn}^{(1)}$$

$${}_oHE_{mn}^{(0)}$$

Beginning with the ${}_eHE_{mn}^{(1)}$ mode, the magnetic and electric fields' axial components for region 1, are given by:

$$\begin{cases} H_{z_1} = A_m Ce_m(\xi) ce_m(\eta) e^{i\beta_1 z} \\ E_{z_1} = B_m Se_m(\xi) se_m(\eta) e^{i\beta_1 z} \end{cases} \quad (0 \le \xi \le \xi_0) \tag{2.20}$$

and for region 0 by

$$\begin{cases} H_{z_0} = \sum_{r=0}^{\infty} L_r Fek_r(\xi) ce_r^*(\eta)\, e^{i\beta_0 z} \\ E_{z_0} = \sum_{r=1}^{\infty} P_r Gek_r(\xi) se_r^*(\eta)\, e^{i\beta_0 z} \end{cases} \quad (\xi_0 \le \xi \le \infty) \tag{2.21}$$

where A_m, B_m, L_m, P_m, are arbitrary constants. In the above relations the harmonic time dependence $e^{-i\omega t}$ is implied and so are the related expressions for the field intensities [33]. The pair of equations (2.20), combined with the four equations (2.4.a - d), produce (after the differentiation is performed) the transverse field components for region 1:

$$H_{\xi_1} = \frac{i\beta}{({k_1}^2 - \beta^2)p} \left\{ A_m Ce'_m(\xi) ce_m(\eta) - \frac{\omega\varepsilon_1}{\beta} B_m Se_m(\xi) se'_m(\eta) \right\} e^{i\beta_1 z} \tag{2.22}$$

$$H_{\eta_1} = \frac{i\beta}{({k_1}^2-\beta^2)p}\left\{A_m Ce_m(\xi)ce'_m(\eta) + \frac{\omega\varepsilon_1}{\beta}B_m Se'_m(\xi)se_m(\eta)\right\}e^{i\beta_1 z} \quad (2.23)$$

$$E_{\xi_1} = \frac{i\beta}{({k_1}^2-\beta^2)p}\left\{\frac{\omega\mu}{\beta}A_m Ce_m(\xi)ce'_m(\eta) + B_m Se'_m(\xi)se_m(\eta)\right\}e^{i\beta_1 z} \quad (2.24)$$

$$E_{\eta_1} = \frac{i\beta}{({k_1}^2-\beta^2)p}\left\{-\frac{\omega\mu}{\beta}A_m Ce'_m(\xi)ce_m(\eta) + B_m Se_m(\xi)se'_m(\eta)\right\}e^{-\beta_1 z} \quad (2.25)$$

where $k_1^2 = \omega^2\mu\varepsilon_1$ and $p = q(\sinh^2\xi + \sinh^2\eta)^{1/2}$.

In a similar way, substituting the pair of equations (2.21) into the group (2.4.a - d), leads to the field components of region 0:

$$H_{\xi_0} = \frac{i\beta}{({k_0}^2-\beta^2)p}\sum_{r=0}^{\infty}\left[L_r Fek'_r(\xi)ce_r^*(\eta) - \frac{\omega\varepsilon_0}{\beta}P_r Gek_r(\xi)se_r^{*'}(\eta)\right]e^{i\beta_0 z} \quad (2.26)$$

$$H_{\eta_0} = \frac{i\beta}{({k_0}^2-\beta^2)p}\sum_{r=1}^{\infty}\left[L_r Fek_r(\xi)ce_r^{*'}(\eta) + \frac{\omega\varepsilon_0}{\beta}P_r Gek'_r(\xi)se_r^*(\eta)\right]e^{i\beta_0 z} \quad (2.27)$$

$$E_{\xi_0} = \frac{i\beta}{({k_0}^2-\beta^2)p}\sum_{r=1}^{\infty}\left[\frac{\omega\varepsilon_0}{\beta}L_r Fek_r(\xi)ce_r^{*'}(\eta) + P_r Gek'_r(\xi)se_r^*(\eta)\right]e^{i\beta_0 z} \quad (2.28)$$

$$E_{\eta_0} = \frac{i\beta}{({k_0}^2-\beta^2)p}\sum_{r=0}^{\infty}\left[-\frac{\omega\varepsilon_0}{\beta}L_r Fek'_r(\xi)ce_r^*(\eta) + P_r Gek_r(\xi)se_r^{*'}(\eta)\right]e^{i\beta_0 z} \quad (2.29)$$

where $k_0^2 = \omega^2\mu\varepsilon_0$. It is noted that as the orthogonality of Mathieu functions dictates [34], when m is odd, then so must be r. This means that for m odd, the series are summed over all the odd values of r [33].

The next step of Yeh's analysis follows with the application of the boundary conditions on the surface of the cylinder where $\xi = \xi_0$. Equation of the tangential electric and magnetic fields H_z, E_z, H_η, E_η, leads to:

$$A_m Ce_m(\xi_0)ce_m(\eta)e^{i\beta_1 z} = \sum_{\substack{r=1\\odd}}^{\infty} L_r Fek_r(\xi_0)ce_r^*(\eta)\,e^{i\beta_0 z} \quad (2.30)$$

$$B_m Se_m(\xi_0)se_m(\eta)e^{i\beta_1 z} = \sum_{\substack{r=1\\odd}}^{\infty} P_r Gek_r(\xi_0)se_r^*(\eta)\,e^{i\beta_0 z} \quad (2.31)$$

$$\frac{\beta_1}{({k_1}^2-{\beta_1}^2)p}\left[A_m Ce_m(\xi_0)ce'_m(\eta) + \frac{\omega\varepsilon_1}{\beta_1}B_m Se'_m(\xi_0)se_m(\eta)\right]e^{i\beta_1 z} =$$

$$\frac{\beta_0}{({k_0}^2-{\beta_0}^2)p}\sum_{\substack{r=1\\odd}}^{\infty}\left[L_r Fek_r(\xi_0)ce_r^{*'}(\eta) + \frac{\omega\varepsilon_0}{\beta_0}P_r Gek'_r(\xi_0)se_r^*(\eta)\right]e^{i\beta_0 z} \quad (2.32)$$

$$\frac{\beta_1}{({k_1}^2-{\beta_1}^2)p}\left[-A_m\frac{\omega\mu}{\beta_1}Ce'_m(\xi_0)ce_m(\eta)+B_mSe_m(\xi_0)se'_m(\eta)\right]e^{i\beta_1 z}=$$

$$\frac{\beta_0}{({k_0}^2-{\beta_0}^2)p}\sum_{\substack{r=1\\odd}}^{\infty}\left[-L_r\frac{\omega\mu}{\beta_0}Fek'_r(\xi_0)ce_r^*(\eta)+P_rGek_r(\xi_0)se_r^{*'}(\eta)\right]e^{i\beta_0 z} \qquad (2.33)$$

At this point the following operations take place:

- $\beta=\beta_0=\beta_1$
- elimination of $ce_r^{*'}(\eta)$ and $se_r^{*'}(\eta)$ via relations (2.30), (2.31)
- elimination of dependence in η
- multiplication of relations (2.30), (2.33) with $ce_s(\eta)$
- multiplication of relations (2.31), (2.32) with $se_s(\eta)$
- integration as per η from 0 to 2π

which eventually lead to

$$A_mCe_m(\xi_0)e_{ms}C_m=\sum_{\substack{r=1\\odd}}^{\infty}L_rFek_r(\xi_0)\,\alpha_{rs} \qquad (2.34)$$

$$B_mSe_m(\xi_0)e_{ms}S_m=\sum_{\substack{r=1\\odd}}^{\infty}P_rGek_r(\xi_0)\,\beta_{rs} \qquad (2.35)$$

$$A_m\left[1-\frac{{k_1}^2-\beta^2}{{k_0}^2-\beta^2}\right]Ce_m(\xi_0)X_{ms}+\frac{\omega\varepsilon_1}{\beta}B_mSe'_m(\xi_0)e_{ms}S_m=$$

$$\left(\frac{{k_1}^2-\beta^2}{{k_0}^2-\beta^2}\right)\frac{\omega\varepsilon_1}{\beta}\sum_{\substack{r=1\\odd}}^{\infty}P_rGek'_r(\xi_0)\,\beta_{rs} \qquad (2.36)$$

$$A_m\frac{\omega\mu}{\beta}\,Ce'_m(\xi_0)e_{ms}C_m-B_m\left[1-\frac{{k_1}^2-\beta^2}{{k_0}^2-\beta^2}\right]Se_m(\xi_0)\delta_{ms}=$$

$$\left(\frac{{k_1}^2-\beta^2}{{k_0}^2-\beta^2}\right)\frac{\omega\mu}{\beta}\sum_{\substack{r=1\\odd}}^{\infty}L_rFek'_r(\xi_0)\,\alpha_{rs} \qquad (2.37)$$

where $s=1,3,5,7,9,\ldots$, $e_{ms}, C_m, S_m, \alpha_{rs}, \beta_{rs}, \delta_{ms}, X_{ms}$, are given by:

$$e_{ms}=1 \qquad \text{for } m=s$$

$$e_{ms}=0 \qquad \text{for } m\neq s$$

$$C_m=\int_0^{2\pi}ce_m^2(\eta)dn$$

$$S_m=\int_0^{2\pi}se_m^2(\eta)dn$$

$$\alpha_{rs} = \int_0^{2\pi} ce_r^*(\eta) ce_s(\eta) dn$$

$$\beta_{rs} = \int_0^{2\pi} se_r^*(\eta) se_s(\eta) dn$$

$$\delta_{ms} = \int_0^{2\pi} se'_m(\eta) ce_s(\eta) dn$$

$$X_{ms} = \int_0^{2\pi} ce'_r(\eta) se_s(\eta) dn$$

Further information about the above integrals is given in Appendix B. In Yeh's analysis, it is also noted that every value of m corresponds to four infinite series of linear algebraic relations whose combination provides the following relations:

$$A_m Ce_m(\xi_0) = L_m Fek_m(\xi_0) M_m(\alpha_{rs}) \tag{2.38}$$

$$B_m Se_m(\xi_0) = P_m Gek_m(\xi_0) N_m(\beta_{rs}) \tag{2.39}$$

$$A_m \left[1 - \frac{{k_1}^2 - \beta^2}{{k_0}^2 - \beta^2}\right] Ce_m(\xi_0)\, Q_m(\beta_{rs}, X_{ms}) + \frac{\omega\varepsilon_1}{\beta} B_m Se'_m(\xi_0) =$$
$$\left(\frac{{k_1}^2 - \beta^2}{{k_0}^2 - \beta^2}\right) \frac{\omega\varepsilon_0}{\beta} P_m Gek'_m(\xi_0) N_m(\beta_{rs}) \tag{2.40}$$

$$A_m \frac{\omega\mu}{\beta}\, Ce'_m(\xi_0) - B_m \left[1 - \frac{{k_1}^2 - \beta^2}{{k_0}^2 - \beta^2}\right] Se_m(\xi_0) R_m(\alpha_{rs}, \delta_{ms}) =$$
$$\left(\frac{{k_1}^2 - \beta^2}{{k_0}^2 - \beta^2}\right) \frac{\omega\mu}{\beta} L_m Fek'_m(\xi_0) M_m(\alpha_{rs}) \tag{2.41}$$

$A_m, B_m, L_m, P_m,$ are coefficients and only their ratios can be obtained, to provide coupling factors between them. The constants $M_m(\alpha_{rs}), N_m(\beta_{rs}), Q_m(\beta_{rs}, X_{ms}), R_m(\alpha_{rs}, \delta_{ms})$, are obtained through a method that is demonstrated in the following example:

Let the mode $m = 1$. The constants are defined as

$$M_1(\alpha_{rs}) = \frac{\begin{vmatrix} \alpha_{33} & \alpha_{53} & \cdots \\ \alpha_{35} & \alpha_{55} & \cdots \\ \cdots & \cdots & \cdots \end{vmatrix}}{\begin{vmatrix} \alpha_{11} & \alpha_{31} & \alpha_{51} & \cdots \\ \alpha_{13} & \alpha_{33} & \alpha_{53} & \cdots \\ \alpha_{15} & \alpha_{35} & \alpha_{55} & \cdots \\ \cdots & \cdots & \cdots & \cdots \end{vmatrix}} \cdot \frac{1}{C_1}$$

$$N_1(\beta_{rs}) = \frac{\begin{vmatrix} \beta_{33} & \beta_{53} & \cdots \\ \beta_{35} & \beta_{55} & \cdots \\ \cdots & \cdots & \cdots \end{vmatrix}}{\begin{vmatrix} \beta_{11} & \beta_{31} & \beta_{51} & \cdots \\ \beta_{13} & \beta_{33} & \beta_{53} & \cdots \\ \beta_{15} & \beta_{35} & \beta_{55} & \cdots \\ \cdots & \cdots & \cdots & \cdots \end{vmatrix}} \cdot \frac{1}{S_1}$$

$$Q_1(\beta_{rs}, X_{1s}) = \left\{ X_{11} - X_{13} \frac{\begin{vmatrix} \beta_{31} & \beta_{51} & \cdots \\ \beta_{35} & \beta_{55} & \cdots \\ \cdots & \cdots & \cdots \end{vmatrix}}{\begin{vmatrix} \beta_{33} & \beta_{53} & \cdots \\ \beta_{35} & \beta_{55} & \cdots \\ \cdots & \cdots & \cdots \end{vmatrix}} + X_{15} \frac{\begin{vmatrix} \beta_{31} & \beta_{51} & \cdots \\ \beta_{33} & \beta_{53} & \cdots \\ \beta_{37} & \beta_{57} & \cdots \\ \cdots & \cdots & \cdots \end{vmatrix}}{\begin{vmatrix} \beta_{33} & \beta_{53} & \cdots \\ \beta_{35} & \beta_{55} & \cdots \\ \cdots & \cdots & \cdots \end{vmatrix}} + \cdots \right\} \cdot \frac{1}{S_1}$$

$$R_1(\alpha_{rs}, \delta_{1s}) = \left\{ \delta_{11} - \delta_{13} \frac{\begin{vmatrix} \alpha_{31} & \alpha_{51} & \cdots \\ \alpha_{35} & \alpha_{55} & \cdots \\ \cdots & \cdots & \cdots \end{vmatrix}}{\begin{vmatrix} \alpha_{33} & \alpha_{53} & \cdots \\ \alpha_{35} & \alpha_{55} & \cdots \\ \cdots & \cdots & \cdots \end{vmatrix}} + \delta_{15} \frac{\begin{vmatrix} \alpha_{31} & \alpha_{51} & \cdots \\ \alpha_{33} & \alpha_{53} & \cdots \\ \alpha_{37} & \alpha_{57} & \cdots \\ \cdots & \cdots & \cdots \end{vmatrix}}{\begin{vmatrix} \alpha_{33} & \alpha_{53} & \cdots \\ \alpha_{35} & \alpha_{55} & \cdots \\ \cdots & \cdots & \cdots \end{vmatrix}} + \cdots \right\} \cdot \frac{1}{C_1}$$

In the above relations $C_1 = \int_0^{2\pi} ce_1^2(\eta)dn$ and $S_1 = \int_0^{2\pi} se_1^2(\eta)dn$. The infinite determinants involved, can be solved by the method of successive approximations. In order to reach a non-trivial solution, the determinant of the set of equations (2.38)-(2.41) must equal to zero:

$$\begin{vmatrix} F_{11} & 0 & F_{13} & 0 \\ 0 & F_{22} & 0 & F_{24} \\ F_{31} & F_{32} & 0 & F_{34} \\ F_{41} & F_{42} & F_{43} & 0 \end{vmatrix} = 0 \qquad (2.42)$$

where

$$F_{11} = Ce_m(\xi_0)$$

$$F_{13} = -Fek_m(\xi_0)M_m(\alpha_{rs})$$

$$F_{22} = Se_m(\xi_0)$$

$$F_{24} = -Gek_m(\xi_0)N_m(\beta_{rs})$$

$$F_{31} = \left[1 - \frac{{k_1}^2 - \beta^2}{{k_0}^2 - \beta^2}\right] Ce_m(\xi_0)\, Q_m(\beta_{rs}, X_{ms})$$

$$F_{32} = \frac{\omega\varepsilon_1}{\beta} Se'_m(\xi_0)$$

$$F_{34} = \left(\frac{{k_1}^2 - \beta^2}{{k_0}^2 - \beta^2}\right) \frac{\omega\varepsilon_0}{\beta} Gek'_m(\xi_0)\, N_m(\beta_{rs})$$

$$F_{41} = \frac{\omega\mu}{\beta}\, Ce'_m(\xi_0)$$

$$F_{42} = -\left[1 - \frac{{k_1}^2 - \beta^2}{{k_0}^2 - \beta^2}\right] Se_m(\xi_0)R_m(\alpha_{rs}, \delta_{ms})$$

$$F_{43} = \left(\frac{{k_1}^2 - \beta^2}{{k_0}^2 - \beta^2}\right) \frac{\omega\mu}{\beta} Fek'_m(\xi_0)M_m(\alpha_{rs})$$

From (2.42) and after setting

$$x^2 = q^2 \cosh^2 \xi_0 \left({k_1}^2 - \beta^2\right)$$

$$y^2 = -q^2 \cosh^2 \xi_0 \left({k_0}^2 - \beta^2\right)$$

the transcendental characteristic equation of mode ${}_eHE_{mn}^{(1)}$ can be obtained:

$$\left[\frac{1}{x^2}\frac{Ce\prime_m(\xi_0)}{Ce_m(\xi_0)} + \frac{1}{y^2}\frac{Fek\prime_m(\xi_0)}{Fek_m(\xi_0)}\right]\left[\frac{1}{x^2}\frac{Se\prime_m(\xi_0)}{Se_m(\xi_0)} + \frac{1}{y^2}\frac{\varepsilon_0}{\varepsilon_1}\frac{Gek\prime_m(\xi_0)}{Gek_m(\xi_0)}\right] +$$

$$\frac{(x^2+y^2)\left(x^2\frac{\varepsilon_0}{\varepsilon_1}+y^2\right)}{x^4y^4} R_m(\alpha_{rs}, \delta_{ms})Q_m(\beta_{rs}, X_{ms}) = 0 \qquad (2.43)$$

Also by $\beta_0 = \beta_1$ the following relation is obtained:

$$x^2 + y^2 = k_0^2 q^2 \cosh^2 \xi_0 \left(\frac{\varepsilon_1}{\varepsilon_0} - 1\right) \qquad (2.44)$$

The transcendental characteristic equation can be used together with relation (2.44) to calculate the propagation constant β depending on the frequency, the dimensions of the waveguide, the eccentricity, the EM constants of the subsequent media and the order of the subsequent mode [33]. The pair of relations (2.43) and (2.44) are also referred to as the dispersion relations for the propagation constant. Also, the pre-mentioned ratios among the arbitrary constants are used to indicate the coupling between amplitude and phase in various field components [33].

Similar to the above analysis, the solutions for the remaining principal modes can be obtained.

For ${}_eHE_{mn}^{(0)}$ the transcendental characteristic equation is

$$\left[\frac{1}{x^2}\frac{Ce'_m(\xi_0)}{Ce_m(\xi_0)}+\frac{1}{y^2}\frac{Fek'_m(\xi_0)}{Fek_m(\xi_0)}\right]\left[\frac{1}{x^2}\frac{Se'_m(\xi_0)}{Se_m(\xi_0)}+\frac{1}{y^2}\frac{\varepsilon_0}{\varepsilon_1}\frac{Gek'_m(\xi_0)}{Gek_m(\xi_0)}\right]+$$
$$\frac{(x^2+y^2)\left(x^2\frac{\varepsilon_0}{\varepsilon_1}+y^2\right)}{x^4y^4}R^*{}_m(\alpha^*{}_{rs},\delta^*{}_{ms})Q^*{}_m\left(\beta^*{}_{rs},X^*{}_{ms}\right)=0 \qquad (2.45)$$

where $R^*{}_m(\alpha^*{}_{rs},\delta^*{}_{ms}), Q^*{}_m\left(\beta^*{}_{rs},X^*{}_{ms}\right)$ are calculated similarly to $R_m(\alpha_{rs},\delta_{ms}), Q_m(\beta_{rs},X_{ms})$ which were evaluated previously for ${}_eHE_{mn}^{(1)}$

For ${}_oHE_{mn}^{(1)}$ the transcendental characteristic equation is

$$\left[\frac{1}{x^2}\frac{Se'_m(\xi_0)}{Se_m(\xi_0)}+\frac{1}{y^2}\frac{Gek'_m(\xi_0)}{Gek_m(\xi_0)}\right]\left[\frac{1}{x^2}\frac{Ce'_m(\xi_0)}{Ce_m(\xi_0)}+\frac{1}{y^2}\frac{\varepsilon_0}{\varepsilon_1}\frac{Fek'_m(\xi_0)}{Fek_m(\xi_0)}\right]+$$
$$\frac{(x^2+y^2)\left(x^2\frac{\varepsilon_0}{\varepsilon_1}+y^2\right)}{x^4y^4}R_m(\alpha_{rs},\delta_{ms})Q_m(\beta_{rs},X_{ms})=0 \qquad (2.46)$$

For ${}_oHE_{mn}^{(0)}$ the transcendental characteristic equation is

$$\left[\frac{1}{x^2}\frac{Se'_m(\xi_0)}{Se_m(\xi_0)}+\frac{1}{y^2}\frac{Gek'_m(\xi_0)}{Gek_m(\xi_0)}\right]\left[\frac{1}{x^2}\frac{Ce'_m(\xi_0)}{Ce_m(\xi_0)}+\frac{1}{y^2}\frac{\varepsilon_0}{\varepsilon_1}\frac{Fek'_m(\xi_0)}{Fek_m(\xi_0)}\right]+$$
$$\frac{(x^2+y^2)\left(x^2\frac{\varepsilon_0}{\varepsilon_1}+y^2\right)}{x^4y^4}R^*{}_m(\alpha^*{}_{rs},\delta^*{}_{ms})Q^*{}_m\left(\beta^*{}_{rs},X^*{}_{ms}\right)=0 \qquad (2.47)$$

2.2.5. Important notes in Yeh's analysis

Comparing the dispersion relations between the modes ${}_eHE_{mn}^{(1)}$ and ${}_eHE_{mn}^{(0)}$ and between ${}_oHE_{mn}^{(1)}$ and ${}_oHE_{mn}^{(0)}$, it can be noticed that the only difference lays in the products $R_m(\alpha_{rs},\delta_{ms})Q_m(\beta_{rs},X_{ms})$ and $R^*{}_m(\alpha^*{}_{rs},\delta^*{}_{ms})Q^*{}_m\left(\beta^*{}_{rs},X^*{}_{ms}\right)$. Except

for the case when $\xi_0 = \infty$, these products do not coincide numerically. Nevertheless, there is a region when $m = 1$ and $n = 1$, where the two products' values are almost identical. In that region the modes ${}_eHE_{mn}^{(1)}$ - ${}_eHE_{mn}^{(0)}$, and ${}_oHE_{mn}^{(1)}$ - ${}_oHE_{mn}^{(0)}$ could be considered degenerate, sharing the same propagation constant.

When it comes to the numerical analysis of the dominant modes, and especially the solutions of the characteristic equations, it has been shown that the constants (i.e. $Q_m(\beta_{rs}, X_{ms}), R_m(\alpha_{rs}, \delta_{ms})$ for ${}_eHE_{mn}^{(1)}$) involved in the solutions are given by sets of infinite determinants. For these determinants, the method of successive approximations is used. For a value of ξ_0 close to 3, eccentricity is reduced and the rod becomes more similar to a cylinder of circular cross section. It has been numerically estimated that for such a case of small eccentricity, less terms of expansions are needed to determine the value of constants $Q_m(\beta_{rs}, X_{ms}), R_m(\alpha_{rs}, \delta_{ms})$ (for ${}_eHE_{mn}^{(1)}$) and the problem becomes simplified by using a "3-term approximation" [33]. However, for eccentricity values equivalent to a flatter elliptical cross-section, then the constants' product becomes significantly prevalent requiring the involvement of more computations and the 3-level approximation is no longer sufficient in terms of accuracy. The method proposed and used in Yeh's analysis is limited to values of $\infty \leq \xi_0 \leq 0.5$.

C. Yeh in his analysis proceeds to determine the cutoff frequencies of the dominant modes, even and odd alike. The analysis concludes that in the case of the elliptical waveguide, the modes ${}_eHE_{mn}^{(1)}$ and ${}_oHE_{mn}^{(1)}$ constitute the only non-degenerate modes and have no cutoff frequencies [33]. As the ellipticity of the dielectric rod's cross-section increases (the elliptical cross-section becomes flatter), x moves towards zero with a slower pace. In relation to the rest of the modes, the cutoff frequencies become higher as the elliptical cross-section of the rod flattens.

2.3. Elliptical fibers' preservation of polarization

R.B. Dyott's contribution to the study of elliptical fibers is substantial while his analysis on their properties has been often used as a basis for many recent related studies. Dyott's theoretical analysis is highly based on Yeh's analysis for the derivation of the wave equations and through the boundary conditions, the estimation of the ${}_eHE_{mn}$ and ${}_oHE_{mn}$ modes. Dyott's research was expanded to the investigation and definition of significant properties of elliptical core fibers; among those, the current

chapter will focus on the presentation of birefringence and the preservation of polarization.

Elliptical fibers' ability to retain polarization constitutes a key feature that renders them an important tool for optical interferometers and other applications. In Dyott's research on polarization preservation in elliptical fibers [29], it is noted that in fibers with broad core-cladding index differences around $7*10^{-2}$ and with ellipticity a/b ratio above the middle range ($a/b \geq 2.5$), the polarization retaining properties are formidable. In waveguides with similar characteristics it is estimated that intermodal coupling is also reduced to values below -40 dB (for a full turn in a dielectric rod of 2mm diameter). A small pitch of 0.75mm, in a presented beat pattern amongst fundamental modes, is demonstrated as an indicator of successful preservation of polarization.

It must be noted that in order to obtain the characteristics of the mode propagation in elliptical fibers, Dyott et al. have constructed a computer based solution of Yeh's analysis. This solution is used to determine the specific conditions under which elliptical fibers with the pre-mentioned characteristics ($\Delta\beta, a/b$) manage to preserve polarization. An interesting result was obtained from plotting the difference in group velocities between the two modes, where group velocity is given by $v_g = {}^{c}/_{n_g}$, c expressing the speed of light in free space and n_g being a group index (Figure 2-2).

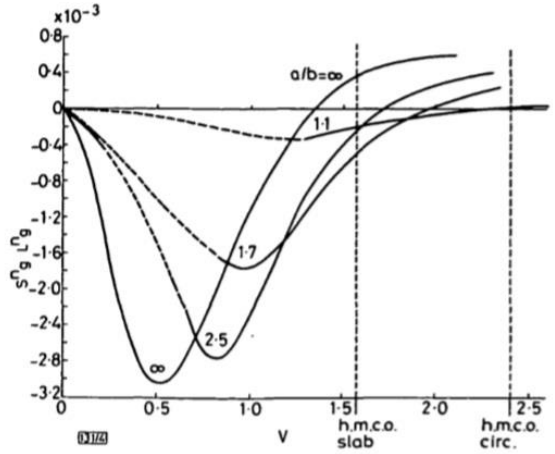

Figure 2-3 Difference in the group indices of the two fundamental modes [29]

It was found that there exists a critical value of ellipticity for which the group velocity difference becomes zero at the higher-mode cutoff point. In another plot where the

elliptical fiber normalized frequency V is plotted against ellipticity a/b at $\Delta n_g = 0$ (Figure 2-3), it is evident that the critical point is found at $a/b = 1.8$.

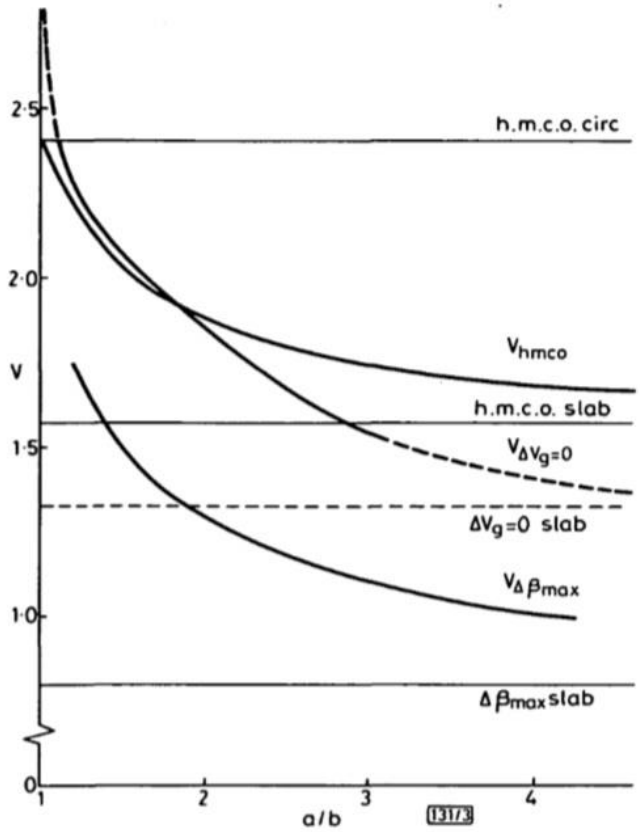

Figure 2-4 Propagation relationships in elliptically cored fiber [29]

It is therefore expected that an elliptical waveguide could be designed with ellipticity higher than 1.8 and be operated at a V value where the group velocities coincide but the difference in phase velocities is sufficient to preserve polarization [29]. Dyott proposed that such a single-mode elliptical core fiber might even be used for telecommunications, which eventually became impossible due to increased attenuation. Nevertheless, elliptical fibers with these characteristics found immediate use in fiber sensors.

2.4. Birefringence

Given a wave propagating inside an elliptical fiber, the propagation constants of the ${}_0HE_{11}$ and ${}_eHE_{11}$ modes are decoupled and this phenomenon is called Birefringence. Birefringence is numerically described as the difference between the normalized propagation constants $\Delta\bar{\beta} = {}_0\bar{\beta} - {}_e\bar{\beta}$. Its' value is therefore dependent on the normalized frequency V and on the difference Δn between the refractive indices in the

core and the cladding. Initially all efforts to estimate birefringence in elliptical fibers were focused on determining the effects of fiber cores whose cross section was deviating from circularity. Such were the cases of fiber systems where differential group delay had a negative effect on bandwidth, and of sensor applications requiring complete absence of birefringence (i.e. in sensors based on Faraday rotation). Adams et al. [35] provides a brief listing of relevant works including Ramaswamy et al. [28], Schlosser [27], Marcuse [36], Snyder and Young [37], using a simplification of Yeh's analysis [33]. Calculations of birefringence based on each of the above analyses exhibit wide variation both in terms of magnitude and in the point where birefringence is maximum. In all analyses, birefringence appears to be proportional to the square of the index difference $(\Delta n)^2$. This leads to the conclusion that, for elliptical fiber applications requiring high birefringence to maintain polarization, a broad index difference between core and cladding is necessary.

2.5. Usability and Applications of Elliptical Fibers

During the early developments in elliptical fibers it was considered that the polarization maintenance property of the propagating modes in birefringent optical fibers might be useful for coherent optical systems which were intensely studied in the 1990s. High birefringence fibers were therefore manufactured either using elliptical shaped core, or using stress elements around the core creating inherent birefringence due to stress, (PANDA fibers). It was generally accepted later, that the relatively high losses of birefringent fibers, when compared to ordinary circular core optical fibers, led researchers to direct the focus of research on birefringent optical fibers for sensor applications and fiber optic devices; therefore circular core fibers progressed to lead on the telecommunications market. Elliptical core optical fibers find themselves today in navigation systems, as part of gyroscopes, and other military and sensor applications. Specifically, polarization-holding fibers have been long used in optical interferometers but the method used for decoupling the light paths within, was based on shifting the index through application of stress.

The use of elliptical fibers as a means to split the fundamental mode in to two distinct orthogonally polarized modes has significant advantages over the stress-induced method:

1. Elliptical fibers are less complicated to manufacture

2. Avoiding stress reduces pressure and heat sensitivity
3. Higher order modes propagating in elliptical fibers are azimuthally more stable than those inside cylindrical fibers, facilitating the creation of over-moded fiber sensors [27].

Basic applications of the elliptical fiber will be presented in the following section.

2.6. Applications of elliptical core fibers

As mentioned in chapter 1, optical fibers with elliptical core hold distinct properties compared to their cylindrical siblings; these properties include polarization retaining ability and increased birefringence, reduced complexity in manufacturing, reduced pressure and heat sensitivity and enhanced azimuthal stability for higher order modes. Thanks to these properties elliptical fibers are being used in various applications mostly related to fiber sensors but also to optical communication systems. Further, the list of applications is presented beginning with a communication related application.

2.6.1. Dispersion readjustment in communication fibers

Elliptical fibers can be used as a means for fixing dispersion in fiber waveguides. As described in the introduction, the BL product is an essential measure of efficiency in communication systems, and optical systems have achieved considerably high BL by increasing repeater spacing. The distance between repeaters though has come with a toll, since, as the distance increases, so does the effect of dispersion. Nevertheless, the effect of dispersion can be counterbalanced with a negative dispersion produced by increasing group velocity via increasing wavelength of an interposed over-moded elliptical fiber. The sequence producing the counterbalancing dispersion can be described as follows: while moving closer to the cutoff, the evanescent field becomes broader and the power shifts to the part of the cladding with lower refractive index. At this point, rising wavelength is coupled with rising group velocity of the primary higher order modes. This procedure has been described experimentally and proposed as an application by Poole et al. [38]. A schematic representation is shown in fig. 6.1

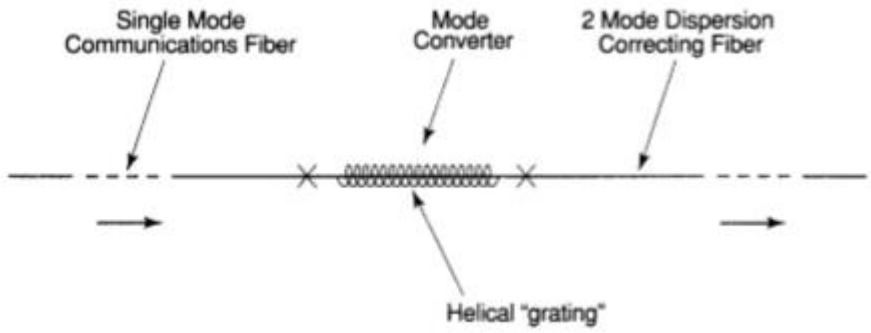

Figure 2-5 Schematic representation of correcting dispersion via overmoded elliptical fiber [39]

2.6.2. Optical Gyroscopes

In Fiber-Optic Gyroscopes (FOGs) a single light path is split into a couple of paths propagating in opposite directions following a circular loop before they reunite back into a single path. A rotation of the loop around its axis causes a phase shift between the split paths of opposite directions. In gyroscope implementations using single mode fibers there are two prominent problems: unwanted azimuthal changes dependent on polarization, caused by bending stress of the fiber, and unwanted temperature changes affecting birefringence. The fact that optical gyroscopes are practically functioning in a wide range of temperatures from -55˚C to 85 ˚C makes it even more difficult to stabilize polarization and birefringence [39]. These problems are tackled with the use of polarizers that suppress unwanted polarization along with polarization-retaining fibers used together with couplers and splices. At this point the use of elliptical core fibers offers significant advantages. Most importantly the effect of temperature changes on birefringence is reduced to 1/7 compared to the effect in stress-induced fibers. Moreover, the use of an elliptical core D-fiber provides the ability to avoid the use of splices further reducing losses.

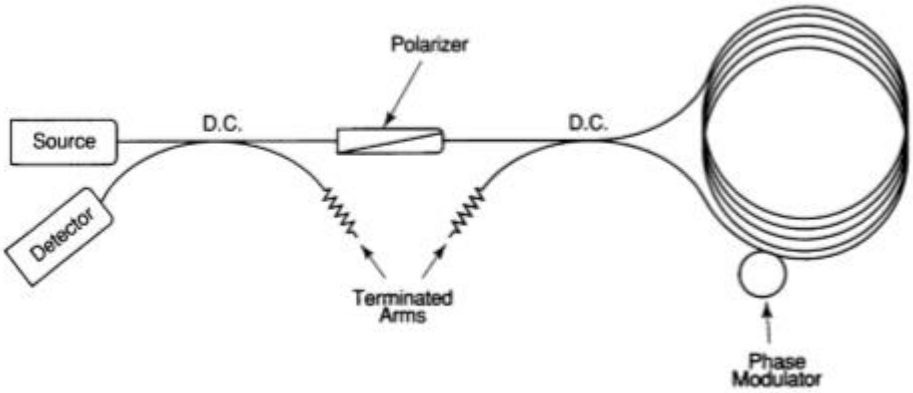

Figure 2-6 Schematic representation of fiber-optic gyroscope [39].

2.6.3. Higher-order-based sensors

Elliptical fibers can be used to create sensing interferometers. Such an application would utilize either of the fundamental even and odd elliptical modes ${}_oHE_{11}$, ${}_eHE_{11}$, together with the first LP_{11}, in a way that the modes interfere when a source is applied. Therefore, changes in pressure, caused by fiber stress or acoustic waves, as well as variations in temperature result in variations of the difference between mode propagation constant [40]. The application of a remote voltage sensor has also been proposed based on double-mode elliptical fibers [41].

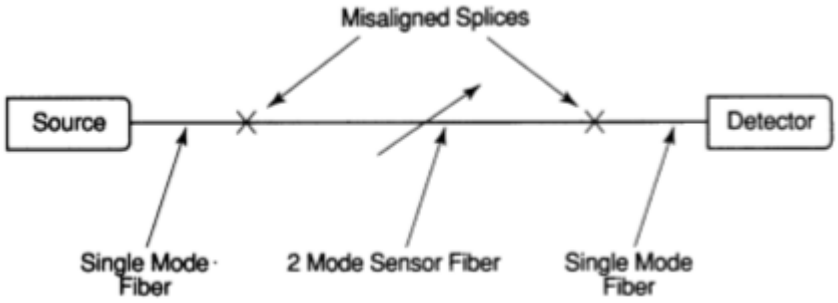

Figure 2-7 Fiber sensor with overmoded elliptical fiber [39]

2.6.4. E-fiber gratings

Gratings are periodical variations in fiber properties (i.e. refractive index). Such variations can be applied on fibers through various methods including applied pressure and exposure to radiation. Elliptical fibers with gratings can be used as sensors or laser tuners.

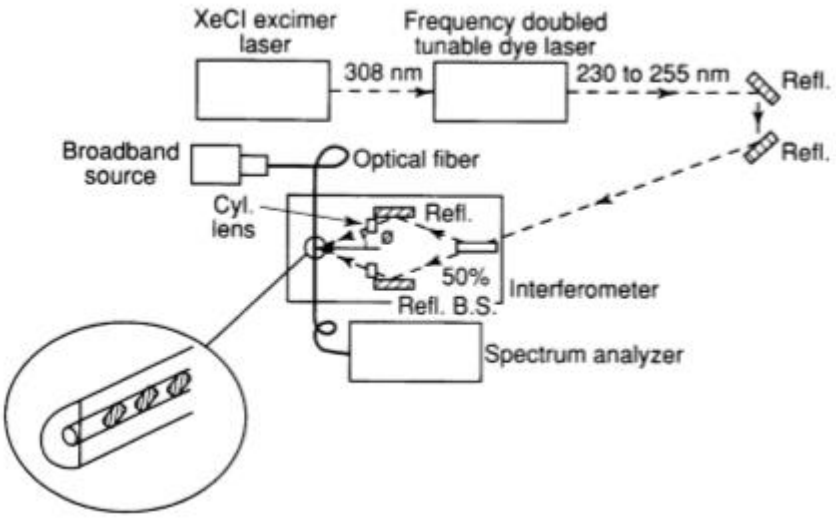

Figure 2-8 Technical representation of grating formation [39]

2.6.5. Acoustic wave coupling

In elliptical core D-fibers, acoustic waves can be used to facilitate mode coupling. It has been experimentally proved [42] that acoustic waves travelling along the D-fiber, interact with the even and odd fundamental modes in a way that the modes are coupled with each other. The frequency, the direction of the wave and the angle of the applied stress over the axis of core's ellipsis, play a significant role on optimizing the mode coupling.

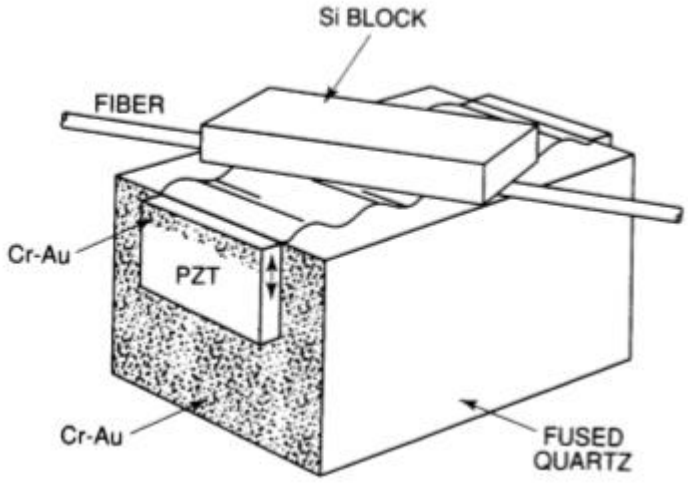

Figure 2-9 D-fiber coupling with surface acoustic wave [39]

2.6.6. Optical Kerr effect

In the optical Kerr effect, an intense optical-electrical field [39] causes a shift in the refractive index which in turn results to a change in the birefringence of the fiber. The Kerr effect can be used in elliptical fibers to locate occurrences of mode coupling along the fibers, as anomalies caused by external factors (i.e. pressure). In such cases, a combination of a high-power pulse and a probe signal travelling the opposite direction, is applied. The resulting changes in couplings on the probe signal and the local anomaly are used together with the timing of the pulse to estimate the position of the anomalies [43]. The optical Kerr effect applied on double mode elliptical fibers can be used as a switch implementation [44]. Another optical Kerr implementation is that of an optical amplifier where a polarizer is used along with a birefringent elliptical fiber, in order to convert a rotation of polarization into amplitude modulation. The modulation is further translated to amplification and change in frequency [45].

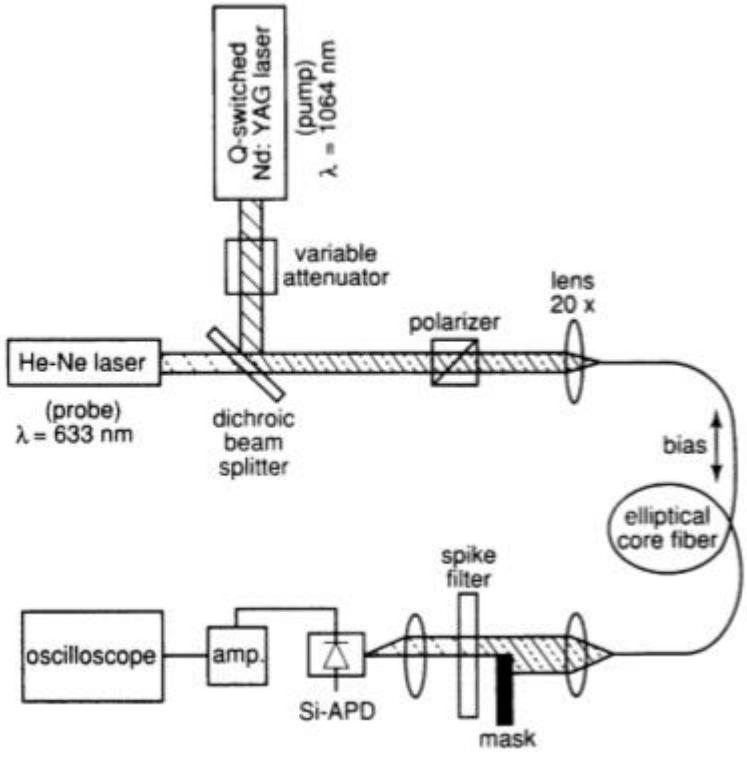

Figure 2-10 Optical switch utilizing Kerr effect [39]

2.6.7. Current sensors

Single mode fibers whose polarization has been rotated have been proposed as means to measure current in conductors. The problem with such implementations is the

inability to achieve the required conditions for coupling the HE_{11}mode due to imperfections of the circular core structure. A solution has been proposed [46] involving an elliptical fiber with strong birefringence that can produce a periodical field with transverse modes in phase. A technique known as Broadbanding can be then used to synchronize the periodical field with the beat length of the fiber in order to achieve polarization rotation.

3 CHAPTER 3

Elliptical core fibers analysis using RTL method – the harmonics method

3.1 The elliptical fiber problem

Yeh's analysis of the propagation phenomena in elliptical waveguides focused on the simple step refractive index profiles. The transcendental equations and the mode field component solutions derived are known to involve Mathieu Functions. Computation of Mathieu Functions used to be a hard task ensuring convergence, but naturally this is easier to achieve with the computing processing power available, today. However, when we consider realistic and non-step index refractive index profiles in the fiber core, the numerical problem is far more complex, and efficient numerical techniques are sought after. Dealing with complexity was the first incentive, and in this aspect the contribution of this study has strong advantages. Through consistent research of the now established technique of transverse resonance [8][10], based on transmission line principles, for circular core fibers, it has been proved that this approach to solving electromagnetic problems is not only intuitive and based on well understood electrical engineering principles, but also very powerful and capable of dealing with many hard problems; not only forward, but also inverse [10]. The other incentive for the analysis in the current chapter was to apply and test the same principles using the elliptical coordinate system. In [47], a first attempt was made towards solving this problem using transmission lines in elliptical coordinates, but the solution was not general. The research presented in the current thesis provides a general solution and expands earlier work by presenting numerical examples of graded index profiles and mode cutoffs.

This chapter describes the analysis and development of a method for solving the optical properties of elliptical core optical fibers of arbitrary refractive index profile using Transmission Line Principles without employing Mathieu Functions. The chapter is organized as follows: it starts with the introduction of the elliptic cylindrical system, followed by an analysis of the EM waves in the elliptical fibers. The mathematical solution to the problem leads to the appearance of factors referred to as harmonics. The chapter continues with the examination of the problem, first, considering no harmonics and then with the full consideration of harmonic analysis. Then follows the examination

of the boundary impedance of elliptical fibers. Example computations are further provided for comparison.

3.2. Maxwell's equations in elliptical coordinate system

The following elliptic coordinate system is used matching the cross section of the elliptical fiber. We use

$$\boldsymbol{W} = \theta + j\varphi, \boldsymbol{Z} = c\cosh(\boldsymbol{W}) = x + jy = c\cosh\theta\cos\varphi + j\sinh\theta\sin\varphi$$

where $\boldsymbol{Z}$ and $\boldsymbol{W}$ are complex variables on the plane (x, y) and c is the semi focal distance of the ellipses

$$\text{Thus } \begin{cases} x = c\sinh\theta\cos\varphi \\ y = c\cosh\theta\sin\varphi \end{cases} \tag{3.1}$$

The function derives from the conformal mapping transformation:

$$h_{(\theta,\varphi)} = \left|\frac{\partial w}{\partial z}\right| = |c\sin h\,\theta\cos\varphi + jc\cos h\,\theta\sin\varphi|$$

From the above relation, we obtain

$$h^2_{(\theta,\varphi)} = \frac{c^2}{2}(\cosh 2\theta - cos2\,\varphi)$$

In the elliptic cylindrical system, Figure 3-1, each θ constant describes an ellipse, with semimajor axis $c\cosh\theta$ and semiminor axis $c\sinh\theta$ matching the fiber's cross section and for φ constant a hyperbola, of the same foci define any point at some complex point $\boldsymbol{Z}$. The ellipses of constant θ are normal to the hyperbolae of constant φ [47].

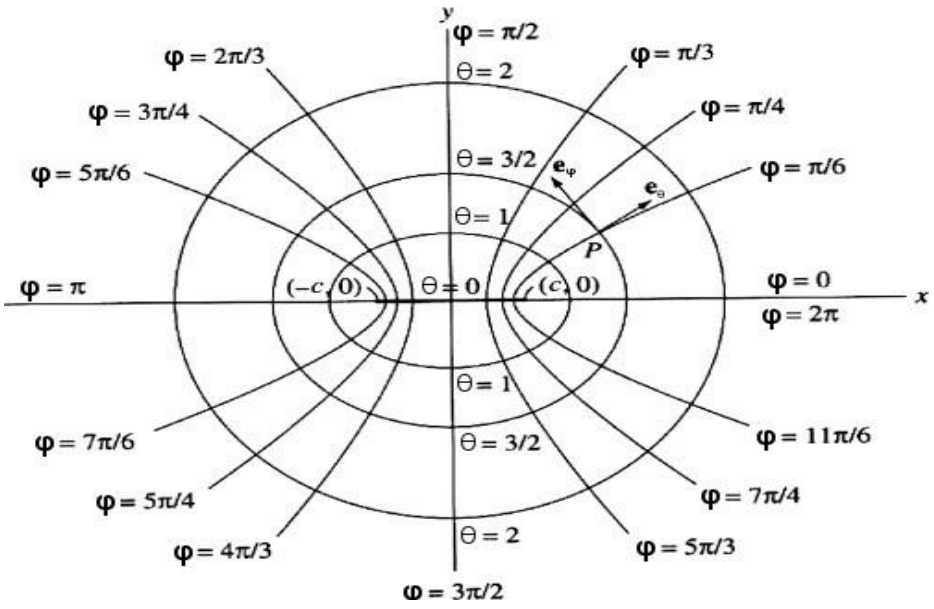

Figure 3-1 Elliptic coordinate system θ+jφ

From Figure 3-1 it is clear that coordinate θ, traces the ellipse of the waveguide and φ deals with the angular degree of freedom of the elliptical coordinate system. As the ellipticity increases, θ tends to zero, and circular cross section fibers have θ tending to infinity, as in Figure 3-1.

Maxwell's equations (for $\frac{\partial}{\partial t} = j\omega$) expressed on a set of elliptic cylindrical coordinates (θ, φ,z), can be written for an infinitesimal small layer of thickness Δθ, for which it can be safely assumed that the refractive index n can be considered constant [47].

$$\nabla \times \vec{E} = -j\omega\mu_0\vec{H}\begin{cases} \frac{\partial E_z}{\partial \varphi} - \frac{\partial (hE_\varphi)}{\partial z} = -j\mu_0\omega(hH_\theta) \\ \frac{\partial (hE_\theta)}{\partial z} - \frac{\partial E_z}{\partial \theta} = -j\mu_0\omega\left(hH_\varphi\right) \\ \frac{\partial (hE_\varphi)}{\partial \theta} - \frac{\partial (hE_\theta)}{\partial \varphi} = -j\mu_0\omega(h^2H_z) \end{cases} \tag{3.2}$$

$$\nabla \times \vec{H} = jn^2\varepsilon_0\omega\vec{E}\begin{cases} \frac{\partial H_z}{\partial \varphi} - \frac{\partial (hH_\varphi)}{\partial z} = jn^2\varepsilon_0\omega(hE_\theta) \\ \frac{\partial (hH_\varphi)}{\partial z} - \frac{\partial H_z}{\partial \theta} = jn^2\varepsilon_0\omega\left(hE_\varphi\right) \\ \frac{\partial (hH_\varphi)}{\partial \theta} - \frac{\partial (hH_\theta)}{\partial \varphi} = jn^2\varepsilon_0\omega(h^2E_z) \end{cases} \tag{3.3}$$

Where in elliptic cylindrical coordinate systems, the scale factor h, is

$h = \sqrt{\ h^2(\theta,\varphi)}\ and\quad h^2(\theta,\varphi) = \frac{c^2}{2}(\cosh 2\theta - cos2\,\varphi)$. The mean value of $h^2(\theta,\varphi)$ along φ is given by: $h_0^2(\theta) = \frac{c^2}{2}\cosh 2\theta$, thus $\frac{\partial h_0^2(\theta)}{\partial\theta} = c^2 \sinh 2\theta$. Thus

$h^2\,(\varphi,\theta) = h_0^2(\theta) - \frac{c^2}{2}(\,cos2\,\varphi) = h_0^2(\theta) - \frac{c^2}{4}(e^{j2\varphi} + e^{-j2\varphi})$.

From this point on we define $h_0^2(\theta) = \ h_0^2$

Considering an exponential dependence along the propagation axis z, the field components will be expressed in terms of $A^{j\beta z}$. Using the Fourier Transform along φ with integer wave numbers *l*, the following is obtained:

$$\begin{cases} jl\overline{E}_z - j\beta\left(\overline{hE_\varphi}\right) = -j\mu_0\omega\left(\overline{hH_\theta}\right) \\ j\beta\overline{(hE}_\theta) - \frac{\partial\overline{E_z}}{\partial\theta} = -j\mu_0\omega(\overline{hH_\varphi}) \\ \frac{\partial(\overline{hE_\varphi})}{\partial\theta} - jl(\overline{hE_\theta}) = -j\mu_0\omega(h^2 \otimes \overline{\mathrm{H_z}}) \end{cases} \tag{3.4}$$

$$\begin{cases} jl\overline{H}_z - j\beta\left(\overline{hH_\varphi}\right) = jn^2\varepsilon_0\omega(\overline{hE_\theta}) \\ j\beta\overline{(hH}_\theta) - \frac{\partial\overline{H_z}}{\partial\theta} = jn^2\varepsilon_0\omega(\overline{hE_\varphi}) \\ \frac{\partial(\overline{hH_\varphi})}{\partial\theta} - jl(\overline{hH_\theta}) = jn^2\varepsilon_0\omega(h^2 \otimes \overline{\mathrm{E_z}}) \end{cases} \tag{3.5}$$

The functions $\{\overline{E}_z\,,\left(\overline{hE_\varphi}\right),\left(\overline{hE_\theta}\right),\overline{H}_z\,,\left(\overline{hH_\varphi}\right),(\overline{hH_\theta})\}$ are the (partial) Fourier Transforms of the respective functions over φ with an integer wave number l. The Fourier Transform of the function product h^2E_z, represents a convolution $h^2 \otimes \overline{\mathrm{E_z}}$ which is calculated as follows

$$\begin{aligned} \left(\overline{h^2E_z}\right) = & \int_{-\infty}^{\infty} h^2(\theta,\varphi)E_z(\theta,\varphi)\exp(jl\varphi)\,d\varphi \\ & = h_0^2(\theta)\overline{E}_z \\ & - \frac{c^2}{4}\int_{-\infty}^{\infty} E_z(\theta,\varphi,\beta)\exp(j(l+2)\varphi)\,d\varphi \\ & - \frac{c^2}{4}\int_{-\infty}^{\infty} E_z(\theta,\varphi,\beta)\exp(j(l-2)\varphi)\,d\varphi \end{aligned}$$

$$= h_0^2(\theta)\overline{E}_z - \frac{c^2}{4}\left[\overline{E_z}(l+2) + \overline{E_z}(l-2)\right]$$

$$= h_0^2(\theta)\overline{E}_z - \frac{c^2}{4}[\Phi_2] \tag{3.6}$$

where $\Phi_2 = \overline{E_z}(l+2) + \overline{E_z}(l-2)$

In the same way

$$\left(\overline{h^2 H_z}\right) = h_0^2(\theta)\overline{H}_z - \frac{c^2}{4}\left[\overline{H_z}(l+2) + \overline{H_z}(l-2)\right]$$

$$= h_0^2(\theta)\overline{H}_z - \frac{c^2}{4}[\Phi_1] \tag{3.7}$$

Where $\Phi_1 = \overline{H_z}(l+2) + \overline{H_z}(l-2)$

Taking into consideration that: $\omega\mu_0 = z_0 k_0$and $\omega\varepsilon_0 = k_0/z_0$, where $z_0 = \sqrt{\frac{\mu_0}{\varepsilon_0}} = 120\pi$ and $k_0 = \omega\sqrt{\mu_0\varepsilon_0} = \frac{2\pi}{\lambda}$, we begin the transformation into transmission lines using the following set of four functions I_M, I_E, V_M, V_E defined:

$$\begin{cases} I_M = -j\left(\overline{hH_\theta}\right) = j\left(l\overline{E_z} - \beta\left(\overline{hE_\varphi}\right)\right) \\ I_E = n^2\left(\overline{hE_\theta}\right) = \left(l\overline{H_z} - \beta\left(\overline{hH_\varphi}\right)\right) \\ V_M = \frac{l\left(\overline{hE_\varphi}\right) + \beta h_0^2(\theta)\overline{E}_z}{jF} \\ V_E = \frac{l\left(\overline{hE_\varphi}\right) + \beta h_0^2(\theta)\overline{E}_z}{F} \end{cases} \tag{3.8}$$

where $F = F_l = l^2 + \beta^2 {h_0}^2$

All the magnetic field components have been multiplied by z_0 in order for the couples $V_M, V_E and I_M,\ I_E$ to have the same units in MKSA. Also the symbol of wave number β in (3.8) and for the rest of the analysis is normalized and represents the ratio β/k_0 The symbol of the semi axis of the ellipses c represents the product $k_0 c$, thus $\beta\ and\ h_0^2(\theta)$ are numbers without units [47].

Using the new functions I_M, I_E, V_M, V_E it can be proved through algebraic analysis (see Appendix B) that the differential equations (3.4), (3.5) derived by the Maxwell equations are equivalent to the following two sets of differential equations representing

two interlinked transmission lines of infinitesimal length $\Delta\theta$ [47].

$$\begin{cases} \frac{\partial V_M}{\partial \theta} = -\frac{\gamma^2}{jF} I_M - jMI_E - \frac{n^2 l}{F}\frac{c^2}{4}[\Phi_2] \\ \frac{\partial I_M}{\partial \theta} = -jFV_M + \beta\frac{c^2}{4}[\Phi_1] \end{cases} \tag{3.9}$$

$$\begin{cases} \frac{\partial V_E}{\partial \theta} = -\frac{\gamma^2}{jn^2F} I_E - jMI_M + jl\frac{c^2}{4F}[\Phi_1] \\ \frac{\partial I_E}{\partial \theta} = -jn^2FV_E + jn^2\beta\frac{c^2}{4}[\Phi_2] \end{cases} \tag{3.10}$$

with

$$\begin{cases} \gamma^2 = l^2 + (\beta^2 - n^2){h_0}^2 \\ h_0^2 = \frac{c^2}{2}\cosh 2\theta \\ \frac{\partial h_0^2}{\partial \theta} = c^2 \sinh 2\theta \\ F = F_l = l^2 + \beta^2{h_0}^2 = \gamma^2 + n^2{h_0}^2 \\ M = \beta l \frac{\partial {h_0}^2}{\partial \theta}/F^2 \end{cases} \tag{3.11}$$

Using algebraic relations (3.8) it can be easily proved that the Fourier Transforms of the Electro Magnetic field components, along z and φ axis, can be calculated by the formulae

$$\begin{cases} \overline{H_z} = {lI_E}/{F} + j\beta V_M \\ \overline{E_z} = {-jlI_M}/{F} + \beta V_E \end{cases} \tag{3.12a}$$

$$\begin{cases} h\overline{H_\varphi} = jlV_M + \frac{\beta h_0^2}{F_l} I_E \\ h\overline{E_\varphi} = \frac{j\beta h_0^2}{F_l} I_M + lV_E \end{cases} \tag{3.12b}$$

3.3. Even and odd modes

Beginning with the analysis of even modes we define a new $U_S = V_M + nV_E$ *and* $I_S = I_M + \frac{I_E}{n}$. It can be proved that the above two interlinked transmission lines differential equations (3.9) and (3.10) will become a set of two differential equations representing one new transmission line as follows

$$\begin{cases} \frac{\partial U_S}{\partial \theta} = -\frac{\gamma^2 - nMF}{jF} I_S + \frac{nlc^2}{4F}[j\Phi_1 - n\Phi_2] \\ \frac{\partial I_S}{\partial \theta} = -jFV_S - \frac{j\beta c^2}{4}[j\Phi_1 - n\Phi_2] \end{cases} \tag{3.13}$$

where

$$\begin{cases} \Phi_1 = H_z^{l-2} + H_z^{l+2} = \frac{l-2}{F_{l-2}} I_E^{l-2} + j\beta V_M^{l-2} + \frac{l+2}{F_{l+2}} I_E^{l+2} + j\beta V_M^{l+2} \\ \Phi_2 = E_z^{l-2} + E_z^{l+2} = -j\frac{(l-2)}{F_{l-2}} I_M^{l-2} + \beta V_E^{l-2} - j\frac{(l+2)}{F_{l+2}} I_M^{l+2} + \beta V_E^{l+2} \end{cases} \tag{3.14}$$

The final terms in the equations (3.9) represent the entanglement of the lth harmonic with the $(l+2)th$ and $(l-2)th$ harmonics (along the angular direction φ). Due to the fact that M takes the sign of l because all the remaining factors are positive, it turns out that positive l instances are representing the HE modes while negative l instances are representing the EH modes.

We can now consider the more general case where the effect of harmonics cannot be ignored. This is the case where either the refractive index difference Δn is high (higher than 1/1000) or the elliptic eccentricity is high (higher than 1.5). In order to examine this case, we calculate Φ1 and Φ2 using eqn. (3.14). Again, we define $V_S = jU_S$, $I_S = I_S$ (all the Vs are defined as imaginary functions in order to have real coefficients in the equations). We then derive the following equations

$$\begin{cases} \frac{\partial V_s^l}{\partial \theta} = -\frac{\gamma^2 - nMF}{F} I_s^l - \\ \frac{lqn}{F}\left[\frac{(l-2)}{F_{l-2}} I_s^{l-2} + \frac{(l+2)}{F_{l+2}} I_s^{l+2}\right] - \frac{q\beta l}{F}[V_s^{l-2} + V_s^{l+2}] \\ \frac{\partial I_s^l}{\partial \theta} = -FV_s^l + q\beta\left[\frac{(l-2)}{F_{l-2}} I_s^{l-2} + \frac{(l+2)}{F_{l+2}} I_s^{l+2}\right] \\ + \frac{q\beta^2}{n}[V_s^{l-2} + V_s^{l+2}] \end{cases} \tag{3.15}$$

where $q = nc^2/4$. It becomes clear that every mode order l, is entangled with orders $l+2$ and $l-2$. From the equation set (3.15) we can generate an infinite set of equations by replacing l with $l \pm 2$. Consequently, we can write (3.15) as a general matrix equation via a parameter which takes care of the order of harmonics and the coefficients of the harmonic values and becomes $l = l \pm k$, $k = 2, 4, 6, ...$

$$\frac{d}{d\theta} V_s^{l+k} = \left[X_{l,k}\right][V_s^{l+k}, V_s^{l+2+k}, V_s^{l-2+k}] \tag{3.16a}$$

$$\frac{d}{d\theta} I_s^{l+k} = \left[Y_{l,k}\right][I_s^{l+k}, I_s^{l+2+k}, I_s^{l-2+k}] \tag{3.16b}$$

When considering the effect of higher harmonics around the harmonic l, i.e. the harmonics $\ldots l+2,\ l+4, l+6\ and\ l-2, l-4, l-6 \ldots$ they result in a set of homogeneous differential equations for the functions $\ldots V_s^{l+6}, I_s^{l+6}, V_s^{l+4}, I_s^{l+4}, V_s^{l+2}, I_s^{l+2},\ V_s^{l}, I_s^{l},\ V_s^{l-2}, I_s^{l-2},\ V_s^{l-4}, I_s^{l-4},\ V_s^{l-6}, I_s^{l-6} \ldots$. The number of the equation coefficients involved in the computation depends on the accuracy required from the system and the number of harmonics involved.

The general matrix $\left[A_{l,k}\right]$ of coefficients from the equations (3.16) $\ldots l+2,\ l+4, l+6\ and\ l-2, l-4, l-6 \ldots$, holds dimensions 14×14 and its elements are in the order shown in Table 3-1. We observe that the diagonal elements of the matrix, all equal to zero. Furthermore, as seen in the table, the parameters k=0, ± 2, ± 4, ± 6… determine the horizontal location of the elements of the matrix. k combined with l, give the general form of $[A(l,k)\ ]$ with coefficients as follows

$\Theta k = -\frac{\gamma_{l+k}^2 - nM_{l+k}F_{l+k}}{F_{l+k}}, \quad \Lambda_k = -F_{l+k},$

$\Lambda 1_k = \frac{-q\beta(l+k)}{F_{l+k}}, \Lambda 2_k = \frac{-qn(l+k)(l+2+k)}{F_{l+2+k}F_{l+k}},$

$\Lambda 3_k = \frac{q\beta^2}{n}, \qquad \Lambda 4_k = \frac{\beta q(l+2+k)}{F_{l+2+k}}.$

$\Lambda 5_k = \frac{-qn(l+k)(l-2+k)}{F_{l-2+k}F_{l+k}}$

$\Lambda 6_k = \frac{\beta q(l-2+k)}{F_{l-2+k}}$

We also notice that

$$F_{l+2+k} = (l+2+k)^2 + \beta^2 {h_0}^2, \gamma_{l+2+k}^2 = (l+2+k)^2 + (\beta^2 - n^2){h_0}^2$$

$$M_{l+2+k} = \beta(l+2+k)\frac{\partial {h_0}^2}{\partial\theta} / \mathrm{F}_{\mathrm{l+2+k}}^2,\ q = nc^2/4.$$

Similar relations for F, M, γ can be written for $l\ and\ l-2$. Using the above coefficients, we can compute the eigenvalues of matrix $\left[A_{l,k}\right]$ for the elliptical layer $\partial\theta$.

		V_s^{l+6}	I_s^{l+6}	V_s^{l+4}	I_s^{l+4}	V_s^{l+2}	I_s^{l+2}	V_s^{l}	I_s^{l}	V_s^{l-2}	I_s^{l-2}	V_s^{l-4}	I_s^{l-4}	V_s^{l-6}	I_s^{l-6}	
	..	..	..	..	..	..	..	..	..	..	..	..	..	..	..	..
$\frac{\partial}{\partial\theta}V_s^{l+6}$	..	0	Θ_6	$\Lambda 1_{\kappa=6}$	$\Lambda 5_{\kappa=6}$	0	0	0	0	0	0	0	0	0	0	..
$\frac{\partial}{\partial\theta}I_s^{l+6}$	..	Λ_6	0	$\Lambda 3_{\kappa=6}$	$\Lambda 6_{\kappa=6}$	0	0	0	0	0	0	0	0	0	0	..
$\frac{\partial}{\partial\theta}V_s^{l+4}$	..	$\Lambda 1_{\kappa=4}$	$\Lambda 2_{\kappa=4}$	0	Θ_4	$\Lambda 1_{\kappa=4}$	$\Lambda 5_{\kappa=4}$	0	0	0	0	0	0	0	0	..
$\frac{\partial}{\partial\theta}I_s^{l+4}$	..	$\Lambda 3_{\kappa=4}$	$\Lambda 4_{\kappa=4}$	Λ_4	0	$\Lambda 3_{\kappa=4}$	$\Lambda 6_{\kappa=4}$	0	0	0	0	0	0	0	0	..
$\frac{\partial}{\partial\theta}V_s^{l+2}$	..	0	0	$\Lambda 1_{\kappa=2}$	$\Lambda 2_{\kappa=2}$	0	Θ_2	$\Lambda 1_{\kappa=2}$	$\Lambda 5_{\kappa=2}$	0	0	0	0	0	0	..
$\frac{\partial}{\partial\theta}I_s^{l+2}$	..	0	0	$\Lambda 3_{\kappa=2}$	$\Lambda 4_{\kappa=2}$	Λ_2	0	$\Lambda 3_{\kappa=2}$	$\Lambda 6_{\kappa=2}$	0	0	0	0	0	0	..
$\frac{\partial}{\partial\theta}V_s^{l}$	..	0	0	0	0	$\Lambda 1_{\kappa=0}$	$\Lambda 2_{\kappa=0}$	0	Θ_0	$\Lambda 1_{\kappa=0}$	$\Lambda 5_{\kappa=0}$	0	0	0	0	..
$\frac{\partial}{\partial\theta}I_s^{l}$	..	0	0	0	0	$\Lambda 3_{\kappa=0}$	$\Lambda 4_{\kappa=0}$	Λ_0	0	$\Lambda 3_{\kappa=0}$	$\Lambda 6_{\kappa=0}$	0	0	0	0	..
$\frac{\partial}{\partial\theta}V_s^{l-2}$	..	0	0	0	0	0	0	$\Lambda 1_{\kappa=-2}$	$\Lambda 2_{\kappa=-2}$	0	Θ_{-2}	$\Lambda 1_{\kappa=-2}$	$\Lambda 5_{\kappa=-2}$	0	0	..
$\frac{\partial}{\partial\theta}I_s^{l-2}$	..	0	0	0	0	0	0	$\Lambda 3_{\kappa=-2}$	$\Lambda 4_{\kappa=-2}$	Λ_{-2}	0	$\Lambda 3_{\kappa=-2}$	$\Lambda 6_{\kappa=-2}$	0	0	..
$\frac{\partial}{\partial\theta}V_s^{l-4}$	..	0	0	0	0	0	0	0	0	$\Lambda 1_{\kappa=-4}$	$\Lambda 2_{\kappa=-4}$	0	Θ_{-4}	$\Lambda 1_{\kappa=-4}$	$\Lambda 5_{\kappa=-4}$	..
$\frac{\partial}{\partial\theta}I_s^{l-4}$	..	0	0	0	0	0	0	0	0	$\Lambda 3_{\kappa=-4}$	$\Lambda 4_{\kappa=-4}$	Λ_{-4}	0	$\Lambda 3_{\kappa=-4}$	$\Lambda 6_{\kappa=-4}$	..
$\frac{\partial}{\partial\theta}V_s^{l-6}$	..	0	0	0	0	0	0	0	0	0	0	$\Lambda 1_{\kappa=-6}$	$\Lambda 2_{\kappa=-6}$	0	Θ_{-6}	..
$\frac{\partial}{\partial\theta}I_s^{l-6}$	..	0	0	0	0	0	0	0	0	0	0	$\Lambda 3_{\kappa=-6}$	$\Lambda 4_{\kappa=-6}$	Λ_{-6}	0	..
	..	..	..	..	..	..	..	..	..	..	..	..	..	..	..	..

Table 3-1 Even Mode Characteristic Matrix [A_(l, k)]for Elliptical Fiber Layers. (Coefficients of (15, 16))

The squares of the eigenvalues of the set of the simultaneous equations give the respective transmission line characteristics γ_l^2. The minimum squared eigenvalue γ_l^2 can be used for determining the fundamental HE and EH respective elliptical modes for $l = 1$ as well as the TM, TE, respective modes for $l = 0$.

Using the layer eigenvalues, the resulting T-circuits for even modes can be formed using γ_l^2 for the corresponding elliptical layer as shown in Figure 3-2, with $\gamma_l^2$and j$F_l = j(l^2 + \beta^2 {h_0}^2)$

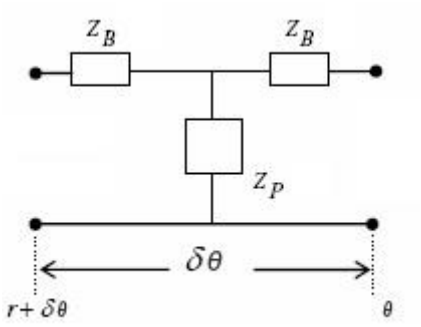

Figure 3-2 Equivalent transmission line circuit of element layer Δθ

$$\begin{cases} Z_B = \gamma_l^2 \Delta\theta/(2jF) \\ Z_P = 1/(jF\Delta\theta) \end{cases} \tag{3.17}$$

Having represented the elliptical thin layer as a T-circuit the series cascade represents successive elliptical thin layers, and we can compute the propagation constants by employing resonance of the assembly.

It is known that elliptical fibers also support odd modes orthogonal to even. This can be derived in a similar manner. From equations (3.9) and (3.10) alternatively we can define parameters

$$V_{SS} = j\left(\frac{V_M}{n} + V_E\right) \qquad I_{SS} = nI_M + I_E \;\; i.e. \;\; I_{SS} = I_S n \qquad V_{SS} = j\frac{V_S}{n}$$

We can in a similar manner as with even modes derive the relations

$$\begin{cases} \frac{\partial V_{SS}^l}{\partial\theta} = -\frac{\gamma_l^2 - nM_l F_l}{n^2 F_l} {I_{SS}}^l - \\ \frac{ql}{nF_l}\left[\frac{(l-2)}{F_{l-2}} I_{SS}^{l-2} - \frac{(l+2)}{F_{l+2}} I_{SS}^{l+2}\right] - \frac{ql\beta}{F_l}\left[V_{SS}^{l-2} + V_{SS}^{l+2}\right] \\ \frac{\partial I_{SS}^l}{\partial\theta} = -F_l n^2 {V_{SS}}^l + q\beta\left[\frac{(l-2)}{F_{l-2}} I_{SS}^{l-2}\right. \\ \left. + \frac{(l+2)}{F_{l+2}} I_{SS}^{l+2}\right] + \beta^2 qn\left[V_{SS}^{l-2} + V_{SS}^{l+2}\right] \end{cases} \tag{3.18}$$

We can show that eqns. (3.18) and (3.15) are equivalent if we multiply both sides of (3.18) by n^2 and substituting $V_{SS}n^2 = W_{SS}^l \;\; and \; I_{SS} = I_{SS}$. Then the same equations are obtained as (3.15) with respect to $W_{SS}^l \;\; and \; I_{SS}$. A homogeneous system of equations can thus be formed again using (3.18) as with even modes.

Similarly to the case of even modes as described before, one can now consider the

effect of higher harmonics, for odd modes, around the harmonic l , i.e. the harmonics $\ldots l+2,\ l+4,\ l+6\ and\ \ l-2, l-4, l-6 \ldots$ which result in a set of homogeneous differential equations for the functions $V_{SS}^{l+6}, V_{SS}^{l+4}, V_{SS}^{l+2}, V_{SS}^{l}, V_{SS}^{l-2}, V_{SS}^{l-4}, V_{SS}^{l-6}, I_{SS}^{l+6}, I_{SS}^{l+4}, I_{SS}^{l+2}, I_{SS}^{l}, I_{SS}^{l-2}, I_{SS}^{l-4}, I_{SS}^{l-6}$. We observe that the eigenvalues of the respective system of equations here representing odd modes are the same as the respective eigenvalues of the system of the previous equations (3.15) for the eigenfunctions shown in Table 3.1. The respective resulting quadrupole however differs and should be formed with the same respective transmission characteristic γ_l^2 but different admitances $n^2F = jn^2(l^2 + \beta^2 {h_0}^2)$. Thus, in general the overall transmission characteristics β of the odd modes are different to those for even modes, (birefringence effect). Therefore, both quadrupoles representing the odd HE and EH modes, will use the same transmission characteristic γ_l^2 and different admittances $jn^2\,F$. The characteristic impedances for odd modes of the T-circuit are given by the equations

$$\begin{cases} Z_B = \gamma_l^2 \Delta\theta/(2jFn^2) \\ \quad and \\ Z_P = 1/(jFn^2\Delta\theta) \end{cases} \tag{3.19}$$

The previous equations were considered for $l \geq 0$. Considering that M is proportional to l we can form sets of similar equations for HE (l positive integer) and for EH (l negative integer). The resonance "frequencies" of the derived "total transmission line of successive layers" are equal to the transmission wave numbers "β" of the respective elliptic fibers' odd modes. The terminal impedances for $\theta = \infty\ and\ \theta = 0$, are the boundary conditions for the transmission line behavior. The full mathematical analysis for the derivation of Maxwell's equations in elliptical coordinate system and the subsequent Transmission Line relations, is given in Appendix B.

3.4. Boundary terminal impedance calculation and resonant solutions

Calculation of terminal impedance at $\theta = \infty$ has been based on the fact that as θ tends to infinity the ellipse becomes a circle, thus the harmonics effect is negligible. Thus the terminal impedance is the limit of the characteristic impedance of the quadruple given by $z_{(\infty)} = \gamma/_{jF_l}$. For θ = ∞ it can be shown that $z_{(\infty)} = 0$.

The terminal impedance for $\theta = 0$ can similarly be calculated taking into consideration that the field components E_z and H_z are symmetric for the y axis. This results from the property that only polarized EM waves are stably transmitted in elliptic fibers. This property means finally that the EM field components are periodic along φ with period π. Thus for $\theta = 0$, the following relations can be written: $E_z(\varphi) = E_z(\varphi - \pi)$ and $H_z(\varphi) = H_z(\varphi - \pi)$.

Hence the Fourier Transform of E_z along φ can be given as

$$\overline{E_z} = \int_{-\pi}^{\pi} E_z(\varphi) e^{-jl\varphi} d\varphi \tag{3.20}$$

It is then easy to prove that

$$\overline{E_z} = \int_{0}^{\pi} E_z(\varphi) e^{-jl\varphi} [1 + e^{-jl\pi}] d\varphi \tag{3.21}$$

Then for $l = even\ (or\ zero)$, $\overline{E_z} \neq 0$ and for $l = odd$, $\overline{E_z} = 0$.

In the same way it can be proved that for $l = even(or\ zero)$, $\overline{H_z} \neq 0$ and for $l = odd$, $\overline{H_z} = 0$. Thus for $l = odd$, $V_M = \overline{hH_\varphi} l / jF$ and $I_M = \beta\, \overline{hE_\varphi} / j$. But for $\theta = 0$ and $l \neq 0, where\ j\, \overline{H_\varphi} = n\overline{E_\varphi}$, $V_M / I_M = Z_M(0) = nl / j\beta F$. Thus $Z_{HE}(0) = nl / j\beta F$ and $Z_{EH}(0) = l / j\beta Fn$. For $l = even\ (or\ zero)$ and $\theta = 0, \{\overline{H_z} \neq 0$ and $\overline{E_z} \neq 0\}$ $thus$ $V_M \neq 0$ and $V_E \neq 0$ while $I_E = n^2 \overline{hE_\theta} = 0$ and $I_M = \overline{hH_\theta} / j = 0$, because $\overline{E_\theta} = 0$ and $\overline{H_\theta} = 0$. Thus for $l = even\ (or\ zero)$, $Z_M(0) = \infty$, $Z_E(0) = \infty$, $Z_{HE}(0) = \infty$, $Z_{EH}(0) = \infty$.

For each of the successive layers of Δθ, length can be represented by a quadrupole like the one shown in Figure 3-2, where

$$\begin{cases} Z_B = (\gamma^2 - nM_l F_l)\delta\theta / (2jF_l n^{tm}) \\ Z_P = \frac{1}{jF_l n^{tm} \delta\theta} \end{cases}, tm = \begin{cases} 0 \\ 2 \end{cases} \tag{3.22}$$

The quadrupoles representing the successive layers can be connected in series, because the equivalent "voltages" and "currents" on their boundaries are continuous due to the fact that V_M, I_M, V_E, I_E are also continuous functions of θ, following the

normal and tangential Magnetic and Electric fields being continuous. Therefore, the set of the successive layers is forming an overall "Transmission Line" with pure imaginary impedances.

Then the fiber mode normalized (/k0 as defined in section 3.2, the paragraph after eq. 3.8) propagation constants "β" are calculated from the resonant "frequencies" of the line. The terminal impedances for $\theta = \infty \; and \; \theta = 0$, are the boundary conditions for the transmission line behavior. The terminal impedances should be calculated using transmission line properties. In the case of elliptic fibers, there are symmetry properties arising from the fact that wave transmission is polarized. The mode cutoff wavelengths can also be computed by setting for $\beta = n_2$ the cutoff condition, i.e. the minimum reduced wave number with which a mode may exist in the fiber. Due to the significance of the harmonics in the calculation of mode propagation constants, and in order to differentiate the current method from other TL methods presented in this thesis, the current method will be henceforth referred to as the harmonics method.

A specific case related to the value of eccentricity is that of small elliptic eccentricity for l = 0 or 1 where the effect of harmonics can be ignored (this case is not applicable for higher harmonics). As a result of small elliptic eccentricity, the effect of harmonics in equations (3.9) becomes negligible and the coefficients of [Φ_1] and [Φ_2] are zero. In this case the equations (3.9) collapse to

$$\begin{cases} \frac{\partial V_S}{\partial \theta} = -\frac{\gamma^2 - nMF}{jF} I_S \\ \frac{\partial I_S}{\partial \theta} = -jFV_S \end{cases} \tag{3.23}$$

Furthermore we can define $V_{SS} = \frac{V_M}{n} + V_E \quad I_{SS} = nI_M + I_E$. It can then be proved that

$$\begin{cases} \frac{\partial V_{SS}}{\partial \theta} = -\frac{\gamma^2 - nMF}{jFn^2} I_{SS} \\ \frac{\partial I_{SS}}{\partial \theta} = -jFn^2 V_{SS} \end{cases} \tag{3.24}$$

The set of equations (3.23) and (3.24) can be written in the following compact form

$$\begin{cases} \frac{\partial V_H}{\partial \theta} = -\frac{(\gamma^2 - nMF)}{jFn^{tm}} I_H \\ \frac{\partial I_H}{\partial \theta} = -jFn^{tm} V_H \end{cases} \text{ for } tm = \begin{cases} 0 \\ 2 \end{cases} \tag{3.25}$$

where V_H, I_H stand for even and odd modes respectively, or the two independent hybrid modes with the same transmission coefficient γ^2-*nMF* and different admittances *jF* and jFn^2. The two modes are related to the birefringence property in elliptic fibres. This method maybe of use, in the case where there is interest in approximate but fast computation of the mode behavior.

3.5. Estimation of the EM Field Components for Elliptical Core Fibers

Taking into consideration the set of equations in (3.12) and due to the fact that the values of the estimated birefringence are very small, it can be assumed that:

$V_E \cong \frac{V_M}{n}$ and $I_E \cong nI_M$

Thus $V_M = \frac{V_S}{2}$ and $I_M = \frac{I_S}{2}$ and $V_E \cong \frac{V_S}{2n}$ and $I_E \cong n\frac{I_S}{2}$

Taking into consideration that $h_0^2 = \frac{c^2}{2}\cosh 2\theta$ the set (3.12) transforms as follows

$$\begin{cases} \overline{H_z} = {lI_E}/{F} + j\beta V_M \\ \overline{E_z} = {-jlI_M}/{F} + \beta V_E \end{cases} \tag{3.26}$$

$$\begin{cases} \overline{H_\varphi} \cong \left(jlV_M + \frac{\beta h_0^2}{F_l} I_E\right)\Big/_{h_0} \\ \overline{E_\varphi} \cong \left(\frac{j\beta h_0^2}{F_l} I_M + lV_E\right)\Big/_{h_0} \end{cases} \tag{3.27}$$

Having calculated β, V_S, I_S for each θ, or, for each $bb(\theta) = \sinh\theta$, the equations in (3.26) and (3.27) can be used for the calculation and plotting the values of the EM field components for the elliptical core fiber for TM (E) and TE (M) modes separately.

3.6. Results

Using the relations of the impedances in section 3.4, for the quadrupoles that make up the Transmission Line, an algorithm can be developed that calculates the mode propagation constant β at the point of resonance. Using the corresponding algorithm, the $\bar{b} - V$ diagram has been computed for a number of low order modes with ellipticity b/a=0.5, versus V defined as $V = \frac{2\pi b}{\lambda}\sqrt{n_1^2 - n_2^2}$, b defined as the semiminor axis of the ellipse and a, is the semi major axis $\bar{b} = \frac{(\frac{\beta}{k_0})^2 - n_2^2}{n_1^2 - n_2^2}$. The wave number β represents the ratio β/k_0.

The results shown in Figure 3-3, agree within the 3rd or 4th decimal place compared to other published results in the literature. The curves in the figures were generated using 5 harmonics. Using only 3 or 4 harmonics the fundamental HE11 produces acceptable accuracy in the value of 'β', but the higher order modes require more harmonics to become more accurate, as shown in Figure 3-4.

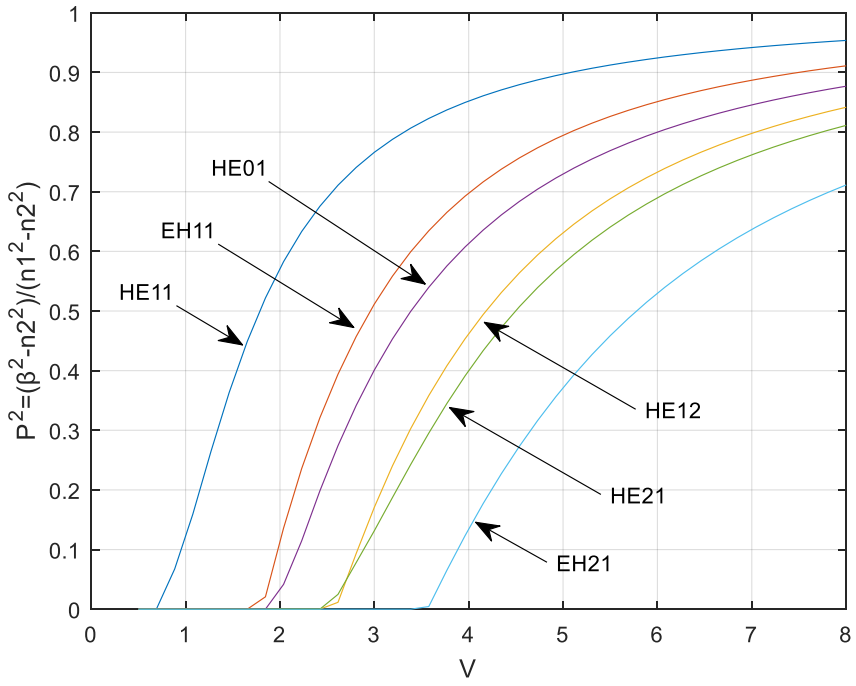

Figure 3-3 The first six normalized modes versus V, of Step Index Elliptical fiber of $\mathbf{n_1 = 1.54}$, $\mathbf{n_2 = 1.47}$, $\mathbf{^a/_b = 2, l = 1 \text{ and } l = 0}$.

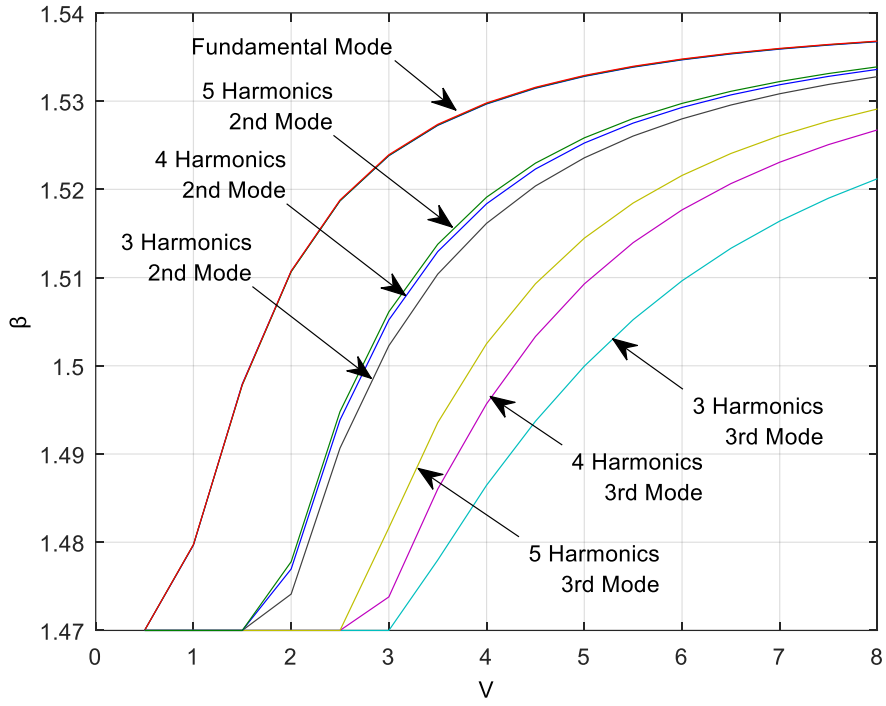

Figure 3-4 The first three normalized modes versus V, of Step Index Elliptical fiber of $\mathbf{n_1 = 1.54}$, $\mathbf{n_2 = 1.47}$, $\mathbf{a/b = 2, l = 1}$ calculated with 3, 4 and 5 harmonics. (The wave number β is normalized by ko)

Table 3-2 presents a comparison of calculated normalized step index core mode propagation constants using only 2x2 matrix Mathieu functions and the Transmission Line method.

a/b=1.3	**Mathieu**	**TR**
V	$\mathbf{b_{11,\ Ne}}$	$\mathbf{b_{11,\ Ne}}$
1.5	1,4907763	1,4907020
2.1	1,5061120	1,5057200
2.5	1,5131290	1,5126423
3.1	1,5203294	1,5198141
a/b=1.3	**Mathieu**	**TR**
V	$\mathbf{b_{11,\ No}}$	$\mathbf{b_{11,\ No}}$
1.5	1,4911885	1,4910277

2.1	1,5064715	1,5063359
2.5	1,5134235	1,5131960
3.1	1,5205393	1,5202285
a/b=1.5	**Mathieu**	**TR**
V	$\mathbf{b_{11,\ Ne}}$	$\mathbf{b_{11,\ Ne}}$
1.5	1,4936200	1,4933413
2.1	1,5085150	1,5078138
2.5	1,5150727	1,5143015
3.1	1,5217244	1,5209683
a/b=1.5	**Mathieu**	**TR**
V	$\mathbf{b_{11,\ No}}$	$\mathbf{b_{11,\ No}}$
1.5	1,4942506	1,4936368
2.1	1,5090391	1,5083152
2.5	1,5154931	1,5147457
3.1	1,522019120000000	1,521299532774000

Table 3-2 Comparison of normalized mode propagation constants calculated using Mathieu functions method and Transmission Line method

The comparison is made for two basic cases of elliptic eccentricity, namely a/b=1.3 and a/b=1.5, for the fundamental modes, both even and odd and for selected numbers of normalized frequency V. The small differences are due to the truncation of the Matrix using Mathieu Functions. The appearance and consideration of more harmonic terms leads to significant accuracy for the TR method; accuracy is the harmonics method's competitive advantage against other existing methods.

3.6.1. Evaluation of the method for different number of harmonics

At this point it would be interesting to investigate the effect of using different numbers of harmonics under various ellipticities. To this end, 4 cases of elliptical fibers are considered, with corresponding ellipticities of ab = 1.5, ab = 2, ab = 3 and ab = 5. For each of these cases, the mode propagation constants are estimated in β-V diagrams for the fundamental mode; the calculations in each case take place using 1, 3 and 5 harmonics and the results are presented below.

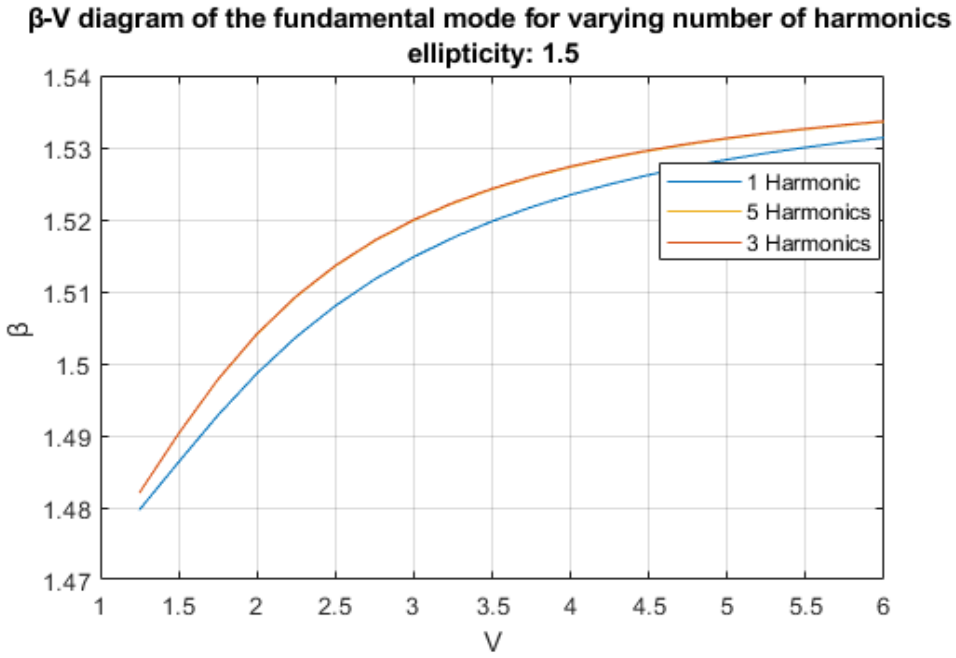

Figure 3-5 β-V diagram of the fundamental mode for varying number of harmonics. Ellipticity: 1.5

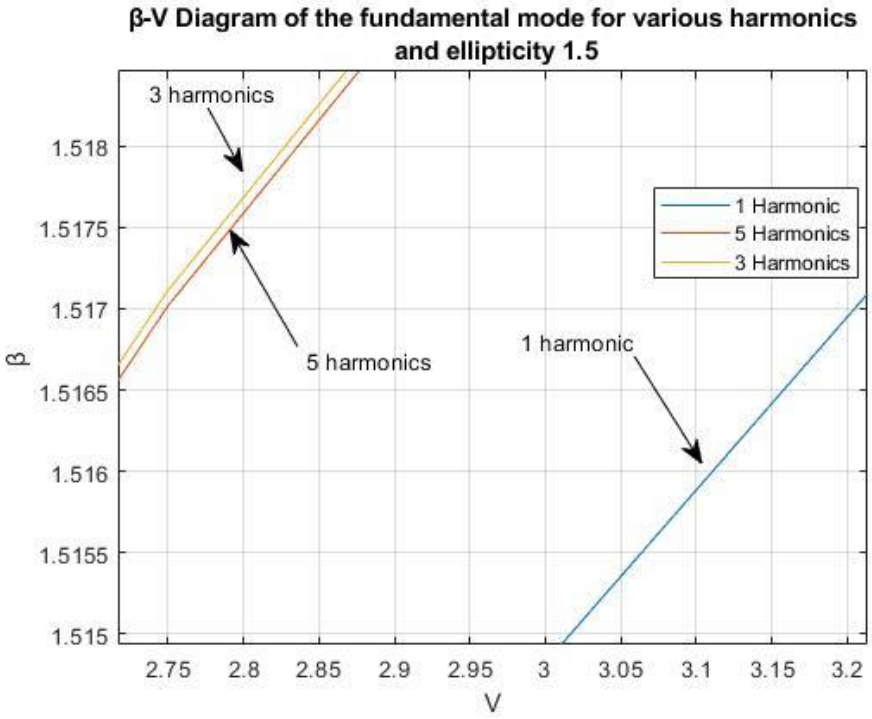

Figure 3-6 Zoomed β-V diagram of the fundamental mode for varying number of harmonics. Ellipticity: 1.5

In the diagram of Figure 3-5, the difference between the β values calculated by 1 harmonic and those calculated by 3 and 5 is very notable and varying between 2×10^{-3} and 6×10^{-3}. In Figure 3-5 however, the difference between the β values calculated by 3 and 5 harmonics is so restricted that the two lines appear as one. In order to better visualize the difference (between 3 and 5), a second figure is deployed, Figure 3-6, which presents a zoomed area of the same diagram where the lines of 3 and 5 harmonics appear distinct. The difference in β is around 8×10^{-5}. The conclusion drawn from the above figure, is that using more than 3 harmonics for the estimation of the β-V diagram, shifts the resulting line merely by a minimum, while beyond 5 harmonics the difference is negligible and the line is stabilized.

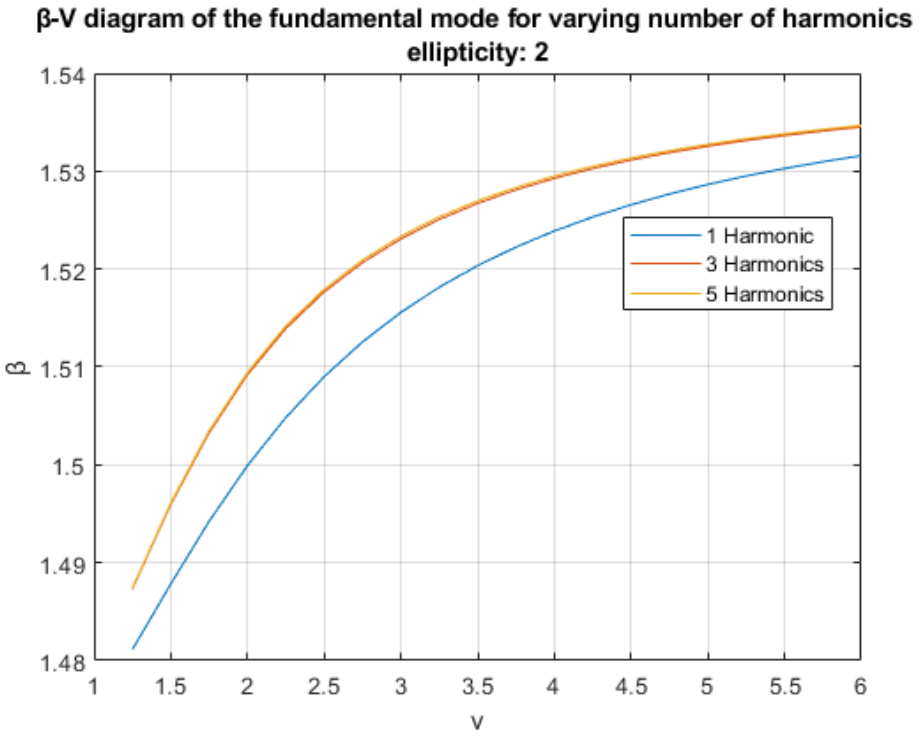

Figure 3-7 β-V diagram of the fundamental mode for varying number of harmonics. Ellipticity: 2

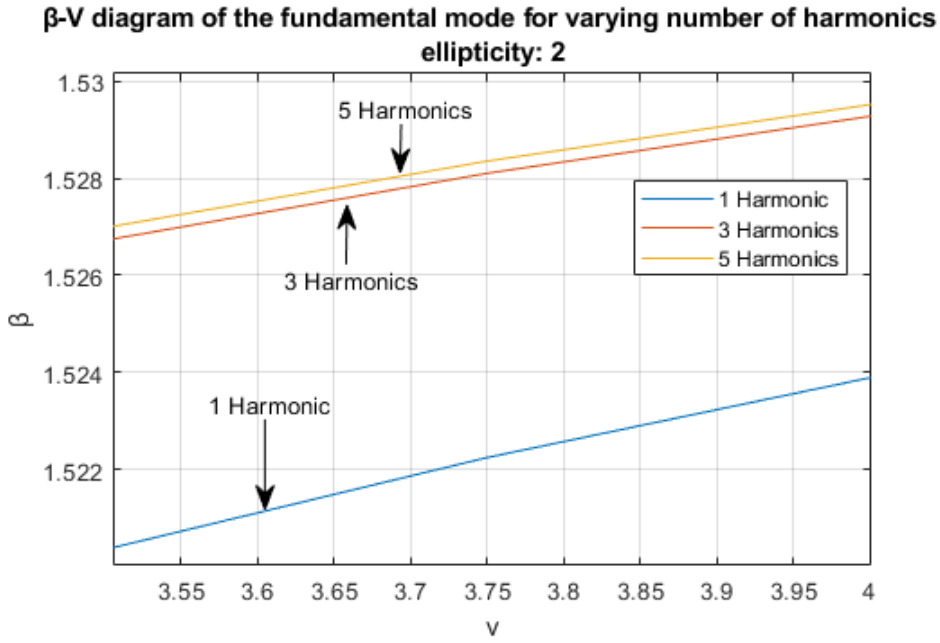

Figure 3-8 Zoomed β-V diagram of the fundamental mode for varying number of harmonics. Ellipticity: 2

In the diagram of Figure 3-7, the value of ellipticity has been increased to 2. The difference between the β values calculated by 1 harmonic and those calculated by 3 and

5 is again quite evident and varying between 6×10^{-3} and 10^{-2}. In Figure 3-7, the difference between the β values calculated by 3 and 5 harmonics is restricted as in Figure 3-5 and the two lines again appear as one. In order to better visualize the difference (between 3 and 5), Figure 3-8 is utilized, presenting a zoomed area of the same diagram where the lines of 3 and 5 harmonics appear distinct. The difference in β for the lines of 3 and 5 harmonics, is around 3×10^{-4}. The conclusion drawn from the above figure, is that using more that 3 harmonics for the estimation of the β-V diagram shifts the resulting line by a difference in β that reaches 3×10^{-4}. The corresponding maximum difference in β under ellipticity 1.5 is 8×10^{-5}. This means that for an ellipticity of 2, using 3 harmonics is less adequate than in the case of ellipticity of 1.5. Still, beyond 5 harmonics the difference is negligible and the line is stabilized.

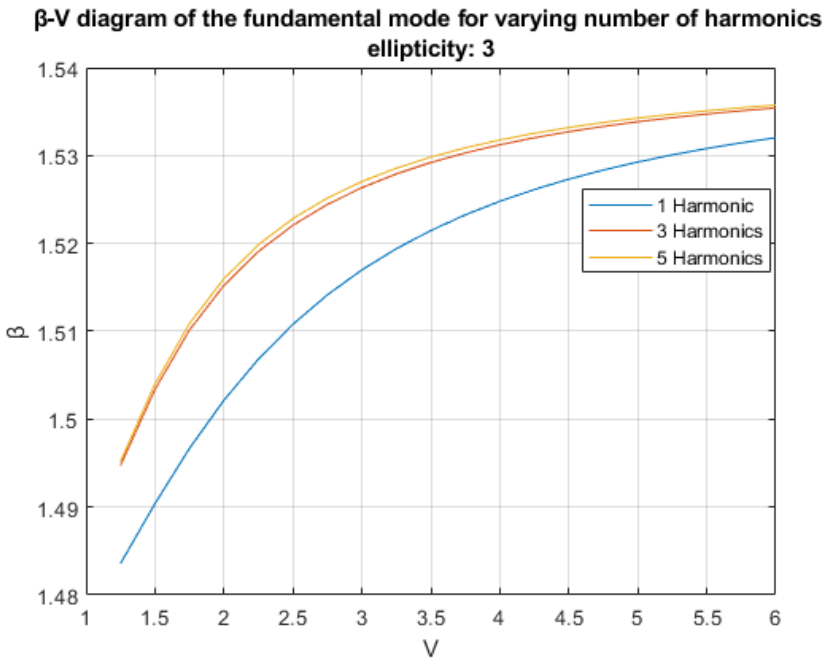

Figure 3-9 β-V diagram of the fundamental mode for varying number of harmonics. Ellipticity: 3

In the diagram of Figure 3-9, β-V lines have been plotted for ellipticity of 3 and for various numbers of harmonics. The difference between the β values calculated by 1 harmonic and those calculated by 3 and 5 is evident and varying between 5×10^{-3} and 1.3×10^{-2}. In Figure 3-9, the difference between the β values calculated by 3 and 5 harmonics is evident and the corresponding lines appear separate without the need of a zoom; the value of this difference reaches its maximum around 10^{-3}. The conclusion drawn from the above figure, is that the use of 3 harmonics may be not enough since

there is an error of 10^{-3} between 3 and 5 harmonics and for V around 2.5. Using 5 harmonics on the other hand is adequate and the line beyond that number of harmonics will not shift.

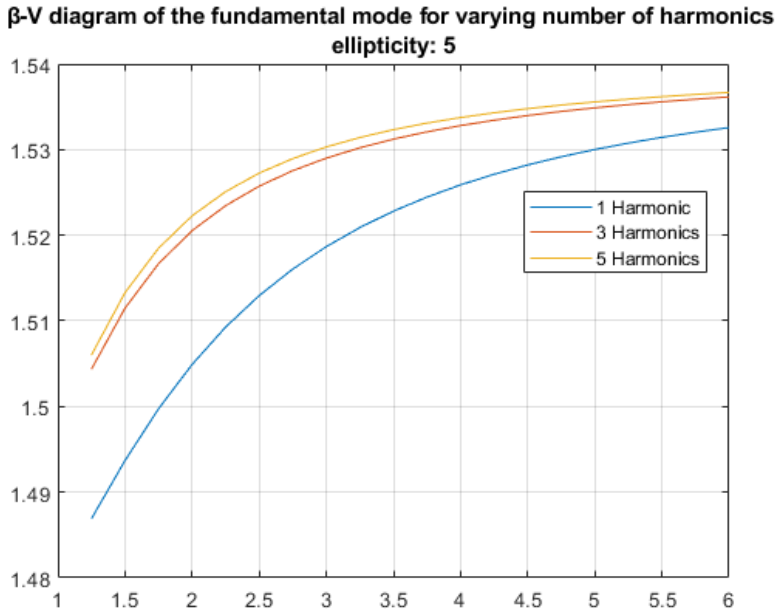

Figure 3-10 β-V diagram of the fundamental mode for varying number of harmonics. Ellipticity: 5

Finally, on Figure 3-10, a diagram is presented with the β-V plots for ellipticity of 5 and for various numbers of harmonics. The difference between the β values calculated by 1 harmonic and 3 is varying between 5×10^{-3} and 1.8×10^{-2}; even wider compared to Figure 3-9. In Figure 3-10, the difference between the β values calculated by 3 and 5 harmonics is again evident and the corresponding lines appear separate without the need of a zoom; the value of this difference reaches its maximum around 2×10^{-3}. The conclusion drawn from the above figure, is that the use of 3 harmonics may be not enough since there is an error of 10^{-3} between 3 and 5 harmonics and for V around 2. Using 5 harmonics even for this value of ellipticity (5) is adequate and the line beyond that number of harmonics will not shift.

Concluding, as the value of ellipticity increases, the difference in β increases significantly. It is therefore concluded that as ellipticity increases, a higher number of harmonics need to be included in order for the results to converge on an accurate β value. However, for all the cases of ellipticity presented above (1.5, 2, 3 and 5), the

use of 5 harmonics has been found adequate to produce results with significant accuracy.

3.6.2. Obtaining Results for Elliptical Fibers with Arbitrary Index Profiles

The power of the Resonant Transmission Line method is not limited to the accurate calculation of mode propagation constants. Perhaps its most powerful feature is the ability to produce results for index profiles, other than the typical step index, such as graded. Graded index fibers do not have a constant refractive index in the core, but a decreasing core index $n(r)$, with radial distance from a maximum value of n_1 at the axis, to a constant value n_2 beyond the core radius 'a' in the cladding. This refractive index variation may be represented as:

$$n(\bar{r}) = \begin{cases} n_1 \times \left[1 - \Delta \times (\frac{\bar{r}}{\bar{a}})^{\alpha}\right] & \bar{r} < \bar{a} \\ n_2 & \bar{r} > \bar{a} \end{cases}$$

where

$\Delta \equiv (n_1 - n_2)/n_1$,

n_1 is the refractive index at the axis of the optical fiber,

α controls the decay or growth of the profile envelope,

$\bar{a}$ is the normalized core radius.

A variety of profiles can be generated by varying α, as shown in Fig. 3-11 below

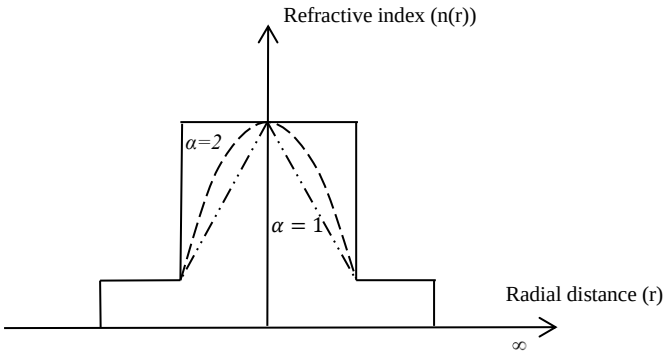

$\alpha = 1$ Triangular index profile

$\alpha = 2$ Parabolic index profile

Figure 3-11 Possible fibre refractive index profiles for different values of α

Linear and parabolic index profiles are often used in the industry as methods for dispersion manipulation. Results for arbitrary index profiles like the ones mentioned above, cannot be easily produced using the Mathieu functions analytical method.

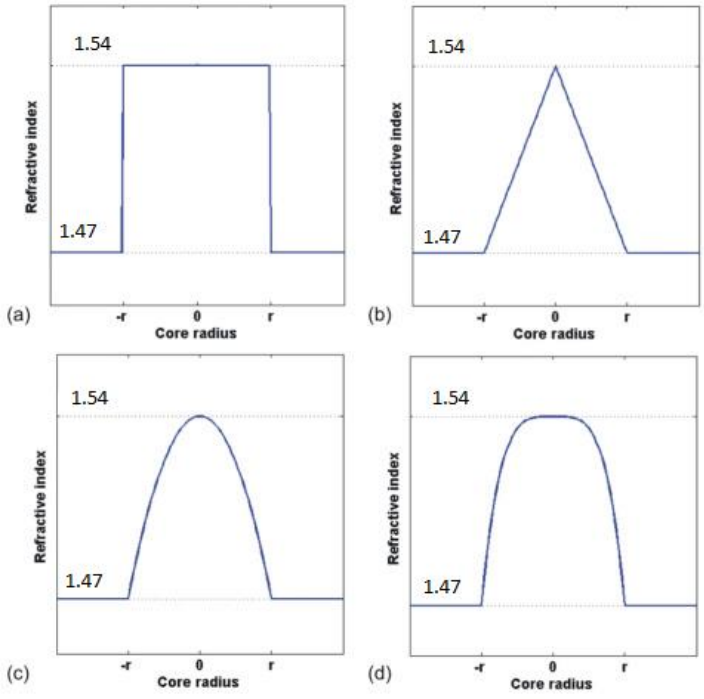

Figure 3-12 (a) Step index profile (b) Linear index profile (c) Parabolic index profile (d) 4th power parabolic index profile

[https://www.osapublishing.org/getImage.cfm?img=LmxhcmdlLG9lLTI1LTExLTEyOTg0LWcwMDI
]

Further follows a demonstration of the calculation of mode propagation constants in elliptical core fibers of arbitrary index profiles, starting with the case of linear index profile. For a linearly varying core index profile, the distribution of the index value in relevance to the core radius can be seen in case (b) of Figure 3-12. Specifically in the case of an elliptical core fiber, let us consider the following case where the variation of the core index starts from $\Theta = 0$ at the core center, from a typical value of $n_1 = 1.54$ down to $n_2 = 1.47$ at the outer core ellipse where $\Theta = \tanh^{-1}(1/ab)$. The values of mode propagation constants under varying normalized frequency V for the fundamental mode in an elliptical core fiber of ellipticity ab=2 have been plotted in Figure 3.13.

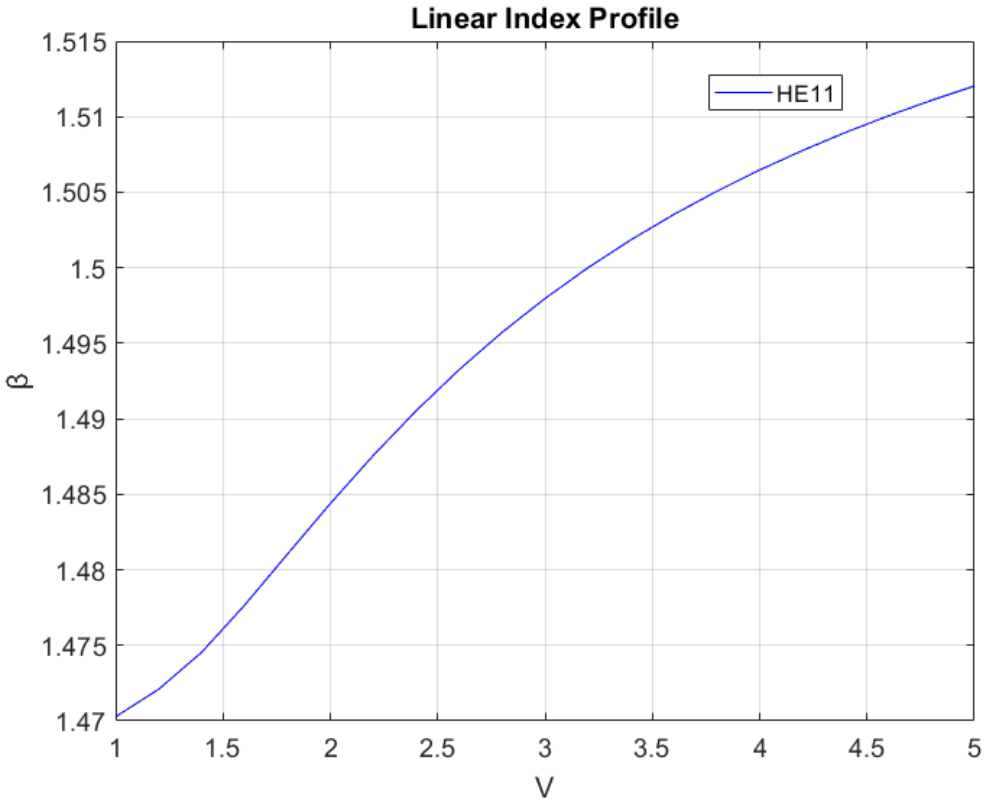

Figure 3-13 The β-V diagram for a linearly varying core index profile, ab=2

Figure 3-14 presents a comparative plot between step and linear index profiles. The upper curve is the standard curve for a constant index value n_1 while the lower curve corresponds to the linearly varying index profile. As one might expect, the curve representing the linear index profile lays below that of the step index, since the core in its entirety is characterized by lower refractive index.

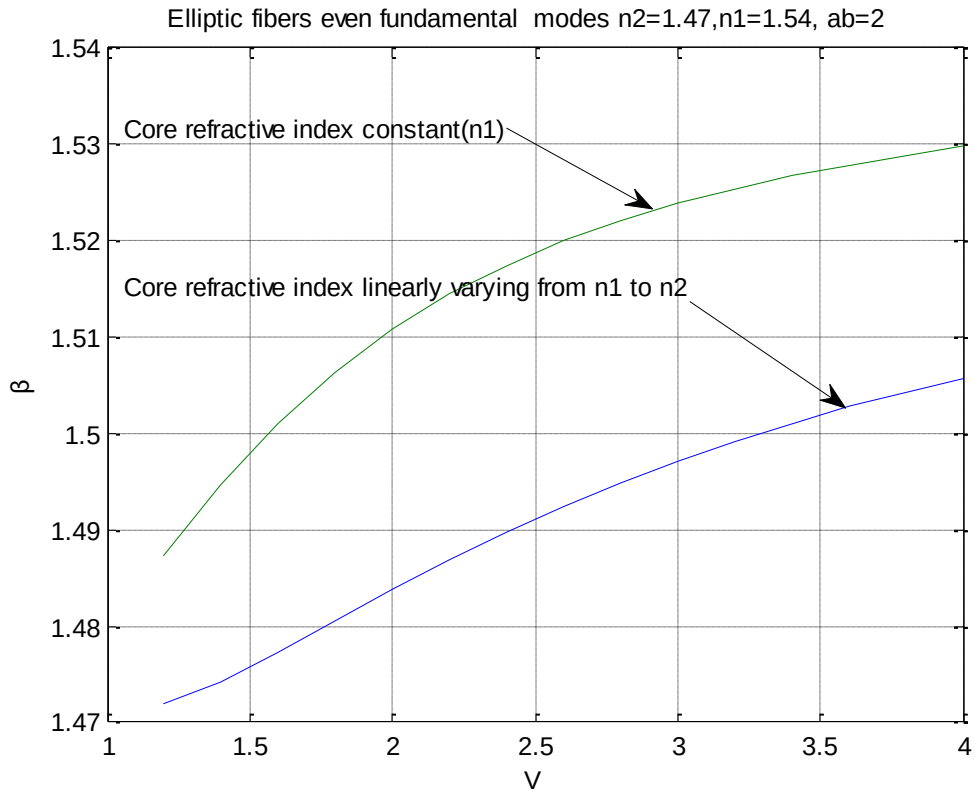

Figure 3-14 *β-v* diagram comparing β values between a linearly varying core index profile and a typical step index profile.

The demonstration continues with the analysis of the case of a parabolic index profile. For a parabolically varying core index profile, the distribution of the index value in relevance to the core radius can be seen in case (c) and (d) of Figure 3-12. Index values variate from n_1 = 1. 54 at the core center (Θ = 0), decreasing to n_2 = 1. 47 at the outer core where $\Theta = \tanh^{-1}(1/ab)$, in a parabolic manner, under a power of two as per case (c) of figure 3.12. The values of mode propagation constants under varying normalized frequency V for the fundamental mode in an elliptical core fiber of ellipticity ab=2 have been plotted in figure 3-15.

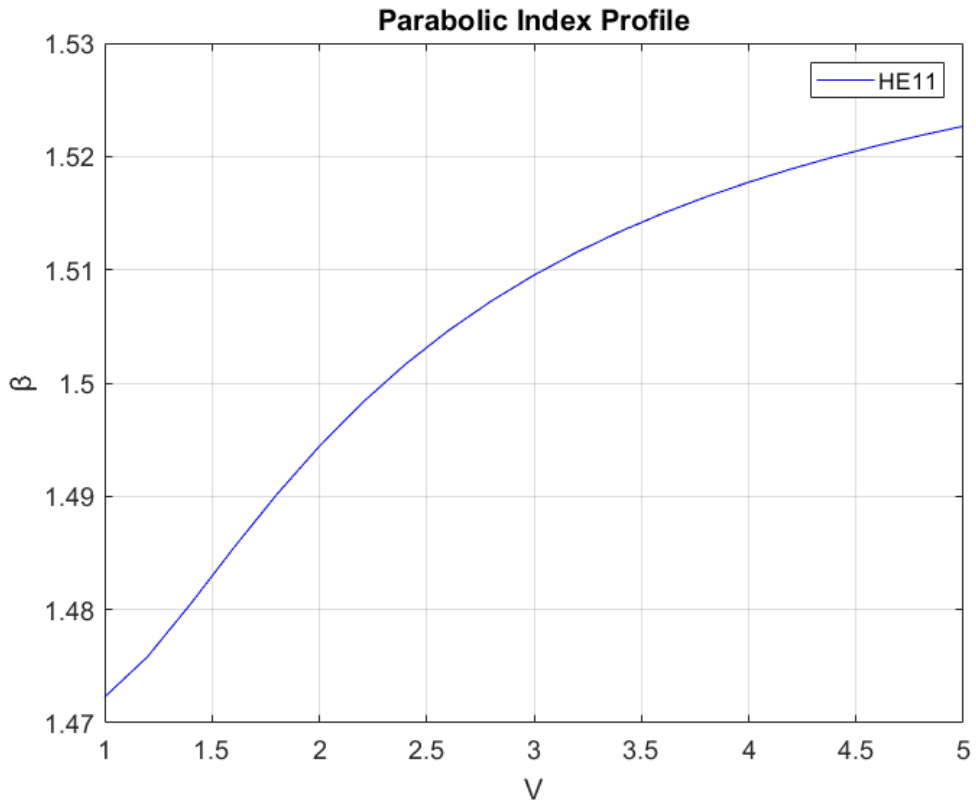

Figure 3-15 β-v diagram for a parabolically varying core index profile

Figure 3-16 presents a comparative plot between step parabolic and linear index profiles. The upper curve is the standard curve for a constant index value n_1 while the middle curve corresponds to the parabolically varying index profile and the lower curve corresponds to the linearly varying index profile. As one might expect, the curve representing the parabolic index profile lays in between those of the step and linear index profiles, since the area covered by a larger index value is lesser than step and greater than the linear profile cases.

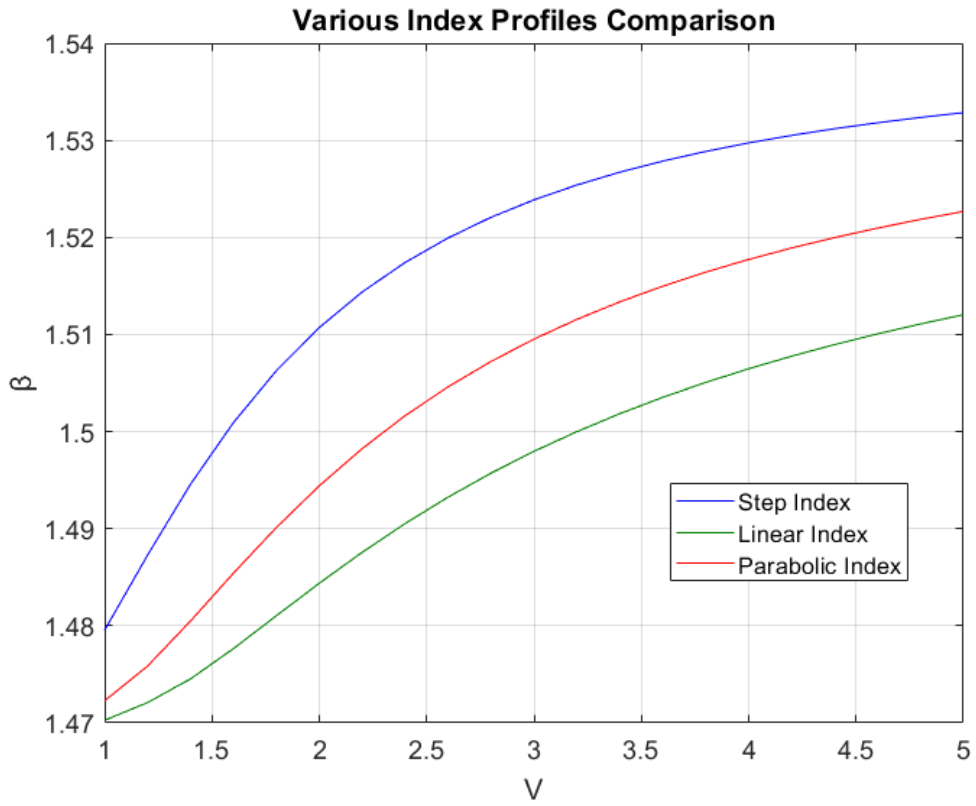

Figure 3-16 *β-v* diagram comparing β values between a typical step index profile, a parabolic and a linear index profile

3.6.3. Calculation of Birefringence and Mode Cutoffs

The current method can be used for the calculation of birefringence and mode cutoffs, with significant accuracy. In Figure 3-17, we study the fundamental mode birefringence for the step index case and for l=1, a/b=3 while we use 3, 4 and 5 harmonics in order to highlight the convergence using higher order harmonics between them. It can be observed that 5 harmonics provide adequate level of accuracy for most applications.

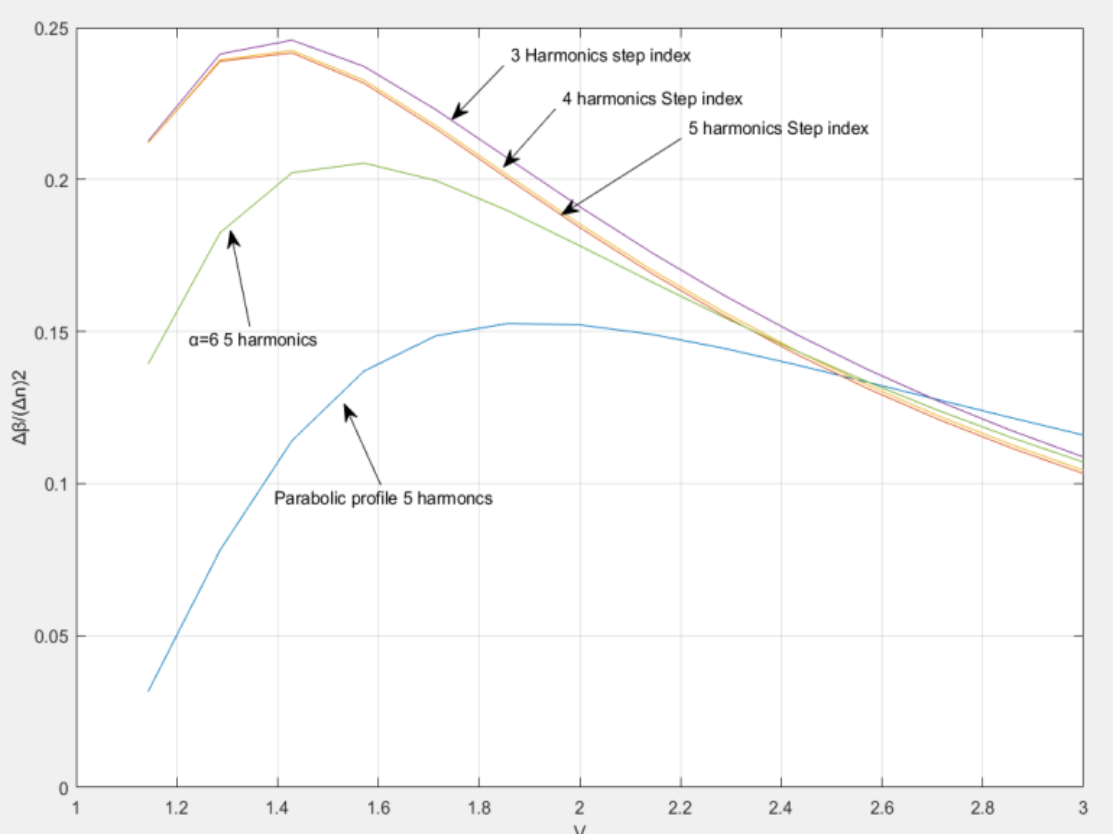

Figure 3-17 Birefringence related to V, of Elliptical Graded Index Core fibers for n_1=1.54 and n_2=1.47, for a/b=3

In the same figure we also calculate the birefringence of graded index elliptical waveguides, using the general refractive index profile formula $n(\theta)=n_1+(n_2-n_1)(\theta/\theta_0)^{\alpha}$ where n_1 is the maximum core refractive index, n_2 is the cladding refractive index and θ_0 is defined by the dimensions of the elliptic core(θ_0=atanh(b/a)). Figure 3-17 also presents two typical birefringence curves for α=2 (parabolic), and α=6. It is evident that birefringence is higher for step index fibers compared to other graded profiles.

Figure 3-18, shows the normalized birefringence versus v-curves, using the ellipticity a/b, as a parameter. The results are identical to the ones presented in the literature.

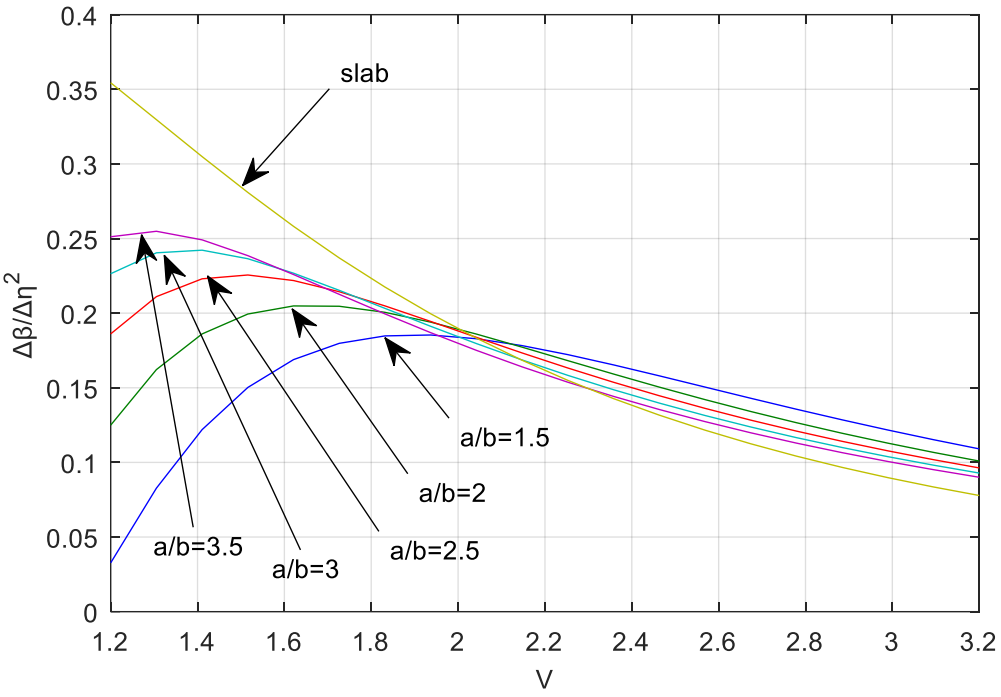

Figure 3-18 Birefringence versus V, of Elliptical Step Index Core fibers forn_1=1.54, n_2=1.47 for a/b=1.5,2,2.5, 3, 3.5 and infinity (slab).

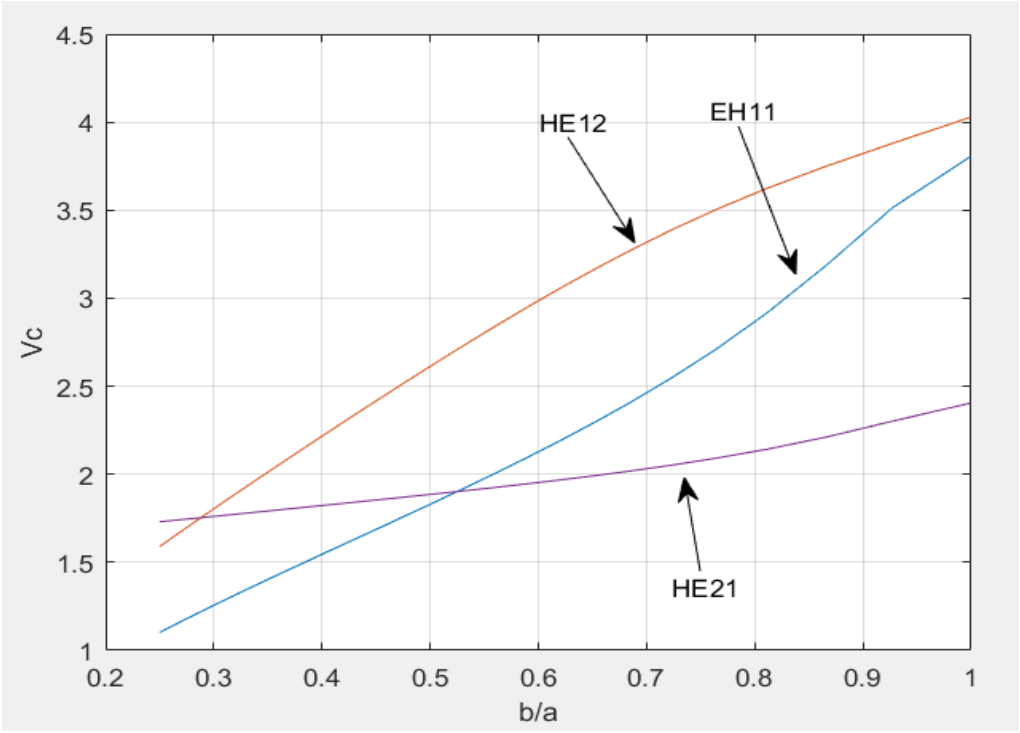

Figure 3-19 Mode cutoff frequencies Vc versus ellipticity b/a for a few low order modes of Step Index Elliptical Waveguides for n1=1.46 and n2=1.34 and l=1 and l=0.

A direct computation is also presented, of the mode cutoff frequencies for specific low order modes in step index elliptical core fibers, in Figure 3-19. The agreement is quite satisfying, considering that all published work take only the minimum size for the transcendental matrix, using Mathieu Functions, while in the method presented, one can simply increase the harmonic terms and reach higher accuracy.

We conclude this chapter by noticing that the harmonics method is computationally exact, producing equivalent results with certain analytical solutions based on Mathieu functions, without using them explicitly. Unlike existing analytical methods, it can be applied to arbitrary refractive index profiles exhibiting remarkable simplicity, accuracy and fast convergence. Additionally, analytical methods such as, Bessel and Mathieu functions based methods are mostly limited to analysing cases where a finite radius core is covered by an infinitely expanded cladding which is unrealistic since optical fibers are covered with more layers of different materials or air. Unlike the complexity limitations of analytical methods, the RTL calculative method can be used for the analysis of more complexed realistic cases that examine mode propagation within multiple layers.

4 CHAPTER 4

A study of Eccentric Core Optical Fibers

4.1 Reasoning and methods for studying eccentricity

In several cases optical fibers for telecommunication applications have cores of non-circular geometry. Fiber optic deformations appear in optical fibers for a variety of reasons. Optical fiber core ellipticity where the fiber optic core is not perfectly circular due to fiber optic manufacturing tolerances is measured and it often becomes a problem. Optical fiber core eccentricity, is defined by the fiber core being not on the axis of the fiber, but is offset by a certain length. This is another very important issue for ensuring performance with low loss splices and connector losses. Both ellipticity and eccentricity are specified in accordance with international standards for fiber optic manufacturing telecommunications grade fibers.

The present chapter studies ellipticity combined with core eccentricity specifically and presents a new method for analyzing their effect. We present an extension of the transmission line technique as a means of studying such fibers and deriving necessary parameters. Conformal mapping on the other hand is a simple mathematical tool by which one can generate sets of orthogonal two-dimensional coordinate systems. Shortly a conformal map of Cartesian two-dimensional space is defined by any analytical function $w(z)$ where z, w, are: $z = x + jy$, $w = \theta + j\varphi$.

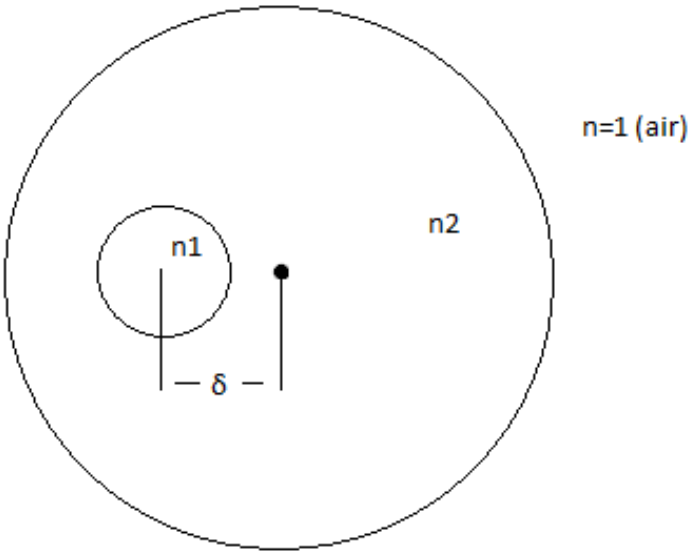

Figure 4-1 Typical eccentric core optical fiber. The core has refractive index n_1 and the cladding n_2

The function deriving by the conformal mapping transformation $h_{(\theta,\varphi)} = \left|\frac{\partial w}{\partial z}\right| = 1/\left|\frac{\partial z}{\partial w}\right|$,can be used in order to define $\nabla \vec{A}$ and $\nabla \times \vec{A}$ where $\vec{A}$ is the magnetic or electric field in the derived orthogonal coordinate system. Useful conformal maps for fiber optics applications should have the property that the equation $\theta(x, y)$= constant, forms closed curves in a Cartesian two-dimensional space (x,y).

The choice of a $\theta(x, y)$ representing a set of co-eccentric circles, leads to the normal case of conventional fibers with circular cores. In case of $\theta(x, y)$ representing a set of ellipses, we have the case of elliptic core optical fibers. The case of $\theta(x, y)$ representing a set of eccentric circles corresponds to optical fibers with eccentric core. The method presented in the current chapter uses the transmission line technique together with conformal mapping as tools for the study of various shaped optical fiber cores and the effect of eccentricity on the fundamental modes of eccentric core fibers.

Orthogonal Curvilinear Coordinates can be generated using a conformal map [48] of Cartesian coordinates (x,y) represented by the complex number z=x+jy. Of current interest are orthogonal coordinate systems where the z coordinate remains Cartesian (as in standard cylindrical coordinates) and furthermore for θ = constant, closed curves are formed on (x,y) plane. Thus, in general a Fourier Transformation along φ has integer

values 'l'. Any function of A(θ,φ,z) can be transformed along z and φ and the derived transformation will be a function of A(θ,l,β)$e^{j\beta z} \cdot e^{jl\varphi}$ such that $\frac{\partial A}{\partial z} = j\beta A$, $\frac{\partial A}{\partial \varphi} = jlA$ $(l = integer)$. The Fourier Transform along φ of the product of $C'(\varphi)A'(\theta,\varphi)e^{j\beta z}$ becomes the convolution

$$e^{j\beta z}[C(l) \oplus A(\theta,l)] \cong C_0 A(\theta,l) + C_1 A(\theta,l \mp 1) + C_2 A(\theta,l \mp 2) + \cdots$$

where

$$C_0 = \frac{1}{2\pi}\int_0^{2\pi} C(\varphi)d\varphi, \quad C_n = \frac{1}{2\pi}\int_0^{2\pi} C(\varphi)e^{jn\varphi}d\varphi$$

In general, Fourier Transforming Maxwell equations, expressed in general orthogonal cylindrical coordinate systems leads to the appearance of certain harmonics. In most cases related to optical fibers the harmonics can be omitted in practical calculations, with a negligible error due to the fact that $\Delta n = n_1 - n_2$ is very small in comparison with n_1. In this chapter these harmonics will be ignored.

4.2. Fourier representation and resonance analysis

Maxwell's equations (see appendix B, for $\frac{\partial}{\partial t} = j\omega$) expressed on a set of orthogonal cylindrical coordinates (θ, φ, z) arising from a conformal mapping $w = w(z)$,can be written for an infinitesimal layer of very small thickness $\Delta\theta$ where refractive index n can be considered constant as follows

$$\begin{cases} \frac{\partial E_z}{\partial \varphi} - \frac{\partial (hE_\varphi)}{\partial z} = -j\mu_0\omega(hH_\theta) \\ \frac{\partial (hE_\theta)}{\partial z} - \frac{\partial E_z}{\partial \theta} = -j\mu_0\omega(hH_\theta) \\ \frac{\partial (hE_\varphi)}{\partial \theta} - \frac{\partial (hE_\theta)}{\partial \varphi} = -j\mu_0\omega(h^2 H_z) \end{cases} \tag{4.1}$$

$$\begin{cases} \frac{\partial H_z}{\partial \varphi} - \frac{\partial (hH_\varphi)}{\partial z} = jn^2\varepsilon_0\omega(hE_\theta) \\ \frac{\partial (hH_\varphi)}{\partial z} - \frac{\partial H_z}{\partial \theta} = jn^2\varepsilon_0\omega(hE_\theta) \\ \frac{\partial (hH_\varphi)}{\partial \theta} - \frac{\partial (hH_\theta)}{\partial \varphi} = jn^2\varepsilon_0\omega(h^2 E_z) \end{cases} \tag{4.2}$$

Where $h^2{}_{(\varphi,\theta)} = \left|\frac{\partial w}{\partial z}\right|^2 = \frac{1}{\left|\frac{\partial z}{\partial w}\right|^2}, h = \sqrt{\left|h^2{}_{(\varphi,\theta)}\right|}$

Fourier Transforming along z and φ gives $FT(\ h^2{}_{(\theta,\varphi)}E'_{z(\theta,\varphi)}) = h^2{}_{(\theta,l)} \oplus E_{z(\theta,l)}$ and omitting the harmonics arising by the F.T. of the product we obtain $FT(\ h^2{}_{(\theta,\varphi)}E'_{z(\theta,\varphi)}) \cong h_0^2(\theta)E_z\ (\theta,l)$ where $h_0^2(\theta) = \int_0^{2\pi} h^2_{(\varphi,\theta)}\, d\varphi$. Substituting $\frac{\partial}{\partial z}\ by\ j\beta$ and $\frac{\partial}{\partial \varphi}\ by\ jl$, where $l\ integer$ the set of six partial differential Maxwell equations, becomes a set of four ordinary differential equations (for the remaining variable) and two algebraic ones as follows

$$\begin{cases} \frac{\partial \dot{E}_z}{\partial \theta} - j\beta\dot{E}_\theta = j\dot{H}_\varphi \\ \frac{\partial \dot{E}_\varphi}{\partial \theta} - jl\dot{E}_\theta = -j\left(h^2 \oplus \dot{H}_z\right) \cong -j({h_0}^2\dot{H}_z) \\ \frac{\partial \dot{H}_z}{\partial \theta} - j\beta\dot{H}_\theta = -jn^2\dot{E}_\varphi \\ \frac{\partial \dot{H}_\varphi}{\partial \theta} - jl\dot{H}_\theta = jn^2(h^2 \oplus \dot{E}_z \cong jn^2{h_0}^2\dot{E}_z \end{cases} \tag{4.3}$$

$$\begin{cases} \beta\dot{E}_\varphi - \lambda\dot{E}_z = \dot{H}_\theta \\ \lambda\dot{H}_z - \beta\dot{H}_\varphi = n^2\dot{E}_\theta \end{cases} \tag{4.4}$$

where as before $\omega\mu_0 = z_0k_0$ and $\omega\varepsilon_0 = k_0/z_0$ as well as $z_0 = \sqrt{\frac{\mu_0}{\varepsilon_0}}$ =120π and $k_0 = \omega\sqrt{\mu_0\varepsilon_0} = 2\pi/\lambda$. Symbols on the above equations represent the Fourier Transforms along z and φ of the electromagnetic field functions via the correspondences $hE_\theta \rightarrow \dot{E}_\theta z_0\ ,\ hE_\varphi \rightarrow \dot{E}_\varphi z_0, hH_\theta \rightarrow \frac{\dot{H_\theta}}{z_0}\ ,\ hH_\varphi \rightarrow \frac{\dot{H_\varphi}}{z_0}\ , E_z \rightarrow \dot{E}_z z_0\ and\ H_z \rightarrow \frac{\dot{H_z}}{z_0}$. The wave number β was also replaced by β/k_0 and h was replaced by hk_0 as well as h_0 with h_0k_0.

We again define a set of four new functions I_M, I_E, V_M, V_E in the two algebraic equations (4.4) as

$$\begin{cases} I_M = \frac{\dot{H}_\theta}{j} = \frac{\beta\dot{E}_\varphi - l\dot{E}_z}{j} \quad I_E = n^2\dot{E}_\theta = (l\dot{H}_z - \beta\dot{H}_\varphi) \\ V_M = \frac{l\dot{H}_\varphi + \beta{h_0}^2\dot{H}_z}{jF} \qquad V_E = \frac{l\dot{E}_\varphi + \beta{h_0}^2\dot{E}_z}{F} \\ F = l^2 + \beta^2{h_0}^2 \end{cases} \tag{4.5}$$

Using the new functions I_M, I_E, V_M, V_E it can be proved as in previous chapters through simple algebraic analysis that the four differential equations (4.3) are equivalent to the following two sets representing two interconnected transmission lines of length $\Delta\theta$.

$$\begin{cases} \frac{\partial V_M}{\partial \theta} = -\frac{\gamma^2 I_M}{jF} - jMI_E \\ \frac{\partial I_M}{\partial \theta} = -jFV_M \end{cases} \tag{4.6}$$

$$\begin{cases} \frac{\partial V_E}{\partial \theta} = -\frac{\gamma^2 I_E}{jn^2 F} - jMI_M \\ \frac{\partial I_E}{\partial \theta} = -jn^2 FV_E \end{cases} \tag{4.7}$$

together with the auxiliary algebraic relations

$$\begin{cases} \gamma^2 = l^2 + (\beta^2 - h^2){h_0}^2 \\ F = l^2 + \beta^2 {h_0}^2 \\ M = \beta l \frac{\partial {h_0}^2}{\partial \theta} / F^2 \end{cases} \tag{4.8}$$

Using (4.6) it can be proven that the Fourier Transforms of the Electric and Magnetic field components can be calculated from

$$\begin{cases} \dot{H}_\theta = jI_M, \;\; \dot{E}_\theta = \frac{1}{n^2} I_E \\ \dot{H}_z = \frac{l}{\varphi} I_E + j\beta V_M, \;\; \dot{E}_z = \frac{jlI_M}{F} + \beta V_E \\ \dot{H}_\varphi = jlV_M - \frac{\beta {h_0}^2}{F} I_E, \;\; \dot{E}_\varphi = lV_E + \frac{j{h_0}^2}{F} I_M \end{cases} \tag{4.9}$$

For $l = 0$ we also have M = 0 so that the set of equations (4.6) and (4.7) are independent and the corresponding transmission lines standing for the Transverse Magnetic and Transverse Electric modes (TM and TE) become decoupled. For $l \neq 0$, the transmission lines are coupled thus each of them represents two modes of transmission (two eigenmodes with eigenvalues $\gamma^2 \pm nMF$), with different transmission parameters. These eigenmodes are "normal" between each other. That means that if the one mode is non-zero, the other is zero. Finally it can be proved that

for $l \neq 0$ the Magnetic field ($\vec{H}$) is related to the respective Electric field ($\vec{E}$) with the relation $\vec{H} = \pm jn\vec{E}/z_0$ in every cylindrical layer.

We shall use symbols M (Magnetic or TE modes) and E (Electric or TM modes) for these modes which can now be written as follows:

$$\begin{cases} \frac{\partial V_M}{\partial \theta} = -\frac{(\gamma^2 - nMF)}{jFn^{tm}} I_M \\ \frac{\partial I_M}{\partial \theta} = -jFn^{tm} V_M \end{cases} \tag{4.10}$$

For $tm = \begin{cases} 0 \\ 2 \end{cases}$ there are two independent modes M

$$\begin{cases} \frac{\partial V_E}{\partial \theta} = -\frac{(\gamma^2 + nMF)}{jFn^{tm}} I_E \\ \frac{\partial I_E}{\partial \theta} = -jFn^{tm} V_E \end{cases} \tag{4.11}$$

For $tm = \begin{cases} 0 \\ 2 \end{cases}$ there are two independent modes E

To apply the resonance technique, we assume again a set of successive layers of length $\delta\theta$ in all cases that can be represented by a quadrupole as that of Figure 3.2. We also define impedances as

$$\begin{cases} Z_B = \frac{1}{2} \frac{\gamma_{HE}^2 \Delta\theta}{jFn^{tm}} \\ Z_P = \frac{1}{jFn^{tm} \Delta\theta} \end{cases} \tag{4.12}$$

for $tm = \begin{cases} 0 \\ 2 \end{cases}$. The quadrupoles representing the successive layers can be connected in series, because the equivalent "voltages" and "currents" on their boundaries are continuous due to the fact that V_M, I_M, V_E, I_E are continuous functions of θ following the normal and tangential Magnetic and Electric fields that are continuous at the boundaries. Thus, the set of the successive layers is forming an overall "Transmission Line" with pure imaginary impedances. The resonance "frequencies" of the line are the transmission wave numbers "β" of the fibers. The terminal impedances for $\theta = \infty \; and \; \theta = 0$, are the boundary conditions for the transmission line behavior. These terminal impedances should be calculated using transmission line properties or symmetry properties. Furthermore for $b = n_2$ we can calculate the cutoff condition, i.e. the minimum wave number k_0 with which a mode may exist in the fiber. For

monomode transmission, the interesting region for monomode transmission is the region between cutoff wave numbers of the fundamental mode LP_{11} and LP_{01} .

4.3. Applications in distinct coordinate systems

The method of conformal mapping for derivation of orthogonal cylindrical coordinate systems will be applied in the following cases of (a) *Elliptic Cylindrical System* (ECS), (b) *Bipolar Cylindrical System* (BCS). Which are examined separately in what follows.

4.3.1. Elliptical Cylindrical System case

We again set $w = \theta + j\varphi$, $z = c\sin(w) = x + jy = c\sinh\theta\cos\varphi + jc\cosh\Theta\sin\varphi$ so that

$$\begin{cases} x = c\sinh\theta\cos\varphi \\ y = c\cosh\theta\sin\varphi \end{cases}$$

These relations prescribe an elliptic coordinate system. In the elliptic cylindrical system for θ constant on the plane (x,y) ellipses (of two foci in distance 2c) are generated, while for φ constant, hyperbolae (of the same foci) are generated that are normal to the previous ellipses. The elliptic system can be used for the study of fibers with an elliptic core [9]. The transmission line technique has already been used for the study of elliptic core fibers. Step index elliptic fibers can be also tackled using the (complicated) Mathieu functions.

In elliptic cylindrical coordinate systems $h^2_{(\theta,\varphi)} = \frac{c^2}{2}(\cosh 2\theta - cos2\,\varphi)$ and thus omitting the harmonics we can use the previous equations via the relation $h^2_{0(\theta)} = \frac{c^2}{2}\cosh 2\theta$ which now gives $\frac{\partial h_0^2}{\partial\theta} = c^2\sinh 2\theta$ resulting in the system

$$\begin{cases} F = l^2 + \beta^2 h_0^2 \\ \gamma^2 = l^2 + (\beta^2 - n^2)h_0^2 \\ M = \beta l\frac{\partial h_0^2}{\partial\theta}/F^2 \\ \gamma_{HE}^2 = \gamma^2 - nMF \text{ and } \gamma_{EH}^2 = \gamma^2 + nMF \end{cases} \tag{4.15}$$

Each couple of modes HE or EH will be then represented by T-quadrupoles with:

$$\begin{cases} Z_B = \frac{1}{2}\frac{\gamma_{HE}^2 \Delta\theta}{jFn^{tm}} \;\; or \; Z_B = \frac{1}{2}\frac{\gamma_{EH}^2 \Delta\theta}{jFn^{tm}} \\ \qquad and \;\; Z_P = \frac{1}{jFn^{tm}\Delta\theta} \end{cases} \tag{4.16}$$

for $tm = \begin{cases} 0 \\ 2 \end{cases}$. Thus, the resonance technique can be applied assuming that $z_{in}(0)$ and $z_{out}(\infty)$ will be defined.

4.3.2. Bipolar Cylindrical fiber analysis

From $z = x + jy \;\; and \; w = \theta + j\varphi = c \bullet ln\left[\frac{z-c}{z+c}\right]$ or, equivalently $z = c\tanh(^{w}/_{2})$ we get a representation of a bipolar orthogonal cylindrical coordinate system.
Furthermore, it can be proven that

$$x = \frac{c\sinh\theta}{\cosh\theta - \cos\varphi} \;\; \text{and} \;\; y = \frac{c\sin\varphi}{\cosh\theta - \cos\varphi}$$

The previous relations for θ constant represent eccentric circles on (x,y) plane. Every eccentric circle has a radius $r_0 = \frac{c}{\sinh\theta}$ centered on (x) axis at $x_0 = \frac{c\cdot\cosh\theta}{\sinh\theta}$ so that $x_0 = r_0 \cdot \cosh\theta$. The relations for φ constant represent circles on (x,y) plane, normal to the previous circles. Every such circle has a radius $r_0 = \frac{c}{\sin\varphi}$ centered at (y) axis at $y_0 = \frac{c\cdot\cos\varphi}{\sin\varphi}$ or $y_0 = r_0 \cdot \cos\varphi$. Via the auxiliary relation

$$\frac{\partial w}{\partial z} = \frac{1}{z-c} - \frac{1}{z+c} = \frac{2c}{z^2 - c^2}$$

it can be shown that

$$h^2 = \left|\frac{\partial w}{\partial z}\right|^2 = \left[\frac{c}{\cosh\theta - \cos\varphi}\right]^2, \;\; or \;\; h = \frac{c}{\cosh\theta - \cos\varphi}$$

Furthermore we can show that

$$h_{0(\theta)}^2 = \frac{1}{2\pi}\int_0^{2\pi} h^2 d\varphi = \frac{c^2\cosh\theta}{\sinh^3\theta}.$$

from which we derive

$$\frac{\partial h_0^2}{\partial \theta} = -c^2 \left[\frac{2}{\sinh^2 \theta} + \frac{3}{\sinh^4 \theta} \right]$$

Using the previous we arrive at the system

$$\begin{cases} F = l^2 + \beta^2 h_0^2 \\ \gamma^2 = l^2 + (\beta^2 - n^2) h_0^2 \\ M = \beta l \frac{\partial h_0^2}{\partial \theta} / F^2 \\ \gamma_{HE}^2 = \gamma^2 + nMF \ and \ \gamma_{EH}^2 = \gamma^2 - nMF \end{cases} \tag{4.17}$$

For each couple of modes HE and EH we use their equivalent representations via T-quadrupoles with impedances as

$$\begin{cases} Z_B = \frac{1}{2} \frac{\gamma_{HE}^2 \Delta\theta}{jFn^{tm}} \qquad or \qquad Z_B = \frac{1}{2} \frac{\gamma_{EH}^2 \Delta\theta}{jFn^{tm}} \\ and \ Z_P = \frac{1}{jFn^{tm} \Delta\theta} \end{cases}$$

for $tm = \begin{cases} 0 \\ 2 \end{cases}$. At this point it must be noted that transmission in eccentric optical fibers has been studied before in several cases [49], [50], [51], yet without the use of the RTL technique. In this chapter it is proved that the transmission modes of the equivalent transmission line of the eccentric fibers can be computed using the RTL technique, with remarkably accurate results.

It can be proven that given eccentric core fiber defined by $r_1, r_2, and\ \delta$ as in figure, θ_1, θ_2 of the eccentric core and gladding can be calculated by the following relations:

$$\cosh \theta_1 = \frac{1}{2r_1} \left(\frac{r_2^2 - r_1^2}{\delta} - \delta \right)$$

$$\cosh \theta_2 = \frac{1}{2r_2} \left(\frac{r_2^2 - r_1^2}{\delta} + \delta \right)$$

Also in order to apply the resonance technique method, $Z_{in}\ and\ Z_{out}$ must be calculated on the periphery of the core circle defined by θ_1. The starting value for the calculation of $Z_{in}\ i.e.\ its\ value\ for\ \theta = 0\ \ is\ Z_{in(0)} = 0$ (derived using the limit $h_{0(0)}^2 \to \infty$) and we proceed up to θ_1 with a constant refractive index $n = n_1$. The starting value for the computation of $Z_{out}\ for\ \theta = \infty$ (where n=1 for air), can be

estimated considering that $h_0^2 = 0, M = 0, \gamma = l$ and $F = l^2$ thus $Z_{out(\infty)} = \frac{\gamma}{jF} = \frac{l}{jl^2} = \frac{1}{jl}$.

Proceeding towards θ_1 , $for\ \theta >\ \theta_2 n = 1,$ while in the gladding i.e. in the region $\theta_1 \leq \theta \leq \theta_2$. The recursive relations within (or outside) are derived by the T-quadrupole as follows

$$Z_{in,n+1} = \frac{(Z_{in,n} + Z_{B,n})Z_{p,n}}{Z_{in,n} + Z_{B,n} + Z_{p,n}} + Z_{B,n}$$

Finally the resonance condition is given by:

$$Z_{in(\theta=\theta_1)} + Z_{out(\theta=\theta_1)} = 0$$

The fundamental mode LP_{11} was calculated for r_2=5•r_1, $n_1$1=1.54, $n_2$2=1.47 and various eccentricities δ=r_1, 2•r_1, 3•r_1.

4.4 Numerical results for a Bipolar Cylindrical fiber

With reference to figure 4-2 it becomes clear that for fixed V values the propagation constant is reduced as the fiber becomes more eccentric. Depending on the level of eccentricity this could cause the field to reach the outer cladding boundary and increase losses. This also translates to a decreased value of W ($W = r_1 k_0 \sqrt{b^2 - n_2^{\ 2}}$) which in effect would broaden the mode field into the cladding.

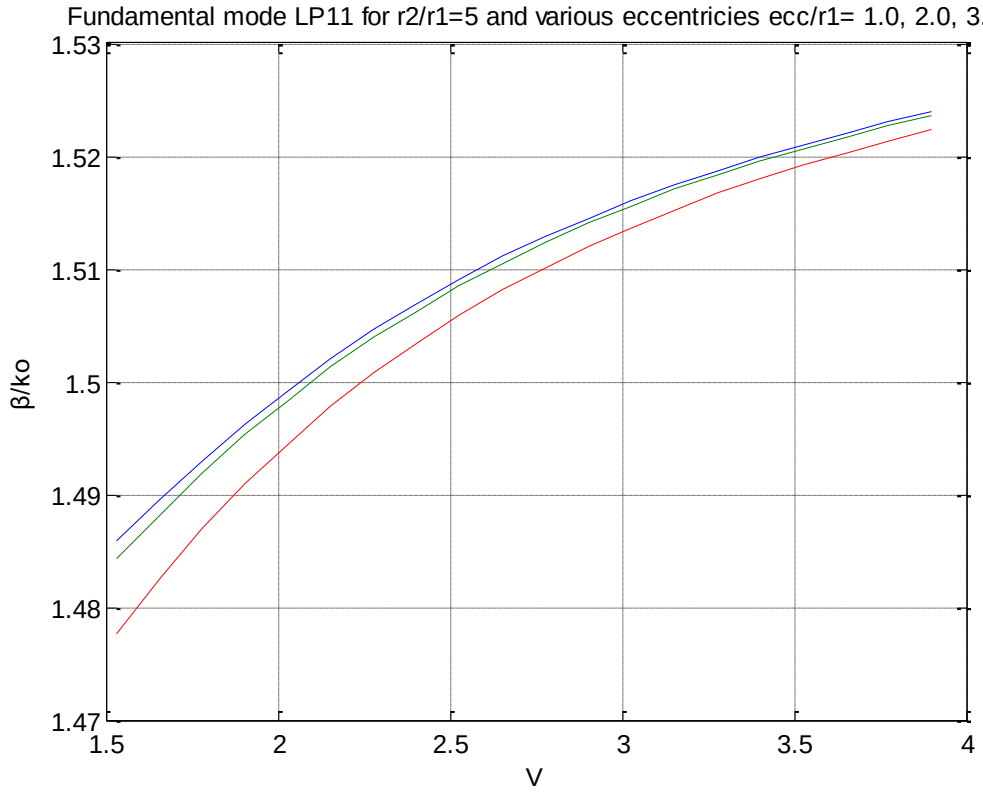

Figure 4-2 Fundamental mode normalized propagation constant, (LP11), for various normalized eccentricities δ for δ/r1 = 1.0 , 2.0 , 3.0 (n1=1.54, n2=1.47)

The fundamental mode LP_{11} can be calculated with a similar procedure as previously for given values of the c/r_1 ratio taking into account that $\theta_1 = \text{arctanh}(\frac{c}{r_1})$, $\theta_2 = \infty$. Initial impedance values are respectively $Z_{in(0)} = 0$ and $Z_{out(\infty)} = \frac{1}{jl}$, for air refractive index $n = 1$. If instead of air another gas of refractive index $n = ref$ was present than the outer terminal initial impedance should be $Z_{out(\infty)} = \frac{1}{jl(ref)}$.

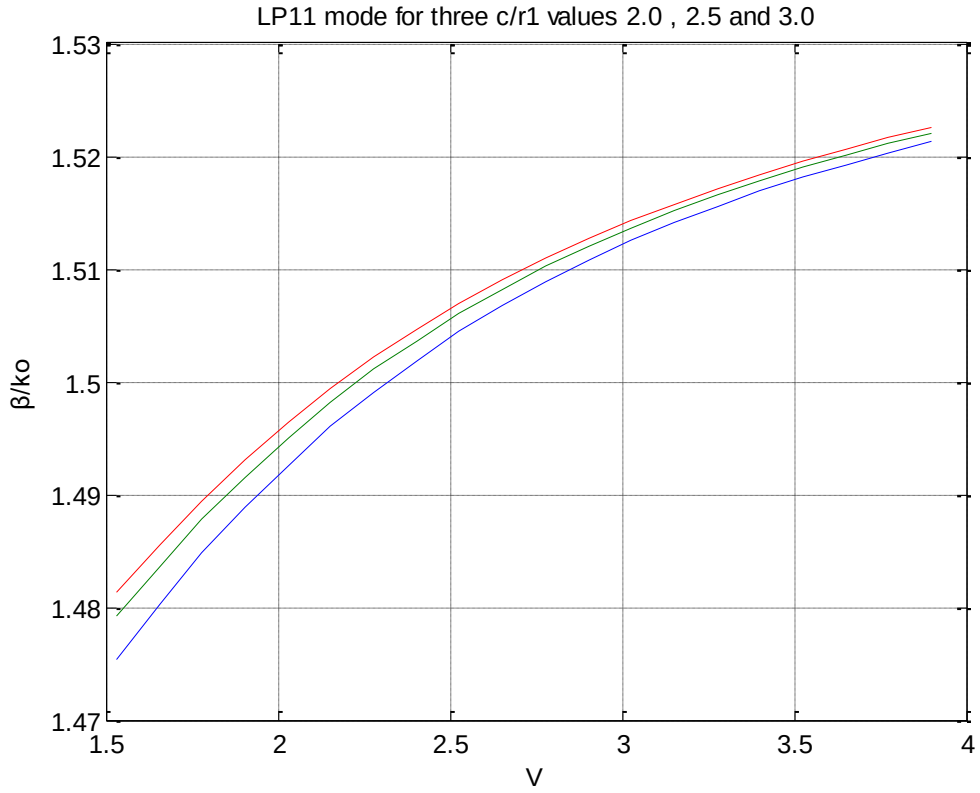

Figure 4-3 Fundamental mode (LP11), for various normalized constants c for c/r1= 2.0 , 2.5 , 3.0 . n1=1.54, n2=1.47.

The fundamental mode LP_{11} wave numbers were calculated for ratio values c/r_1=2, 2.5 and 3, as functions of $V = r_1 k_0 \sqrt{n_1^2 - n_2^2}$ as shown in figure 4-3.

4.5 The D Fiber

The analysis that takes place in the current chapter is of special interest due to its potential application to the case of the D-shaped fiber. The D-fiber is a specific type of optical fiber that combines ellipticity and eccentricity, its name deriving from the shape of its section which is shown in Figure 4-4. When it comes to fibers that retain polarization, the D fiber has two important benefits: an accurate location of the birefringence axes and an efficient way to form power splitters or directional couplers. D fiber achieves both goals by having a guiding domain that is easy to reach and a cross section that facilitates the locating of the birefringent axes. In the cross section of the D fiber, the straight part of the D is parallel to the major axis of the elliptical core.

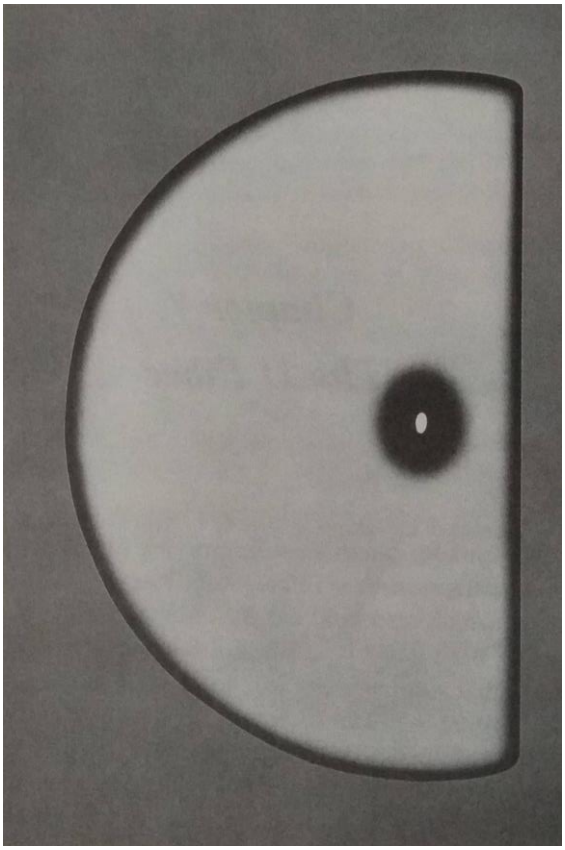

Figure 4-4 Image of a section of a D fiber [39].

The D fiber can be used in various fabrications including the loop mirror which can be applied for monitoring coupling coefficients, Indium-coated polarizers, and optoelectronic devices.

4.6 Conclusions

Conclusively, this chapter presents the combined use of Fourier Transforms, Orthogonal Curvilinear Transforms, Conformal Mapping and their application into Maxwell's Equations towards deriving Transmission Line Models of Optical Fibers with ellipticity or eccentricity in the core. The analysis reveals the modal perturbation of the perfectly circular and non-eccentric fibers. This novel method has wide range applications in D-shape optical Fiber sensing where the core is on purpose located near the surface of the flat of the D in order to increase sensitivity of the surroundings. It can be applied to fiber optic device and component manufacturing and for the study of connector losses, as well as fiber to device losses.

5 CHAPTER 5

Study of Optical Fibers with Angular Asymmetry

5.1 The case of angular dependency

This chapter presents a new approach towards the study of special types of optical fibers with altered geometry which can be characterized as unconventional fibers. At first, we shall define as conventional optical fibers all the cylindrical fibers that can be separated in a set of very thin successive cylindrical layers of average radius r of uniform refractive indexes η. The refractive indexes of the successive thin cylindrical layers in general are different for instance when the refractive index profile is solely a function of r. This profile variation from the center of the fiber up to the outer air limit, uniquely specifies the properties of each fiber.

At this point we can define as unconventional fibers the ones in which at least in some of its successive thin cylindrical layers the refractive index is varying also along its radial coordinate in general as $\eta(r,\varphi)$. This includes all fibers in which their cores are non-circular as are for example the elliptic core fibers, non-symmetric or eccentric core fibers. In these fibers all the cylindrical layers that include parts of core and parts of gladding, they have varying refractive indexes along (φ). Specifically, there will be three main aspects of altered geometry of the cross section of such fibers including eccentricity of the central hole, asymmetry, and elliptic boundary.

All the cylindrical optical fibers shall therefore be referred to as the class of conventional optical fibers (COF) for as long as they can be separated in a set of n very thin successive cylindrical layers of average radius r of uniform refractive index values ηi. Indices of successive layers will be allowed in general to be different for each step as say, η(ri). The resulting, total index profile η(r) variation from the center of the fiber up to the limit outer air medium, completely defines the propagation properties inside the fiber.

The class of unconventional optical fibers (UOF) will additionally be defined as including fibers in which at least in some of their successive thin cylindrical layers present an additional variation of the total index profile along the radial coordinate φ in the form η(r,φ). Such cases include elliptic core, non-symmetric or eccentric core fibers

and in general, all cases of not strictly circular core fibers. In these cases, any discretization into thin cylindrical layers that “cuts” through the core and cladding, results in a variation of the refractive index along φ. In figure 5-1 a related case is presented, of a thin circular cylindrical layer cutting an elliptic core fiber. As is evident in the schematic representation, the variation is analogous to the arc length of the circular sector cut by the ellipse for each discretization step.

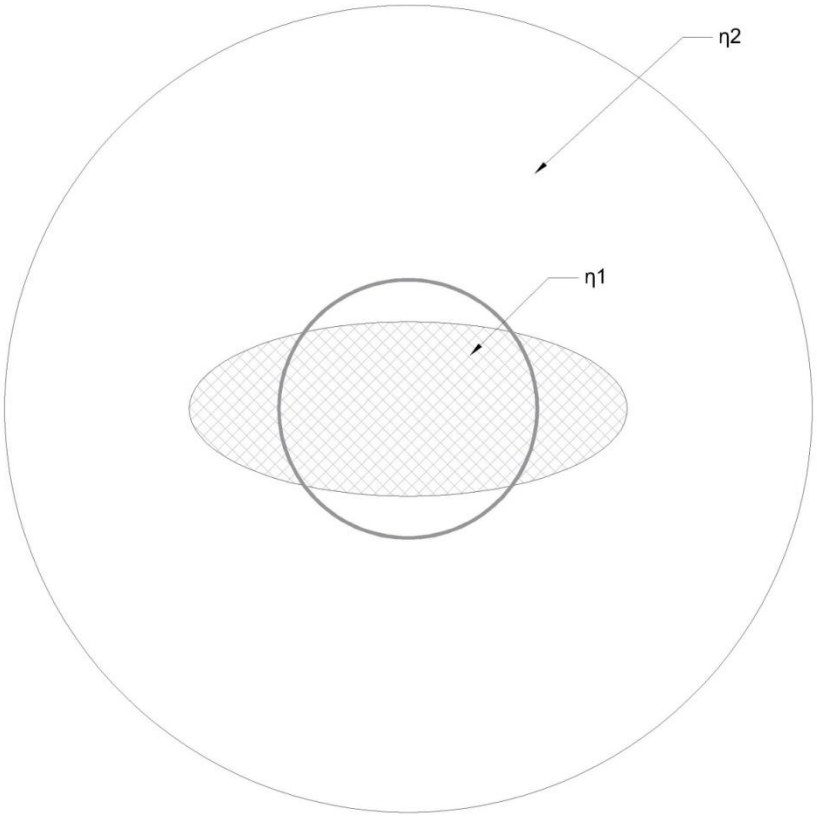

Figure 5-1 Example of the alternating character of the local index value from a thin shell radial discretization.

Additionally, photonic fibers made of silica with a set of small air holes around their centers will have many cylindrical layers of varying refractive indexes along θ. In figure 5-2, an example is shown, of a PCF with a hexagonal lattice of seven rows of air holes.

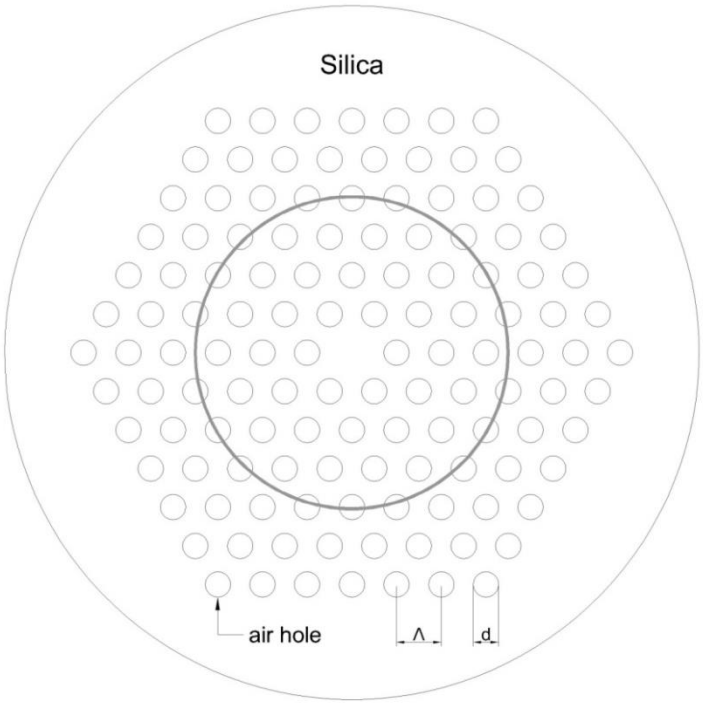

Figure 5-2 Schematic depiction of the alternating step index resulting from radial discretization in PCF.

Again, radial discretization with thin circular cylindrical layers results in alternatively cutting through air holes and silica of a PCF as depicted in the schematic. As part of the main research, this chapter presents the development of an RTL-based method aiming to include all such UOF cases via an appropriate transformation to mathematically equivalent COF cases.

5.2 Mathematical equivalence of homogeneous circular cylindrical layers to electric transmission lines

The basis for the application of the previously introduced RTL is the radial discretization of all cylindrical fibers via a separation into a succession of thin cylindrical layers each one with its own constant refractive index η. These layers can be extended outside of the cladding in order to take into consideration the effect of the surrounding air (η=1).

Following the analysis presented in chapter 2 section 6, the Maxwell equations take the forms:

$$\begin{cases} \frac{jl}{r}\overline{E_z} - j\beta\overline{E_\varphi} = -j\overline{H_r} \\ j\beta\overline{E_r} - \frac{\partial\overline{E_z}}{\partial r} = -j\overline{H_\varphi} \\ \frac{1}{r}\frac{\partial\left(r\overline{E_\varphi}\right)}{\partial r} - \frac{jl}{r}\overline{E_r} = -j\overline{H_z} \end{cases} \tag{5.1}$$

and

$$\begin{cases} \frac{jl}{r}\overline{H_z} - j\beta\overline{H_\varphi} = jn^2(r)\overline{E_r} \\ j\beta\overline{H_r} - \frac{\partial\overline{H_z}}{\partial r} = jn^2(r)\overline{E_\varphi} \\ \frac{1}{r}\frac{\partial\left(r\overline{H_\varphi}\right)}{\partial r} - \frac{jl}{r}\overline{H_r} = jn^2(r)\,\overline{E_z} \end{cases} \tag{5.2}$$

Finally it is possible to prove that the system of equations (5.1) and (5.2) can be transformed in a set of four differential equations (5.4), relating the equivalent "voltage' and "current" functions V_M, I_M, V_E, I_E defined as follows:

$$V_M = \frac{l\overline{H_\varphi}+\beta r\overline{H_z}}{jF}$$

$$I_M = \frac{r\overline{H_r}}{j} = \frac{\beta r\overline{\overline{E_\varphi}} - l\overline{E_z}}{j} \tag{5.3}$$

$$V_E = \frac{l\overline{E_\varphi}+\beta r\overline{E_z}}{F}$$

$$I_E = n^2 r\overline{E_r} = l\overline{H_z} - \beta r\overline{H_\varphi}$$

where we use the notation $F = \frac{(\beta r)^2+l^2}{r}$

$$\begin{cases} \frac{\partial V_M}{\partial r} = -\frac{\gamma^2}{jF}I_M - jMI_E \\ \frac{\partial I_M}{\partial r} = -jFV_M \\ \frac{\partial V_E}{\partial r} = -\frac{\gamma^2}{jn^2F}I_E - jMI_M \\ \frac{\partial I_E}{\partial r} = -jn^2FV_E \end{cases} \tag{5.4}$$

In (5.4) we introduced the total propagation factor $\gamma^2 = \frac{l^2}{r^2} + \beta^2 - n^2$ and the auxiliary function $M = \frac{2l\beta}{[(\beta r)^2+l^2]F}$.

At this point it is noticed that V_M, I_M, V_E, I_E are continuous functions at the boundaries because the tangential components of electric and magnetic fields $\overrightarrow{H_\varphi}\ \overrightarrow{H_z}$ and $\overrightarrow{E_\varphi}\ \overrightarrow{E_z}$ on the cylindrical surface are continuous functions passing the boundaries of the cylindrical layer. Using the previous relations, the Fourier Transforms of the Electro-Magnetic field components along (r, l, β) can be expressed as functions of their equivalent "voltages" and "currents" functions with the auxiliary relations

$$\overline{H_r} = {jI_M}/{r}\,, \qquad \overline{E_r} = \frac{I_E}{n^2 r}$$

$$\overline{H_\varphi} = jlV_M\ /r - \frac{\beta}{F} I_E$$

$$\overline{E_\varphi} = lV_E/r + j\frac{\beta}{F} I_M$$

$$\overline{H_z} = \frac{l}{Fr} I_E + j\beta V_M$$

$$\overline{E_z} = -j\frac{l}{Fr} I_M + \beta V_E$$

It becomes evident by inspection that the final equations (5.4) represent two coupled electric transmission lines.

5.3 Decoupling the transmission line equations

Following the analysis from chapter 2.7

$$\begin{cases} \frac{\partial V_M}{\partial r} = -\frac{\xi^2}{jF} I_M \\ \frac{\partial I_M}{\partial r} = -jF I_M \end{cases} \tag{5.5}$$

$$\begin{cases} \frac{\partial V_E}{\partial r} = -\frac{\xi^2}{jn^2 F} I_E \\ \frac{\partial I_E}{\partial r} = -jFn^2 I_E \end{cases} \tag{5.6}$$

Thus the set of two coupled transmission lines (5.4) is equivalent to two independent transmission lines (5.5) and (5.6).

The two waves represented by the equations of transmission lines (5.5) and (5.6), are geometrically normal because the first is related to Magnetic field and the second to

Electric field that are geometrically normal for transmitted EM waves. This property is an inherent property of EM modes in optical fibers related to birefringence phenomena. However, the β respective values, for any mode, are always found to be very close and can be considered as practically equal.

5.4. Equivalent circuits for cylindrical layers, boundary conditions and birefringence

Taking into consideration the transmission line theory, it can be proved that each layer of infinitesimal thickness δr is equivalent to a T-circuit as the one shown in Figure 3

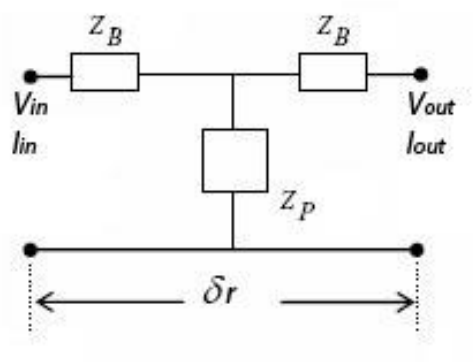

Figure 5-3 The equivalent quadrupole for each cylindrical sector.

$$\begin{cases} Z_B = \dfrac{\xi}{jF}\tanh\left[{}^{(\xi\delta r)}/_{2}\right] \\ Z_p = \dfrac{\xi}{jF\sinh(\xi\delta r)} \end{cases}$$

For $\xi\delta r \ll 1$ the impedances can be approximated by the equivalent relations

$$\begin{cases} Z_B = \dfrac{\xi^2\left({}^{\delta r}/_{2}\right)}{jF} \\ Z_p = \dfrac{1}{jF\delta r} \end{cases} \tag{5.7}$$

If $\xi^2 > 0$, both Z_B, Z_p are "capacitive" reactances, for $\xi^2 < 0$ however Z_B becomes "inductive" reactance. For (V_E, I_E) the approximate respective impedances of the T-circuit are given as

$$\begin{cases} Z'_B = \frac{\xi^2\left(\delta r/_2\right)}{jn^2F} \\ Z'_p = \frac{1}{jn^2F\delta r} \end{cases} \tag{5.8}$$

As previously stated the functions (V_M, I_M) of each layer are continuous at the cylindrical boundaries of the layer, thus if we divide the fiber (including a sufficient number of air layers) in successive thin layers and replace them by their equivalent T-circuits, an overall lossless transmission line is formed with only reactive elements. For given 'l', the 'β'' values that lead to the resonance of the overall transmission line are the eigenvalues of the whole optical fiber.

When a transmission line is in resonance, at any arbitrary point r_0 of the line, the sum of reactive impedances arising from the successive T-circuits on the left and right sides of r_0 should be equal to zero, thus the equation giving the eigenvalues of the transmission line is the following :

$$\{\dot{Z}_{L.r_0} + \dot{Z}_{R.r_0} = 0 \tag{5.9}$$

Equation (5.9) provides the eigen-values 'β ' for a given 'l' , where $\dot{Z}_{L.r_0}$, $\dot{Z}_{R.r_0}$ are the overall reactive impedances of successive T-circuits on the left and right of r_0, using (5.7) or (5.8). The value of r_0 is usually given by the core radius. For the same 'l' the equations (5.7) and (5.8) give usually slightly different values of *'β'*, this phenomenon has already been defined as "Birefringence". For circular step index fibers the birefringence is negligible, however for elliptic fibers and fibers of any other non-circular cores the birefringence phenomenon could be significant.

In order to calculate the overall reactive impedances on the left and right of r_0 we should find the impedances for $r \to 0$ and for $r \to \infty$. As we proceed to 0 or to ∞ the remaining piece of transmission line becomes "homogeneous" i.e. its overall reactive impedance is equal to its characteristic impedance given by $Z = \frac{\xi}{jF}\left(or\ \frac{\xi}{jn^2F}\right)$. Then we must have

$$r \to \infty: F \to \beta^2 r, MF \to 0, \xi \to \sqrt{\beta^2 - n^2} \rightarrow Z_{r\to\infty} = 0$$

$$r \to 0: F \to \frac{l^2}{r},\ \xi \to \frac{l}{r} \rightarrow Z_{r\to 0} = \frac{1}{j|l|}\left(or\ \frac{1}{jn^2|l|}\right)$$

For $l=0$ $Z_{r\to 0}=\infty$ (open circuit at the center of the equivalent transmission line) It is useful to notice that there is an equivalence between our formulation and the classic formulation modes of optical fibers. In particular, for $l=0$, the modes (V_M,I_M) are the TM modes ,while the modes (V_E,I_E) are the TE modes. For $l>0$, the modes (V_M,I_M) are the HE modes ,while the modes (V_E,I_E) are their HE birefringence modes. For $l<0$ the modes (V_M,I_M) are the EH modes ,while the modes (V_E,I_E) are their EH birefringence modes.

5.5. Calculating "Voltages" V_M , V_E and "Currents" I_M , I_E and resulting fields

For any given l, using the resonance technique the β values of the two birefringence modes can be calculated. These β values are practically the same, thus we can consider them as equal or we can consider as the proper value of β the mean value of the two modes.

Taking $V_M=1$ at the center point of the fiber($r=0$) , the respective value of I_M at the same point can be calculated by the respective terminal impedance. Using the matrix relations between input-output for the equivalent successive T-circuits, the values of V_M and I_M at the rest thin cylindrical layers can be calculated. In fact from the general theory of the telegrapher's equation we know that the inputs and outputs are associated via a transfer matrix as follows

$$\begin{cases} [V_{out}I_{out}]=\begin{pmatrix}\cosh(\xi(r)\cdot\delta r) & Z(r)\cdot\sinh(\xi(r)\cdot\delta r)\\ \sinh(\xi(r)\cdot\delta r)/Z(r) & \cosh(\xi(r)\cdot\delta r)\end{pmatrix}\begin{bmatrix}V_{in}\\ I_{in}\end{bmatrix}\approx \\ \approx\begin{pmatrix}1 & Z(r)\cdot(\xi(r)\cdot\delta r)\\ (\xi(r)\cdot\delta r)/Z(r) & 1\end{pmatrix}\begin{bmatrix}V_{in}\\ I_{in}\end{bmatrix}= \\ =\begin{pmatrix}1 & \xi^2(r)\cdot\delta r/jF(r)\\ jF(r)\cdot\delta r & 1\end{pmatrix}\begin{bmatrix}V_{in}\\ I_{in}\end{bmatrix}\end{cases} \tag{5.10}$$

In (5.10), the characteristic impedance should be taken as $Z(r)=\xi(r)/jF(r)$ to fit with the previous analysis. Using the relations $nV_E=V_M$ and $nI_M=I_E$ the respective values of their birefringence equivalents can also be calculated for every thin cylindrical layer r_i.

5.6. Unconventional fibers

The refractive index n(r,φ) of the fiber with a UOF profile in general can be described as a function of both *r* and φ. Each cylindrical layer of an average radius r is considered to have a local value η (φ) for $r = \frac{r_1+r_2}{2}$. Again, we make use of the generic form of Maxwell equations as in the previous section. Fourier Transforming the first vector equation gives the same set of equations as in (5.1), since there is no difference with the UOF case, however the second Maxwell vector equation due to presence of the general *n* function should now be written as

$$\begin{cases} \frac{jl}{r}\overline{H_z} - j\beta\overline{H_\varphi} = jn(\varphi)^2 \otimes \overline{E_r} \\ j\beta\overline{H_r} - \frac{\partial\overline{H_z}}{\partial r} = jn(\varphi)^2 \otimes \overline{E_\varphi} \\ \frac{1}{r}\frac{\partial(r\overline{H_\varphi})}{\partial r} - \frac{jl}{r}\overline{H_r} = jn(\varphi)^2 \otimes \overline{E_z} \end{cases} \quad (5.11)$$

The symbol $\otimes$ means convolution arising by the product of two functions of the variable φ. In the following paragraphs it will be shown how to escape this mathematical difficulty for the usual unconventional optical fibers.

5.7. UOF with non-circular, non-symmetric or eccentric cores

For unconventional fibers of non-circular cores there are a set of circular layers where the refractive index varies between the inner and outer core and cladding values respectively. In any such case, the function $n(\varphi)^2$ is a sum of a steady component n^2 and a periodic function of φ of period 2π thus can be written as a Fourier series $n(\varphi)^2 = n^2 + \sum_{-\infty}^{+\infty} N_k \exp(jk\varphi)$. Thus $< n(\varphi)^2 >= n^2$.

Taking into consideration that the convolution of the product of an exponential function $\exp(jk\varphi)$ with any function A(φ) of a Fourier Transform $A(l)$ is equal to $A(l+k)$, i.e. the convolution generates "harmonics". The function $n(\varphi)^2$ is in a set of cylindrical thin layers, a sum of step functions alternating between the values n_1^2 *and* n_2^2 , where n_1 *and* n_2 are refractive indexes of core and gladding. Considering that in optical fibers the refractive indices of core and cladding are very close, it can be effectively assumed that $(n_1 - n_2)/n_1 \ll 1$. As a result, any harmonic factors N_k of

the function $n(\varphi)^2$ are negligible in comparison to its steady component n^2 and can be omitted.

As an example, the harmonics become maximal for equal alternation steps. In this case the first harmonic, that has the maximum value among all other harmonics, is equal to $A_1 = \frac{2(n_1^2 - n_2^2)}{\pi}$, while the steady component n^2 equals $(n_1^2 + n_2^2)/2$ and we can make an approximation as $A_1/n^2 \simeq (4/\pi)(n_1 - n_2)/n_1 \ll 1$.

Thus, for optical fibers we can always assume that $< n(\varphi)^2 >= n^2$. Then the system (5.11) will become equivalent to the following

$$\begin{cases} \frac{jl}{r}\overline{H_z} - j\beta\overline{H_\varphi} = jn^2\overline{E_r} \\ j\beta\overline{H_r} - \frac{\partial\overline{H_z}}{\partial r} = jn^2\overline{E_\varphi} \\ \frac{1}{r}\frac{\partial(r\overline{H_\varphi})}{\partial r} - \frac{jl}{r}\overline{H_r} = jn^2\overline{E_z} \end{cases} \quad (5.12)$$

We can then follow the analysis that we did with the conventional fibers, where n^2 is the average value of the $\eta^2(\varphi)$ of each layer along φ in the [0, 2π] interval.

5.8. Application to elliptic core fibers

The method was applied to the calculation of fundamental modes of a fiber of elliptic core of *a* and *b* major and minor semi-axis respectively with refractive index n1=1.54, and a cladding value of n2=1.47 (figure 5-1) for various wavelengths (defined by various V factor values $V = b * 2 * \pi\sqrt{n_1^2 - n_2^2}$) and four ratios *a/b*=1.1,1.3,1.5,2.0. Results are compared with previous results calculated with Mathieu functions with the results differing only by 0.01÷ 0.123 %.

The steady component of the refractive index for the calculations for each radius *r* is defined as n1 for r<b, n2 for r>a and as $(n_1 * \varphi_1 + n_2 * \varphi_2)/\pi$ when b<r<b, where φ_1 ,φ_2 are the arcs of the circle of radius r, inside and outside the ellipse in the upper semi ellipse.

COMPARISON OF ELLIPSE FOR THE FUNDAMENTAL MODES				
a/b=1.1	**Mathieu**	**TR**		
V	**$b_{11,\,No}$**	**$b_{11,\,No}$**	**DIFF**	**relDIFF(0/00)**
1.5	1,487454917000000	1,487538376725580	-0,000083459725580	0,056109079
1.7	1,493245000000000	1,493450986151880	-0,000205986151880	0,137945315
1.9	1,498457700000000	1,498722795582640	-0,000265095582640	0,17691229
2.1	1,503029750000000	1,503312465850780	-0,000282715850780	0,188097309
2.3	1,506994250000000	1,507270533663140	-0,000276283663140	0,183334252
2.5	1,510418500000000	1,510675880979590	-0,000257380979590	0,170403752
2.7	1,513376830000000	1,513609496242670	-0,000232666242670	0,153739794
2.9	1,515936970000000	1,516144774928280	-0,000207804928280	0,13708019
3.1	1,518160870000000	1,518344840727660	-0,000183970727660	0,121179996
3.3	1,520101500000000	1,520262686679180	-0,000161186679180	0,106036787

Table 5-1 Elliptic fiber with three indicative elliptic thin layers. Inside the ellipse $r<b(n=n_1)$, outside the ellipse $r>a(n=n_2)$ and partly outside $b<r<a$ $(n_1>n>n_2)$. Ellipticity: 1.1

COMPARISON OF ELLIPSE FOR THE FUNDAMENTAL MODES				
a/b=1.3	**Mathieu**	**TR**		
V	**$b_{11,\,No}$**	**$b_{11,\,No}$**	**DIFF**	**relDIFF(0/00)**
1.5	1,491188512000000	1,491027765079550	0,000160746920450	0,107797853
1.7	1,497028990000000	1,496897637511800	0,000131352488200	0,087742114
1.9	1,502119714000000	1,501986592174880	0,000133121825120	0,088622647
2.1	1,506471523000000	1,506335918376860	0,000135604623140	0,090014727
2.3	1,510205927000000	1,510039049600890	0,000166877399110	0,110499764
2.5	1,513423500000000	1,513196002523000	0,000227497477000	0,150319773
2.7	1,516170122000000	1,515897403413190	0,000272718586810	0,179873342
2.9	1,518513480000000	1,518220317018870	0,000293162981130	0,193059189
3.1	1,520539300000000	1,520228501721160	0,000310798278840	0,204400030
3.3	1,522298190000000	1,521974104375010	0,000324085624990	0,212892341

Table 5-2 Elliptic fiber with three indicative elliptic thin layers. Inside the ellipse $r<b(n=n_1)$, outside the ellipse $r>a(n=n_2)$ and partly outside $b<r<a$ $(n_1>n>n_2)$. Ellipticity: 1.3

COMPARISON OF ELLIPSE FOR THE FUNDAMENTAL MODES				
a/b=1.5	**Mathieu**	**TR**		
V	**$b_{11,\ No}$**	**$b_{11,\ No}$**	**DIFF**	**relDIFF(0/00)**
1.5	1,494250610000000	1,493636836360350	0,000613773639650	0,410756827
1.7	1,499922346000000	1,499340905733040	0,000581440266960	0,387646913
1.9	1,504818670000000	1,504203108321470	0,000615561678530	0,409060368
2.1	1,509039170000000	1,508315227121150	0,000723942878850	0,479737633
2.3	1,512533150000000	1,511793195339390	0,000739954660610	0,489215500
2.5	1,515493100000000	1,514745797603970	0,000747302396030	0,493108412
2.7	1,518011570000000	1,517265908951310	0,000745661048690	0,491209068
2.9	1,520166130000000	1,519429880525980	0,000736249474020	0,48432172
3.1	1,522019120000000	1,521299532774000	0,000719587226000	0,472784617
3.3	1,523620800000000	1,522924688766490	0,000696111233510	0,456879582

Table 5-3 Elliptic fiber with three indicative elliptic thin layers. Inside the ellipse $r<b(n=n_1)$, outside the ellipse $r>a(n=n_2)$ and partly outside $b<r<a$ $(n_1>n>n_2)$. Ellipticity: 1.5

COMPARISON OF ELLIPSE FOR THE FUNDAMENTAL MODES				
a/b=2	**Mathieu**	**TR**		
V	**$b_{11,\ No}$**	**$b_{11,\ No}$**	**DIFF**	**relDIFF(0/00)**
1.5	1,499390500000000	1,497675992184210	0,001714507815790	1,143469840
1.7	1,504727250000000	1,502885066432660	0,001842183567340	1,224264110
1.9	1,509110880000000	1,507251064452310	0,001859815547690	1,232391584
2.1	1,512712190000000	1,510915134944720	0,001797055055280	1,187968913
2.3	1,515667864000000	1,514006539095880	0,001661324904120	1,096100896
2.5	1,518085750000000	1,516632675098700	0,001453074901300	0,957175773
2.7	1,520047200000000	1,518879733445780	0,001167466554220	0,768046252
2.9	1,521631209000000	1,520816115931370	0,000815093068630	0,535670578
3.1	1,522869900000000	1,522496060692140	0,000373839307860	0,245483418
3.3	1,523799100000000	1,523962746538420	0,000163646538420	0,107393775

Table 5-4 Elliptic fiber with three indicative elliptic thin layers. Inside the ellipse $r<b(n=n_1)$, outside the ellipse $r>a(n=n_2)$ and partly outside $b<r<a$ $(n_1>n>n_2)$. Ellipticity: 2.0

In the following figure 5-4 the β diagram of the fundamental even mode of an elliptic fiber with semi axis ratio aa/bb=2, n_1=1.54 and n_2=1.47 and variable factor defined by : $V = bb \cdot k_0 \cdot \sqrt{n_1^2 - n_2^2}$) is shown

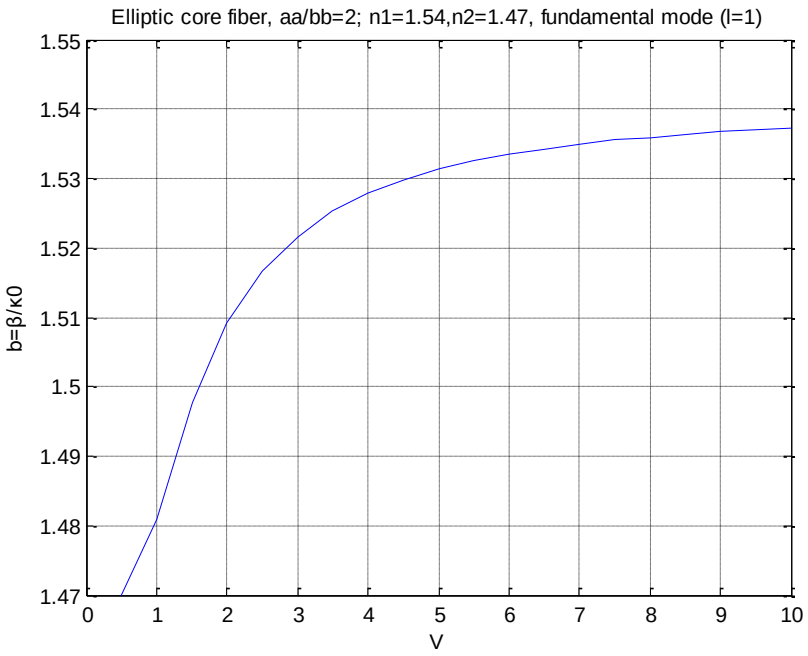

Figure 5-4 β-V diagram of the even fundamental mode an elliptic fiber of semi axis ratio aa/bb=2 and core refractive index 1.54 and gladding index 1.47

5.9. Application to rectangular core fiber

The method was applied also in the calculation of fundamental modes of a fiber with an rectangular core (see figure 5-5) of aa and bb semi sides, with refractive index n1=1.54, and a gladding of refractive index n2=1.47, for various wavelengths, defined by various V factor values $V = bb \cdot k_0 \cdot \sqrt{n_1^2 - n_2^2}$ and four ratios a/b=1.1,1.3,1.5,2.0.

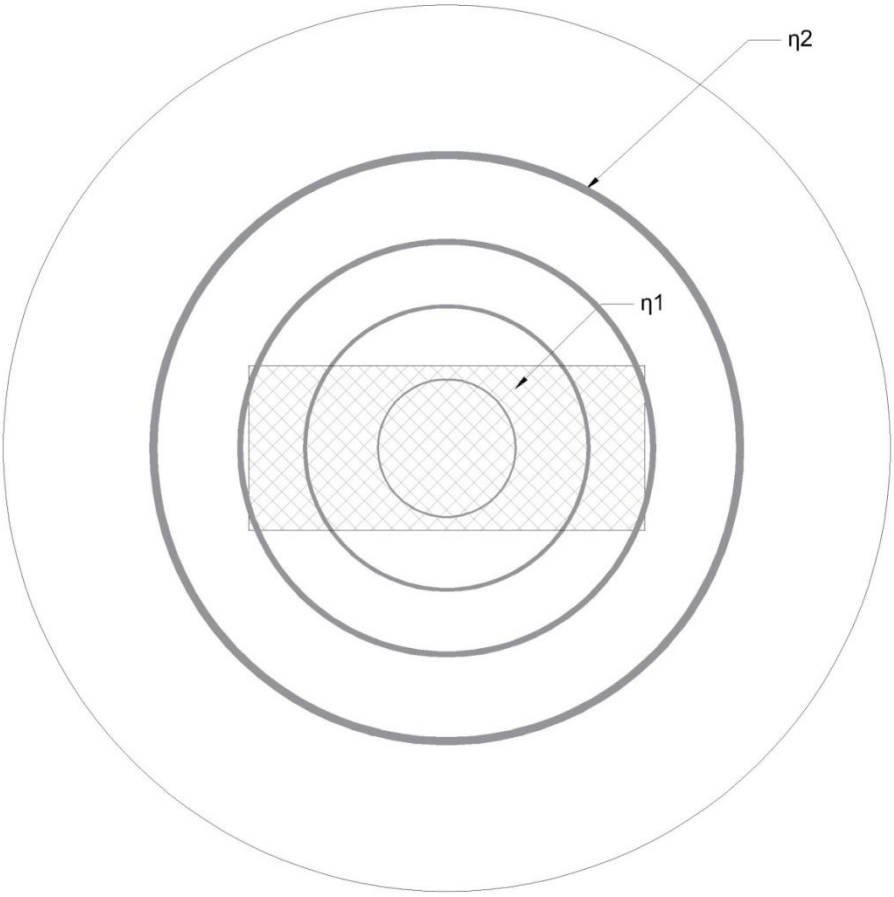

Figure 5-5 Rectangular core fiber of semi sides aa and bb , for r<bb, $n=n_1$, for r>aa, $n=n_2$, for bb<r<aa, $n_2<n<n_1$

The birefringence results are compared with the birefringence results of the elliptic core fiber with equal semi axis. The steady component of the refractive index for the calculations for each radius r is defined as n1 for r<b, n2 for r>a and as $(n_1 * \varphi_1 + n_2 * \varphi_2)/\pi$ when b<r<b, where φ_1 ,φ_2 are the arcs of the circle of radius r, inside the orthogonal and outside the orthogonal in the upper semi orthogonal.

COMPARISON OF BIREFRINGENCE FOR ELLIPTICAL AND ORTHOGONAL CORE FIBERS

	Rectangular core		Elliptic core
a/b=1.1 V	Fundamental Mode Values	Birefringence (TR)	Birefringence (TR)
1.5	1,492539945916010	0,000346704531850	0,000303585935370
1.7	1,498357447022790	0,000513384576600	0,000575417316090
1.9	1,503350570368440	0,000576764589930	0,000712035787010
2.1	1,507590076049970	0,000580793732230	0,000757892695190
2.3	1,511183551577450	0,000554099561380	0,000750121835720
2.5	1,514237341469060	0,000513428535340	0,000713597265680
2.7	1,516844499544290	0,000468033918970	0,000663528284040
2.9	1,519082616576080	0,000422786387590	0,000608733773240
3.1	1,521015087494710	0,000380083447450	0,000554096605350
3.3	1,522693317372840	0,000340959781570	0,000502161305990

Table 5-5 Comparison of birefringence values between fibers of rectangular and elliptical core. Ellipticity 1.1

COMPARISON OF BIREFRINGENCE FOR ELLIPTICAL AND ORTHOGONAL CORE FIBERS

	Rectangular core		Elliptic core
a/b=1.3 V	Fundamental Mode Values	Birefringence (TR)	Birefringence (TR)
1.5	1,495847758922450	0,000344065006270	0,000325722889410
1.7	1,501459058153440	0,000451639480470	0,000520210503450
1.9	1,506179273220210	0,000480411129310	0,000601842058430
2.1	1,510134432440230	0,000468166987430	0,000615857816190
2.3	1,513456882268610	0,000436878544030	0,000593498171210
2.5	1,516262818410440	0,000398422704380	0,000553682765940
2.7	1,518648025192190	0,000358904227450	0,000507155757960
2.9	1,520689537973830	0,000321272665480	0,000459732120240
3.1	1,522448794667530	0,000286796641510	0,000414381305640
3.3	1,523974761485380	0,000255871394240	0,000372472456950

Table 5-6 Comparison of birefringence values between fibers of rectangular and elliptical core. Ellipticity 1.3

COMPARISON OF BIREFRINGENCE FOR ELLIPTICAL AND ORTHOGONAL CORE FIBERS

	Rectangular core		Elliptic core
a/b=1.5 V	Fundamental Mode Values	Birefringence	Birefringence (TR)
1.5	1,498120450723510	0,000278361237480	0,000295449461120
1.7	1,503463400911670	0,000357573590440	0,000442306154260
1.9	1,507908503417930	0,000376605061620	0,000497613358440
2.1	1,511610102671980	0,000365648210230	0,000501375052490
2.3	1,514709614765410	0,000341283334480	0,000478771792790
2.5	1,517324041962060	0,000312143747180	0,000444266137270
2.7	1,519546684126380	0,000282536889750	0,000405759261530
2.9	1,521451022056960	0,000254483058070	0,000367378187930
3.1	1,523094834995030	0,000228815613970	0,000331142666700
3.3	1,524523718254910	0,000205765806060	0,000297919827130

Table 5-7 Comparison of birefringence values between fibers of rectangular and elliptical core. Ellipticity 1.5

COMPARISON OF BIREFRINGENCE FOR ELLIPTICAL AND ORTHOGONAL CORE FIBERS

	Rectangular core		Elliptic core
a/b=2 V	Fundamental Mode Values	Birefringence (TR)	Birefringence (TR)
1.5	1,501154370588750	0,000115100455570	0.00017851280204
1.7	1,505905455821760	0,000185956233950	0.00028097261437
1.9	1,509839664490200	0,000217496051150	0.00032331073887
2.1	1,513123501262850	0,000227441962700	0.00033221109868
2.3	1,515890438928040	0,000225620967080	0.00033221109868
2.5	1,518243818452060	0,000217498908240	0.00030589412246
2.7	1,520263082984900	0,000206163759050	0.00028459934024
2.9	1,522009559228890	0,000193389032200	0.00026227629912
3.1	1,523531014266760	0,000180203858540	0.00024038749997
3.3	1,524865056067340	0,000167204354840	0.00021967555642

Table 5-8 Comparison of birefringence values between fibers of rectangular and elliptical core. Ellipticity 2.0

For comparison reasons the average refractive indexes as functions of r, for an elliptic core fiber and for a rectangular core fiber of the same aa and bb and aa/bb=2, are shown in figure 5-6.

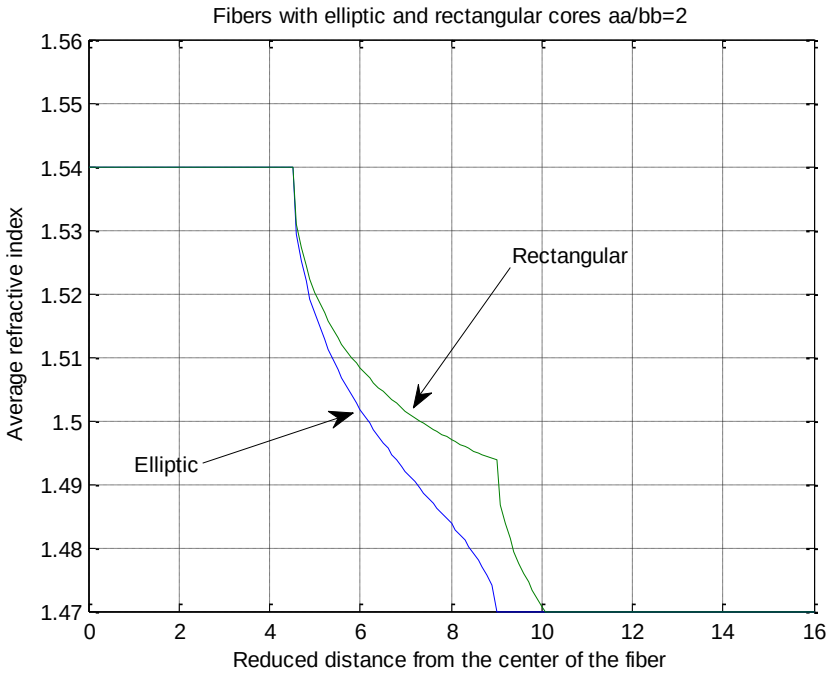

Figure 5-6 Average refractive indexes of circular thin layers of elliptic and rectangular core fibers

5.10. The PCF case

In case of a holey fiber, we separate the whole fiber circular cross-section into a set of thin cylindrical layers variable η along φ extending beyond the cladding to take into account the surrounding air with η=1. Each layer's thickness is $\delta r = r_1 - r_2$. We can then approximate $n(r,\varphi)$ as $n(\varphi)$ for the average r $<r> = r + \delta r/2$. The refractive index can be written as a Fourier series i.e. as $n(\varphi)^2 = < n >^2 + \sum_{-\infty}^{+\infty} N_k \exp(jl\varphi)$. Taking into account the properties of the Fourier transform we see that $FT(\exp(jl\phi)\cdot f(\varphi)) = f(l + l')$ so that the expressions in the second terms of equation (5.11) spread around a spectrum of harmonics. This is also to be understood as a result of successive scatterings from the bored air holes. We can now use the natural geometry of the usual hexagonal lattice to see that for each set of holes we can have either 6k harmonics. For the fundamental harmonic of l'=1 the derived harmonics passing through a layer of 6k holes should be 6k+1. Thus the fundamental wave crossing the successive layers, "sees" a different set of periodic rectangle functions that will be shown rigorously to contribute a different number of harmonics (7,13,19, etc.).

For a common harmonic to pass through, an integer product must be considered which leads to higher and higher harmonics thus cutting out the entire spectrum apart from the last highest frequency. We conclude that for holey optical fibers the approximation for any of its cylindrical thin layers, $\eta(r,l)^2 \approx \eta^2(r) = \eta^2$ suffices for further analysis of the resulting equations. Thus the original system (5.11) becomes

$$\begin{cases} \frac{jl}{r}\overline{H_z} - j\beta\overline{H_\varphi} = jn^2\overline{E_r} \\ j\beta\overline{H_r} - \frac{\partial\overline{H_z}}{\partial r} = jn^2\overline{E_\varphi} \\ \frac{1}{r}\frac{\partial(r\overline{H_\varphi})}{\partial r} - \frac{jl}{r}\overline{H_r} = jn^2\overline{E_z} \end{cases} \quad (5.13)$$

For the usual hexagonal pattern of holes we may utilize elementary analytical geometry to derive the two separate regions where the refractive index alternates between the air refractive index η=1 value and the higher value of the crystal material. We assume that along each separate layer a large circle corresponding to each cylindrical shell of radius r from the center of the fiber to the center of a smaller hole of radius *r << r0* is cut while moving clockwise along the large circle.

Prescribing a set of circles of successive radii r, for each of which we can find the air holes (in 1/6 angle of the PCF) which are cut by the corresponding radius each time. Each arc is computed inside its respective air hole and the total sum of them divided by π/3 expresses the average squared refractive index. As a matter of fact, the square of the refractive index in this sum is equal to one, while the refractive index in the rest arc is the square of the silica refractive index. Hence the average refractive index can be easily calculated along *r*. Figures 5-7, 5-8 and 5-9, present the average refractive index and the Electric field of a hexagonal PCF, of η=1.46 with a twelve layers lattice, as functions of the reduced distance from the center of the fiber for the fundamental mode. The figures were generated by a MATLAB code for air-hole diameter equal to 0.8 of the air-hole distance and the air hole diameter was 3.87 times the transmitted wavelength. We also notice the parametrization used as $= (\Lambda - d/2) * 2 * \pi\sqrt{n_1^2 - n_2^2}$), $n_{1\text{ for the}}$ silica refractive index , n_2 ≃minimum refractive index=1.123, Λ for the reduced air hole distance, d for the reduced air hole diameter and, $\Lambda - d/2$=reduced inner core of PCF.

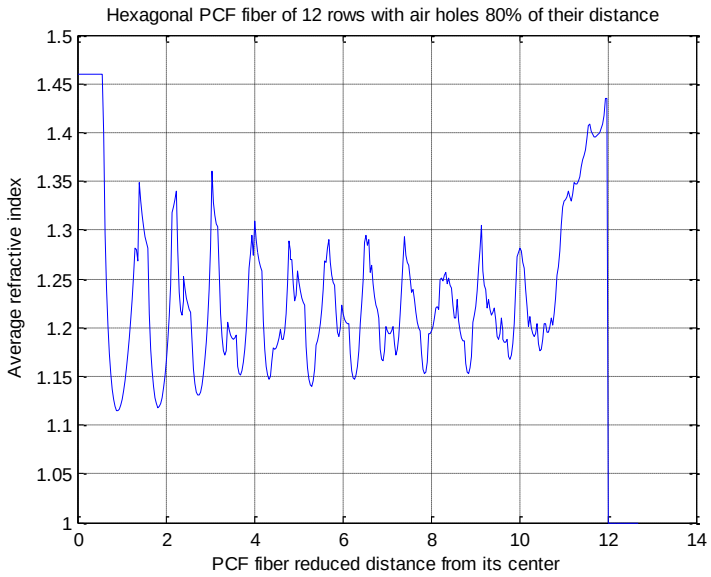

Figure 5-7 Average refractive index for fundamental mode β= 1.343357214454637

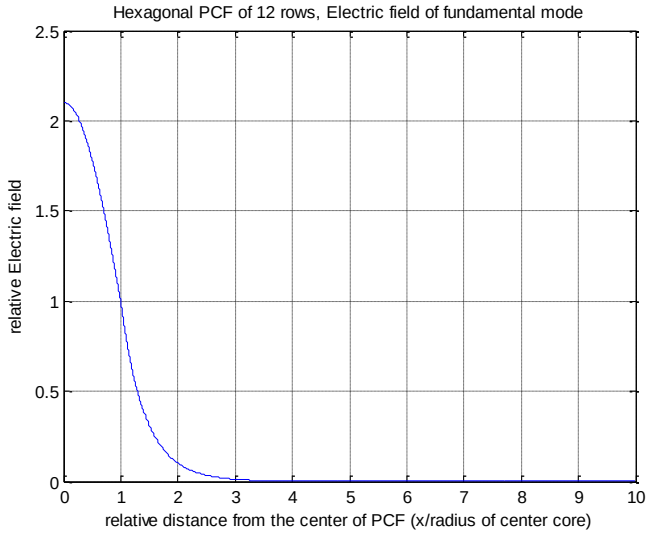

Figure 5-8 Relative Electric Field distribution for Hexagonal PCF

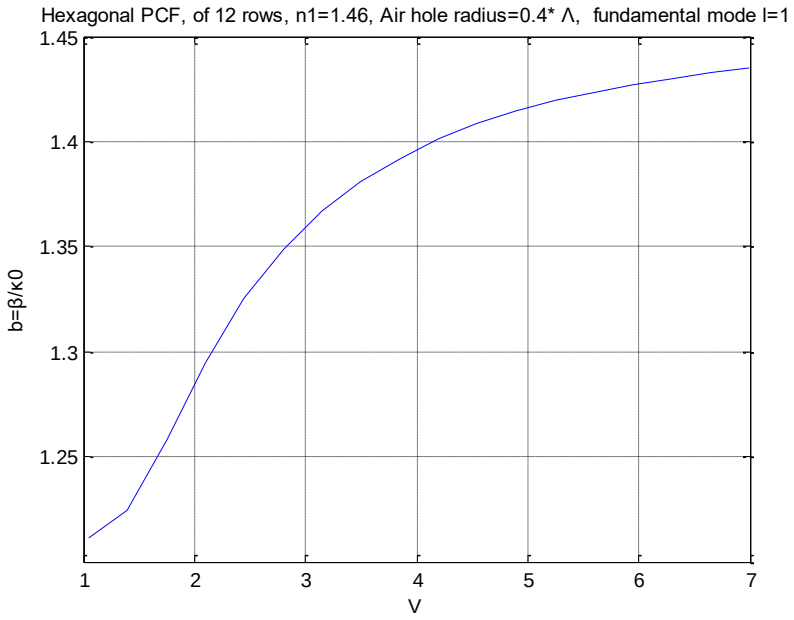

Figure 5-9 b-V diagram for fundamental mode in Hexagonal PCF

5.11 Conclusion

The presented resonance technique can be used for the study of unconventional fibers i.e. fibers with cores of any shape, as long as the difference between core and cladding refractive indices is sufficiently small which holds true for almost all the monomode and holey fibers. The unconventional case is proven reducible to the same technique of conventional fibers, where for each l we can approximate by a set of two, independent and non-homogeneous, Resonant Transmission Lines (RTLs), each one representing one mode of the birefringence.

The simulation of unconventional fibers with RTLs, gives a new, simple and effective method for computing the eigenvalues of the RTLs representing elliptical core fibers. The current method can also be utilized to compute the eigenvalues for various modes of the holey fibers. Furthermore, for each eigenvalue, the average values of E.M. fields for every thin cylindrical layer of radius r of the unconventional fiber is directly computable from the relevant eigenfunctions of the RTLs.

6 CHAPTER 6

Conclusions, applications and suggestions for further research

6.1. Conclusions

In the process of this thesis, the development of a non-analytical technique for the study and determination of key propagation characteristics of elliptical fibers, has been successful. This thesis' specific contributions to the study of elliptical fibers are listed below:

6.1.1. Development of an innovative method for the study of elliptical fibers

The development of a new improved method has been the main objective of the current thesis. The harmonics method is based on RTL and estimates the mode propagation constant β with significant accuracy. It avoids the cumbersome and complex theoretical analysis including Yeh's infinite matrices and avoids the use of Mathieu functions. As a result, the presented method does not use the simplifications and limitations ($\infty \leq \xi_0 \leq 0.5$) [33] that are necessary in Yeh's analysis. The harmonics method is based on valid mathematical analysis, applying Maxwell's equations on elliptical coordinates, yet proceeds with the adaptation of Transmission Lines which are utilized for the estimation of the requested value β. The resulting relations can be easily transformed into computational programs using tools like Matlab or Octave that calculate the results with significant accuracy and speed of convergence.

6.1.2. Simplified calculation of birefringence and cutoffs

Using the already existing programs that estimate the mode propagation constant, the calculation of birefringence becomes simple and fast. A demonstration is presented in chapter 3, comparing the estimated birefringence for different numbers of harmonics and different values of ellipticity. Birefringence is a major feature of elliptical fibers that renders them important for a series of applications including optical sensors. In a similar manner, the presented method has simplified the procedure of calculating the mode cutoff frequencies and investigating correlations with factors of interest like ellipticity.

6.1.3. Design and study of elliptical fibers with arbitrary index profiles

Up to now, the investigation of elliptical fibers with index profile other than step-index was based on analytical methods and was significantly complex. The harmonics method provides the tools for a much simplified and accurate estimation of the mode propagations constant β in elliptical fibers with arbitrary index profiles including triangular, parabolic, and tubular. Another advantage of the current method is its potential application on pragmatic cases of a finite cladding surrounded by air, other substances of a given index, and even multiple layers surrounding the core.

6.1.4. Development of two additional methods for the study of elliptical, eccentric, and fibers with angular asymmetry

Throughout the process of investigating new ways for estimating key properties of elliptical core fibers, 3 different methods are described and presented throughout this thesis. The first method presented in chapter 3, with the resulting harmonics, has the advantage of increased accuracy in the calculation of propagation constants and estimation of birefringence. The second method presented in chapter 4, follows a different analysis resulting in the estimation of β in eccentric core fibers and addresses the cases under which the fiber core is positioned asymmetrically within the cladding. This method lays the basis for approaching the D-shaped fiber which is a subcategory of elliptical core fibers. The third and final method, presented in chapter 5, defines unconventional fibers and approaches the study of elliptical fibers from a broader-to-narrower perspective. In estimating β, this method, although not significantly inferior in accuracy, has the advantage of speed and simplicity while avoiding the complexity of harmonics.

6.2 Suggestions for further study

The resulting methods and algorithms developed in the course of the study throughout this thesis can be used as tools for further study not only of elliptical optical fibers but also of other fiber categories including the D-shaped fiber and the PCF, also known as holey fibers.

6.2.1 Analysis of field components in elliptical fibers

Basic definitions of EM field components are given throughout this thesis for cylindrical and elliptical core fibers alike. However, the exact course of the field's

angular and radial components, as well as the resultant total field measure in the direction z of propagation, need to be investigated. Relevant studies have already been conducted as for example in Li Hui-Rong et al. [52] where field components are numerically calculated and analyzed for the case of elliptical dielectric hollow fiber. An innovative approach using the RTL method would surpass existing analytical methods in simplicity and converging speed, but it would also be easily expandable to various categories of elliptical fibers, simply by changing the index profile of the fiber.

Another suggestion for further study would be the reconstruction of an elliptical core fiber from the mode electric field. Reconstruction of cylindrical core fibers has already been successfully analyzed using the RTL method in AC Boucouvalas, CA Thraskias [53], [54]. A relevant study for elliptical fibers would be innovative and would provide significant design tools to manufacturers supplying fibers for a series of applications that require specific propagation characteristics such as birefringence mode propagation constants.

6.2.1 Estimation of propagation characteristics of the D-shaped fiber

D-shaped fiber is a specific type of fiber used primarily in pressure and temperature sensors. It has an estimated high dependence on cut off wavelength upon polarization and low intrinsic birefringence. An efficient study of their propagation properties can be based on analyses provided in this thesis, either as a combination of the harmonic-based method with the eccentric fiber analyses or using the unconventional-fiber method presented in chapter 5. For a study that focuses more on birefringence, the harmonic-based method should be preferred as it provides more accurate results in relation to mode decoupling.

6.2.2 Estimation of propagation characteristics of PCFs

In chapter 5 of the current thesis, the unconventional fibers are defined as a generic super-category that includes elliptical fibers. Photonic-Crystal fibers or PCFs are a category on their own, yet they fall into the defined super-category of unconventional fibers. An innovative approach could utilize the RTL technique as modified in chapter 5 in order to study and calculate propagation characteristics of holey fibers.

REFERENCES

[1] M. Schwartz, Information Transmission, Modulation, and Noise, 4th ed., McGraw-Hill, New York, 1990

[2] L. W. Couch II, Digital and Analog Communication Systems, 5th ed., Prentice Hall, Upper Saddle River, NJ, 1995.

[3] Agrawal, Govind P. Fiber-optic communication systems. Vol. 222. John Wiley & Sons, 2012.

[04] Jackson, J. D. (1999) "*Classical Electrodynamics*", NY:Wiley.

[05] Clarricoats, P. J. B., (1976) "*Optical fiber wave-guides*" in "*PROGRESS IN OPTICS XIV*" North-Holland.

[06] Takanori O. (1982), "*Optical Fibers*", Academic Press.

[07] Senior, J. M. (1985) "*Optical Fiber Communications*", Prentice-Hall Int., London.

[08] Sujecki, S. (2015) "*Photonics Modelling & Design*", CRC Press, Taylor & Francis.

[09] Yeh, C., Shimabukuro, F. I., (2008) "*The Essence of Dielectric Waveguides*", Springer Sci.+Business Media LLC.

[10] Alexandrov, O. (2004) "*Wave propagation in optical fibers: Analysis and optimization*", PhD thesis, Univ. Minnesota.

[11] Gallawa, R. L., "*Propagation in non-uniform waveguides with impedance walls*", Radio Sci. J. Res., NBC/USNC-URSI, **68**D(11) (1964) pp 1201-1213.

[12] Clarricoats, P. J. B., Oliner, A. A., "*Transverse-network representation for inhomogeneously filled circular waveguide*", Proc. IEE, 112(5) (1965) pp 883-894

[13] Oliner, A. A., Clarricoats, P. J. B., "*Transverse equivalent networks for slotted inhomogeneous circular waveguides.*", Proc. IEE, 114(4) (1967) pp 445-456.

[14] Shigezawa, H, Tsuzi, M., "*A new equivalent network approach to electromagnetic wave problems*", PIER 13, (1996) pp 243-291.

[15] C. D. Papageorgiou, A. C. Boucouvalas, "*Propagation constants of cylindrical dielectric waveguides with arbitrary refractive index profile using the 'Resonance' technique*.", Electronics Letters, 18(18), (1982) pp. 768-788.

[16] A. C. Boucouvalas, C. D. Papageorgiou, "*Cutoff frequencies in optical fibres of arbitrary refractive index profile using the 'resonance' technique*.", IEEE Journal of Quantum Electronics, QE-18(12), (1982) pp. 2027-2031.

[17] Pryce, J. D. (1993) "*Numerical Solution of Sturm–Liouville Problems*.", Oxford: Clarendon Press.

[18] A. C. Boucouvalas, X. Qian, "*Optical fiber refractive index profile synthesis from near field*" ,Proc. IEEE GLOBECOM, San Francisco, CA, 2003, pp. 2669–2673.

[19] Papageorgiou, C. D., T. E. Raptis, and A. C. Boucouvalas. "Simulation of Quantum Wires with Resonant Transmission Lines."

[20] Desoer, Charles A. *Basic circuit theory*. Tata McGraw-Hill Education, 2010.

[21] Ni, W-M., Lambertus A. Peletier, and James Serrin, eds. *Nonlinear Diffusion Equations and Their Equilibrium States II: Proceedings of a Microprogram Held August 25–September 12, 1986*. Vol. 13. Springer Science & Business Media, 2012.

[22] Chu, Lan Jen. "Electromagnetic waves in elliptic hollow pipes of metal." *Journal of Applied Physics* 9.9 (1938): 583-591.

[23] Karbowiak, A. E. "The elliptic surface wave." *British Journal of Applied Physics* 5.9 (1954): 328.

[24] Lyubimov, L. A., G. I. Veselov, and N. A. Bei. "Dielectric waveguide with elliptical cross-section." *Radio Eng. Electron.(USSR)* 6 (1961): 1668-1677.

[25] C. Yeh, “ Elliptical Dielectric Waveguides”, J. Appl. Phys. (1962) 33, pp3235-3243.

[26] Dyott, R. B., and J. R. Stern. "Group delay in glass-fibre waveguide." *Electronics Letters* 7.3 (1971): 82-84.

[27] Schlosser, W. O. "Delay distortion in weakly guiding optical fibers due to elliptic deformation of the boundary." *Bell System Technical Journal* 51.2 (1972): 487-492.

[28] Ramaswamy, V., William G. French, and R. D. Standley. "Polarization characteristics of noncircular core single-mode fibers." *Applied optics* 17.18 (1978): 3014-3017.

[29] Dyott, Ro B., J. R. Cozens, and D. G. Morris. "Preservation of polarisation in optical-fibre waveguides with elliptical cores." *Electronics Letters* 15.13 (1979): 380-382.

[30] S.M. Saad, “*On the higher order modes of elliptical optical fibers*”, IEEE Trans. MTT, Vol. MTT-33, (1985) pp. 1110-1112.

[31] S.R. Rengarajan, “*On the higher order mode cut-off frequencies in elliptical step index fibers*”, IEEE Trans on MTT vol. 37,1989, pp.1244-1248.

[32] Dyott, R.B., “*Cut-off of the first higher order modes in elliptical dielectric waveguide- An experimental approach*” Electronic Letters, Vol.26, (1990) pp.1721-1722.

[33] C. Yeh, “Electromagnetic Surface Wave Propagation Along a Dielectric Cylinder of Elliptical Cross Section”, Calif. Inst. Of Techn. Antenna Laboratory Technical Report No 27. (1962), pp1-202.

[34] N.W. McLachlin, (1947) “*Theory and applications of Mathieu functions*”, Oxford Univ. Press, London.

[35] Adams, M. J., D. N. Payne, and C. M. Ragdale. "Birefringence in optical fibres with elliptical cross-section." *Electronics Letters* 15.10 (1979): 298-299.

[36] Marcuse, Dietrich. *Theory of dielectric optical waveguides*. Elsevier, 2013.

[37] Snyder, Allan W., and William R. Young. "Modes of optical waveguides." *JOSA* 68.3 (1978): 297-309.

[38] Poole, Craig D., et al. "Broadband dispersion compensation by using the higher-order spatial mode in a two-mode fiber." Optics letters 17.14 (1992): 985-987.

[39] Dyott, Richard B. *Elliptical fiber waveguides*. Artech House, 1995.

[40] Blake, James N., et al. "Strain effects on highly elliptical core two-mode fibers." Optics Letters 12.9 (1987): 732-734.

[41] Bohnert, Klaus M., H. Brändle, and G. Frosio. "Field test of interferometric optical fiber high-voltage and current sensors." Tenth International Conference on Optical Fibre Sensors. Vol. 2360. International Society for Optics and Photonics, 1994.

[42] Risk, W. P., et al. "Acousto-optic frequency shifting in birefringent fiber." Optics letters 9.7 (1984): 309-311.

[43] Cokgor, I., V. A. Handerek, and A. J. Rogers. "Distributed optical-fiber sensor for spatial location of mode coupling by using the optical Kerr effect." Optics letters 18.9 (1993): 705-707.

[44] Park, Hee Gap, C. C. Pohalski, and Byoung Yoon Kim. "Optical Kerr switch using elliptical-core two-mode fiber." Optics letters 13.9 (1988): 776-778.

[45] Park, Hee Gap, Shang-Yuan Huang, and Byoung Yoon Kim. "All-optical intermodal switch using periodic coupling in a two-mode waveguide." Optics letters 14.16 (1989): 877-879.

[46] Stolen, R. H., and E. H. Turner. "Faraday rotation in highly birefringent optical fibers." Applied optics 19.6 (1980): 842-845.

[47] E. Georgantzos, C. D. Papageorgiou, A. C. Boucouvalas, "*A transmission line model for propagation in elliptical core optical fibers.*", Int. Conf. Comp. Meth. Sci. Eng. ICCMSE 2015.

[48] Schinzinger, R., P. A. A. Laura, “Conformal Mapping: Methods and Applications”, Courier Corporation, pp. 21-25, 2003.

[49] Naoto Kishi, Eikichi Yamashita, “*Realization of Broad-Band Phase Devices by Using W-Type Eccentric-Core Oprical Fibers*”, J. Lightwave Technology, 8(8), (1990).

[50] Hyunkieu Y., S. Lee, “*A Variational Calculation of TE and TM Cutoff Wavenumbers in Circular Eccentric Guides by Conformal Mapping*”, MICROWAVE AND OPTICAL TECHNOLOGY LETTERS, 31, (2001).

[51] C. Guan, L. Yuan, F. Tian, Q. Dai, X. Tian, “*Mode field analysis of eccentric optical fibers by conformal mapping*”, SPIE, 7753, (2011).

[52] Hui-Rong, Li, and Yin Jian-Ping. "Propagation properties of electromagnetic fields in elliptic dielectric hollow fibres and their applications." *Chinese Physics B* 19.8 (2010): 083204.

[53] Boucouvalas, A. C., and C. A. Thraskias. "Accurate optical fiber refractive index reconstruction from near field." *2008 6th International Symposium on Communication Systems, Networks and Digital Signal Processing*. IEEE, 2008.

[54] Boucouvalas, Anthony C., and Christos A. Thraskias. "*Design of arbitrary modal electric field in cylindrical waveguides.*" IEEE Journal of Quantum Electronics 50.10 (2014): 840-847.

7 APPENDICES

Appendix A. Mathematical Analysis for the Derivation of Propagation Relations in Cylindrical Core Fibers

$$\nabla \times \vec{E} = -j\vec{H}$$

$$\nabla \cdot \vec{H} = 0$$

$$F = \frac{(\beta r)^2 + l^2}{r}$$

$$\frac{\partial(rH_r)}{\partial r} + jlH_\varphi + j\beta rH_z = 0 \quad \text{(A.1)}$$

$$rH_r = jI_M \Rightarrow -jrH_r = I_M \quad \text{(A.2)}$$

From the above, we obtain

$$\frac{\partial I_M}{\partial r} = -j\left(lH_\varphi + \beta rH_z\right)$$

$$\frac{\partial(rH_r)}{\partial r} = -jF\frac{\left(lH_\varphi + \beta rH_z\right)}{jF}$$

Further we define

$$V_M = \frac{lH_\varphi + \beta rH_z}{jF} \quad \text{(A.3)}$$

Thus

$$\frac{\partial I_M}{\partial r} = -jFV_M \quad \text{(A.4)}$$

By the relation $\nabla \times \vec{E} = -j\vec{H}$, the following equations are obtained

$$\begin{cases} jl\frac{E_z}{r} - j\beta \mathrm{E}_\varphi = -jH_r & \text{(A. 5.1)} \\ j\beta E_r - \frac{\partial \mathrm{E}_z}{\partial r} = -jH_\varphi & \text{(A. 5.2)} \\ \frac{\partial(r\mathrm{E}_\varphi)}{\partial r} - jlE_r = -jrH_z & \text{(A. 5.3)} \end{cases} \quad \text{(A.5)}$$

From (A.5.1) it is derived that

$$-j(rH_r) = jlE_z - j\beta r\mathrm{E}_\varphi$$

Thus

$$I_M = j\left(lE_z - \beta r\mathrm{E}_\varphi\right) \tag{A.6}$$

In the same way, by $\nabla \times \vec{H} = -jn^2\vec{E}$, it can be proved that

$$\nabla\left(n^2\vec{E}\right) = 0$$

Defining

$$I_E = n^2 rE_r \tag{A.7}$$

we obtain

$$\frac{\partial(n^2 r\mathrm{E}_r)}{\partial r} + jln^2E_\varphi + j\beta rn^2E_z = 0$$

Additionally defining

$$V_E = \frac{lE_\varphi + \beta rE_z}{F} \tag{A.8}$$

$$\frac{\partial I_E}{\partial r} = -jn^2F\left(\frac{lE_\varphi + \beta rE_z}{F}\right) = -jn^2FV_E \tag{A.9}$$

Again, by $\nabla \times \vec{H} = -jn^2\vec{E}$, we get

$$\begin{cases} jl\frac{H_z}{r} - j\beta\mathrm{H}_\varphi = jn^2E_r & (\mathrm{A.10.1}) \\ j\beta H_r - \frac{\partial \mathrm{H}_z}{\partial r} = jn^2E_\varphi & (\mathrm{A.10.2}) \\ \frac{\partial(r\mathrm{H}_\varphi)}{\partial r} - jlH_r = -jn^2rE_z & (\mathrm{A.10.3}) \end{cases} \tag{A.10}$$

From (A.10.1), it results

$$n^2rE_r = lH_z - \beta rH_\varphi$$

Thus

$$I_E = lH_z - \beta r H_\varphi \tag{A.11}$$

Furthermore (A.2) and (A.7) define $H_r = \frac{jI_M}{r}$, $E_r = \frac{I_E}{n^2 r}$

And (A.3), (A.6), (A.8), (A.11), in order to express $H_\varphi, H_z, E_\varphi, H_z$ by I_M, I_E, V_M, V_E as follows:

$$\begin{cases} jFV_M = lH_\varphi + \beta r H_z \\ I_E = -\beta r H_\varphi + lH_z \end{cases}$$

With $Fr = l^2 + (\beta r)^2$

$$H_\varphi = \frac{\begin{vmatrix} jFV_M & \beta r \\ I_E & l \end{vmatrix}}{Fr} = \frac{jFlV_M - \beta r I_E}{Fr} = \frac{jlV_M}{r} - \frac{\beta}{F} I_E$$

$$=> H_\varphi = \frac{jlV_M}{r} - \frac{\beta}{F} I_E$$

$$H_z = \frac{\begin{vmatrix} l & jFV_M \\ -\beta r & I_E \end{vmatrix}}{Fr} = \frac{l}{Fr} I_E + j\beta V_M$$

$$=> H_z = \frac{l}{Fr} I_E + j\beta V_M$$

And

$$H_r = j\frac{I_M}{r}$$

Furthermore

$$\begin{cases} FV_E = lE_\varphi + \beta r E_z \\ I_M = -\beta r E_\varphi + lE_z \end{cases}$$

With $Fr = l^2 + (\beta r)^2$

$$E_\varphi = \frac{\begin{vmatrix} FV_E & \beta r \\ -jI_M & l \end{vmatrix}}{Fr} = \frac{(FlV_E)}{Fr} + \frac{j\beta r}{Fr} I_M$$

$$=> E_\varphi = \frac{l}{r} V_E + j\frac{\beta}{F} I_M$$

$$E_z = \frac{\begin{vmatrix} l & FV_E \\ -\beta r & -jI_M \end{vmatrix}}{Fr} = \frac{\beta r F}{Fr} V_E - \frac{jlI_M}{Fr}$$

$$=> E_z = \beta V_E - \frac{jl}{Fr} I_M$$

And

$$E_r = \frac{I_E}{n^2 r}$$

Further follows the calculation of the relation $\frac{\partial V_M}{\partial r}$

$$j\frac{\partial(FV_M)}{\partial r} = jF\frac{\partial V_M}{\partial r} + jV_M\frac{\partial F}{\partial r}$$

$$j\frac{\partial(FV_M)}{\partial r} = l\frac{\partial H_\varphi}{\partial r} + \beta r\frac{\partial H_z}{\partial r} + \beta H_z \tag{A.12}$$

$$\frac{\partial(rH_\varphi)}{\partial r} = jlH_r + jrn^2E_z$$

$$r\frac{\partial H_\varphi}{\partial r} = jlH_r + jrn^2E_z - H_\varphi$$

$$\frac{\partial H_\varphi}{\partial r} = \frac{jl^2H_r}{r} + jln^2E_z - \frac{lH_\varphi}{r} \tag{A.13}$$

$$\frac{\partial H_z}{\partial r} = j\beta H_r - jn^2E_\varphi$$

$$\beta r\frac{\partial H_z}{\partial r} = j\beta^2 rH_r - j\beta rn^2E_\varphi \tag{A.14}$$

Combining (A.12), (A.13) and (A.14), results in

$$j\frac{\partial(FV_M)}{\partial r} = jn^2\left(lE_z - \beta rE_\varphi\right) + jFH_r - \frac{lH_\varphi}{r} + \beta H_z$$

$$=> j\frac{\partial(FV_M)}{\partial r} = n^2I_M + \frac{jF}{r}(rH_r) - \frac{lH_\varphi}{r} + \beta H_z$$

$$=> j\frac{\partial(FV_M)}{\partial r} = n^2I_M - \frac{F}{r}I_M - \frac{lH_\varphi}{r} + \beta H_z$$

$$j\frac{\partial(FV_M)}{\partial r} = -\gamma^2 I_M - \frac{lH_\varphi}{r} + \beta H_z \quad \text{(A.15)}$$

Where $\gamma^2 = \beta^2 - n^2 + \frac{l^2}{r^2}$

Combining (A.1) and (A.5) the following relation is obtained

$$jF\frac{\partial V_M}{\partial r} + j\frac{\partial F}{\partial r}V_M = -\gamma^2 I_M - \frac{lH_\varphi}{r} + \beta H_z \quad \text{(A.16)}$$

$$\begin{cases} H_\varphi = \dfrac{jlV_M}{r} - \dfrac{\beta}{F} I_E \\ H_z = \dfrac{l}{Fr} I_E + j\beta V_M \end{cases}$$

$$-\frac{lH_\varphi}{r} = -\frac{jl^2}{r^2}V_M + \frac{\beta l}{Fr}I_E$$

$$\beta H_z = \frac{\beta l}{Fr}I_E + j\beta^2 V_M$$

$$-j\frac{\partial F}{\partial r}V_M = j\left(\beta^2 - \frac{l^2}{r^2}\right)V_M$$

$$=> jF\frac{\partial V_M}{\partial r} = \frac{2\beta l}{Fr}I_E - \gamma^2 I_M$$

$$\frac{2\beta l}{Fr} = \frac{2\beta l}{(\beta r)^2 + l^2} = MF$$

$$M = \frac{2\beta l}{((\beta r)^2 + l^2)F}$$

Thus

$$\frac{\partial V_M}{\partial r} = -\frac{\gamma^2}{jF}I_M - jMI_E$$

Following a similar approach, we obtain:

$$\frac{\partial V_E}{\partial r} = -\frac{\gamma^2}{jn^2 F}I_E - jMI_M$$

Appendix B: Mathematical analysis for elliptical waveguides

Orthogonality Relations of Mathieu Functions:

a. For all γ^2

$$\int_0^{2\pi} ce_m(\eta,\gamma^2)ce_p(\eta,\gamma^2)d\eta = 0 \qquad m \neq p$$

$$\int_0^{2\pi} se_m(\eta,\gamma^2)se_p(\eta,\gamma^2)d\eta = 0 \qquad m \neq p$$

$$\int_0^{2\pi} ce_m(\eta,\gamma^2)se_p(\eta,\gamma^2)d\eta = 0 \qquad m \neq p$$

b. For $\gamma^2 \geq 0$

$$\int_0^{2\pi} ce^2{}_{2n}(\eta,\gamma^2)d\eta = 2\pi\left[A_o^{(2n)}\right]^2 + \pi\sum_{r=1}^{\infty}\left[A_{2r}^{(2n)}\right]^2$$

$$\int_0^{2\pi} ce^2{}_{2n+1}(\eta,\gamma^2)d\eta = \pi\sum_{r=0}^{\infty}\left[A_{2r+1}^{(2n+1)}\right]^2$$

$$\int_0^{2\pi} se^2{}_{2n+1}(\eta,\gamma^2)d\eta = \pi\sum_{r=0}^{\infty}\left[B_{2r+1}^{(2n+1)}\right]^2$$

$$\int_0^{2\pi} se^2{}_{2n+2}(\eta,\gamma^2)d\eta = \pi\sum_{r=0}^{\infty}\left[B_{2r+2}^{(2n+2)}\right]^2$$

c. For $\gamma^2 \leq 0$

$$\int_0^{2\pi} ce^2{}_{2n}(\eta,|\gamma^2|)d\eta = 2\pi\left[A_o^{(2n)}\right]^2 + \pi\sum_{r=1}^{\infty}\left[A_{2r}^{(2n)}\right]^2$$

$$\int_0^{2\pi} ce^2{}_{2n+1}(\eta,|\gamma^2|)d\eta = \pi \sum_{r=0}^{\infty} \left[B_{2r+1}^{(2n+1)}\right]^2$$

$$\int_0^{2\pi} se^2{}_{2n+1}(\eta,|\gamma^2|)d\eta = \pi \sum_{r=0}^{\infty} \left[A_{2r+1}^{(2n+1)}\right]^2$$

$$\int_0^{2\pi} se^2{}_{2n+2}(\eta,|\gamma^2|)d\eta = \pi \sum_{r=0}^{\infty} \left[B_{2r+2}^{(2n+2)}\right]^2$$

Derivation of Maxwell equations in elliptical coordinate system

Using the definitions of equations (3.8) we proceed in the analysis as follows: Using the so called second couple of Maxwell equations (3.5) and (3.6) we can facilitate the derivation.

$$\nabla \bullet \vec{H} = 0 \qquad \text{(B.1)}$$

$$\nabla \bullet \vec{E} = 0 \qquad \text{(B.2)}$$

Equations (B.1) and (B.2) are not independent from the six equations arising from (3.2) and (3.3) as they can be derived from them, however they are useful in order to have the first set of the differential equations relating the equivalent currents and voltages I_M, I_E, V_M, V_E.

Writing the equations (B.1) and (B.2) in an elliptic coordinate system the following partial differential equations we arrive at

$$\frac{\partial(hH_\theta)}{\partial\theta} + \frac{\partial(hH_\varphi)}{\partial\varphi} + \frac{\partial(h^2H_z)}{\partial z} = 0$$

$$\frac{\partial(hE_\theta)}{\partial\theta} + \frac{\partial(hE_\varphi)}{\partial\varphi} + \frac{\partial(h^2E_z)}{\partial z} = 0$$

Fourier transforming the above equations as along $\varphi and z with\ wavenumbers \beta and\ l\ an\ integer$ and using the previous convolution relations, the following ordinary differential equations are derived

$$\frac{\partial\overline{(hH_\theta)}}{\partial\theta} + l\left(\overline{hH_\varphi}\right) + {h_0}^2\beta\overline{H}_z - \beta\frac{c^2}{4}[\Phi_1] = 0$$

$$\frac{\partial\overline{(hE_\theta)}}{\partial\theta} + l\left(\overline{hE_\varphi}\right) + {h_0}^2\beta\overline{E}_z - \beta\frac{c^2}{4}[\Phi_2] = 0$$

$\Phi_1$and Φ_2 are defined in (3.6) and (3.7) respectively. Thus the previous relations can be written in terms of the defined functional parameters (B.7) as follows

$$\frac{\partial I_M}{\partial\theta} = -jFV_M + \frac{\beta c^2}{4}[\Phi_1] \qquad \text{(B.3.1)}$$

$$\frac{\partial I_E}{\partial\theta} = -jFn^2V_E + \frac{jn^2\beta c^2}{4}[\Phi_2]$$

Using the definitions of V_M, V_E, I_M, I_E

$$\begin{cases} I_M = -j\left(\overline{hH_\theta}\right) = j\left(l\overline{E_z} - \beta\left(\overline{hE_\varphi}\right)\right) \\ I_E = n^2\left(\overline{hE_\theta}\right) = \left(l\overline{H_z} - \beta\left(\overline{hH_\varphi}\right)\right) \\ V_M = \frac{l\left(\overline{hE_\varphi}\right) + \beta h_0^2(\theta)\overline{E}_z}{jF} \\ V_E = \frac{l\left(\overline{hE_\varphi}\right) + \beta h_0^2(\theta)\overline{E}_z}{F} \end{cases}$$

And following a cumbersome procedure another set of two differential equations can be derived

$$\frac{\partial V_M}{\partial\theta} = -\frac{\gamma^2}{jF}I_M - jMI_E - \frac{n^2lc^2}{4F}[\Phi_2] \qquad \text{(B.3.2)}$$

$$\frac{\partial V_E}{\partial\theta} = -\frac{\gamma^2}{n^2F}I_E - jMI_M + j\frac{lc^2}{4F}[\Phi_1]$$

These four differential equations (B 3.1 & B3.2) along θ are representing two interlinked transmission lines, where furthermore their values for a wave number l are related with their values for the wave numbers $l+2$ and $l-2$. We call them "harmonics" appearing because of the relation ${h^2}_{(\varphi,\theta)} = h^2_{0(\theta)} - \frac{c^2}{4}(e^{j2\varphi} + e^{-j2\varphi})$ being a function of φ. In the case where the circular layers h^2 is independent of φ, there are no "harmonics" and the analysis becomes much simpler.

The proof for B 3.2 relations is shown below:

By the intermediate relations:

$$h^2 \otimes \overline{H_z} = h_0^2 \overline{H_z} - \frac{c^2}{4}[\Phi_1]$$

$$h^2 \otimes \overline{E_z} = h_0^2 \overline{E_z} - \frac{c^2}{4}[\Phi_2]$$

$$h_0^2 = \frac{c^2}{2}\cosh 2\theta \qquad F = l^2 + \beta^2 h_0^2 \qquad \frac{\partial F}{\partial \theta} = \beta^2 \frac{\partial h_0^2}{\partial \theta}$$

$$\left\{\frac{\partial (jFV_M)}{\partial \theta} = jF\frac{\partial V_M}{\partial \theta} + j\frac{\partial F}{\partial \theta}V_M = jF\frac{\partial V_M}{\partial \theta} + j\beta^2\frac{\partial h_0^2}{\partial \theta}V_M \right. \tag{B.4}$$

$bu\square$ $jFV_M = l\left(\overline{hH_\varphi}\right) + \beta h_0^2(\overline{H_z})$ so that finally:

$$\frac{\partial (jFV_M)}{\partial \theta} = l\frac{\partial\left(\overline{hH_\varphi}\right)}{\partial \theta} + \beta\frac{\partial h_0^2}{\partial \theta}(\overline{H_z}) + \beta^2 h_0^2\frac{\partial(\overline{H_z})}{\partial \theta}$$

Taking into consideration that$\overline{H_z} = l\frac{I_E}{F} + j\beta V_M$we also derive

$$\frac{\partial (jFV_M)}{\partial \theta} = l\frac{\partial\left(\overline{hH_\varphi}\right)}{\partial \theta} + \beta h_0^2\frac{\partial(\overline{H_z})}{\partial \theta} + \frac{\beta l}{F}\frac{\partial h_0^2}{\partial \theta}I_E + j\beta^2\frac{\partial h_0^2}{\partial \theta}V_M \tag{B.5}$$

Thus we obtain

$$jF\frac{\partial V_M}{\partial \theta} = l\frac{\partial\left(\overline{hH_\varphi}\right)}{\partial \theta} + \beta h_0^2\frac{\partial(\overline{H_z})}{\partial \theta} + \frac{\beta l}{F}\frac{\partial h_0^2}{\partial \theta}I_E \tag{B.6}$$

Using the differential relations of the previous paragraph we also obtain

$$l\frac{\partial\left(\overline{hH_\varphi}\right)}{\partial \theta} = jl^2\left(\overline{hH_\theta}\right) + jn^2 l h_0^2\overline{E_z} - \frac{jn^2lc^2}{4}[\Phi_2] \tag{B.7}$$

$$\beta h_0^2\frac{\partial(\overline{H_z})}{\partial \theta} = j\beta^2 h_0^2\left(\overline{hH_\theta}\right) - jn^2\beta h_0^2\left(\overline{hE_\varphi}\right) \tag{B.8}$$

Thus

$$jF\frac{\partial V_M}{\partial\theta} = j(l^2+\beta^2h_0^2)\left(\overline{hH_\theta}\right) + jn^2lh_0^2\left(\overline{E_z}\right) + \frac{\beta l}{F}\frac{\partial h_0^2}{\partial\theta}I_E - jn^2\beta h_0^2\left(\overline{hE_\varphi}\right) - \frac{jn^2lc^2}{4}[\Phi_2]$$

We also know that

$$l\left(\overline{E_z}\right) - \beta\left(\overline{hE_\varphi}\right) = -\left(\overline{hH_\theta}\right)$$

Thus

$$jF\frac{\partial V_M}{\partial\theta} = j(l^2+\beta^2h_0^2-n^2h_0^2)\left(\overline{hH_\theta}\right) + \frac{\beta l}{F}\frac{\partial h_0^2}{\partial\theta}I_E - \frac{jn^2lc^2}{4}[\Phi_2] \qquad \text{(B.9)}$$

This is simplified as

$$jF\frac{\partial V_M}{\partial\theta} = j\gamma^2\left(\overline{hH_\theta}\right) + MFI_E - \frac{jn^2lc^2}{4}[\Phi_2] \qquad \text{(B.10)}$$

with the introduction of the auxiliary variable

$$\gamma^2 = l^2 + h_0^2(\beta^2-n^2), \qquad M = \frac{\beta l}{F^2}\frac{\partial h_0^2}{\partial\theta}$$

Taking into account that $\left(\overline{hH_\theta}\right) = jI_M$ we further get

$$jF\frac{\partial V_M}{\partial\theta} = -\gamma^2I_M + MFI_E - \frac{jn^2lc^2}{4}[\Phi_2]$$

and finally

$$\frac{\partial V_M}{\partial\theta} = -\frac{\gamma^2}{jF}I_M - jMI_E - \frac{n^2lc^2}{4F}[\Phi_2] \qquad \text{(B.11)}$$

Following a similar approach we can prove that

$$\frac{\partial V_E}{\partial \theta} = -\frac{\gamma^2}{jn^2F} I_E - jMI_M + j\frac{lc^2}{4F}[\Phi_1] \qquad \text{(B.12)}$$

Where: $\gamma^2 = l^2 + (\beta^2 - n^2){h_0}^2$, $M = \beta l \frac{\partial {h_0}^2}{\partial \theta}/F^2$,$F = l^2 + \beta^2 {h_0}^2$

A useful remark is that along θ the "Currents" are continuous because $\overline{hH_\theta} and n^2(\overline{hE_\theta})$ as (i.e. the F.T. of the normal induction field components $\mu_0 H_\theta and n^2 \varepsilon_0 E_\theta$) on the surface (φ, z) are continuous. The "Voltages" are also continuous because the tangential field components $H_\varphi H_z E_\varphi E_z$along θ and the function h are continuous "passing" the surface(φ, z) and every linear combination of them is continuous on the surface(φ, z).

Finally to derive an equivalent transmission line of the two interlinked transmission lines we
we define a new "voltage"V_S and a new "current"I_S by the relations
$V_S = V_M + nV_E I_S = I_M + \frac{I_E}{n}$ representing even modes.

Using relations (B.18) we get

$$\begin{cases} \dfrac{\partial V_M}{\partial \theta} = -\dfrac{\gamma^2}{jF} I_M - jM\dfrac{I_E}{n} - \dfrac{nlc^2}{4F}[n\Phi_2] \\ \dfrac{\partial (nV_E)}{\partial \theta} = -\dfrac{\gamma^2}{jF}\dfrac{I_E}{n} - jnMI_M + \dfrac{nlc^2}{4F}[j\Phi_1] \end{cases}$$

Thus we also obtain

$$\frac{\partial V_S}{\partial \theta} = -\frac{\gamma^2 - nMF}{jF} I_S + \frac{nlc^2}{4F}[j\Phi_1 - n\Phi_2] \qquad \text{(B.13)}$$

Using also (B.3.1 & B 3.2)

$$\begin{cases} \frac{\partial I_M}{\partial \theta} = -jFV_M - \frac{\beta c^2}{4}[j\Phi_1] \\ \frac{\partial \left(I_E/n\right)}{\partial \theta} = -jFnV_E + j\frac{\beta c^2}{4}[n\Phi_2] \end{cases} \text{ thus:}$$

$$\frac{\partial I_S}{\partial \theta} = -jFV_S - \frac{j\beta c^2}{4}[j\Phi_1 - n\Phi_2] \quad \text{(B.14)}$$

We also have that

$$\begin{cases} [\Phi_1] = \frac{l-2}{F_{l-2}} I_E^{l-2} + j\beta V_M^{l-2} + \frac{l+2}{F_{l+2}} I_E^{l+2} + j\beta V_M^{l+2} \\ [\Phi_2] = -\frac{j(l-2)}{F_{l-2}} I_M^{l-2} + \beta V_E^{l-2} - \frac{j(l+2)}{F_{l+2}} I_M^{l+2} + \beta V_E^{l+2} \end{cases}$$

Thus we obtain

$$[j\Phi_1 - n\Phi_2] = \frac{j(l-2)n}{F_{l-2}}\left[\left[\frac{I_E^{l-2}}{n} + I_M^{l-2}\right] + j\left[\frac{I_E^{l+2}}{n} + I_M^{l+2}\right]\right] - \beta\left[\left[V_M^{l-2} + nV_E^{l-2}\right] + \left[V_M^{l+2} + nV_E^{l+2}\right]\right]$$

$$[j\Phi_1 - n\Phi_2] = \frac{j(l-2)n}{F_{l-2}} I_S^{l-2} + \frac{j(l+2)n}{F_{l+2}} I_S^{l+2} - \beta\left[V_S^{l-2} + V_S^{l+2}\right] \quad \text{(B.15)}$$

Thus for $q = \frac{nc^2}{4}$, $and A = \frac{ql}{F_l} and B = \frac{\beta q}{n}$ we will get

$$\frac{\partial V_S^l}{\partial \theta} = -\frac{\gamma_l^2 - nM_l F_l}{jF_l} I_S^l + jA\frac{(l-2)n}{F_{l-2}} I_S^{l-2} + jA\frac{(l+2)n}{F_{l+2}} I_S^{l+2} - A\beta\left[V_S^{l-2} + V_S^{l+2}\right] \quad \text{(B.16)}$$

$$\frac{\partial I_S^l}{\partial \theta} = -jF_l V_S^l + B\frac{(l-2)n}{F_{l-2}} I_S^{l-2} + B\frac{(l+2)n}{F_{l+2}} I_S^{l+2} + jB\beta\left[V_S^{l-2} + V_S^{l+2}\right] \quad \text{(B.17)}$$

where

$F_{l+2} = (l+2)^2 + \beta^2 {h_0}^2, F_{l-2} = (l-2)^2 + \beta^2 {h_0}^2, F_l = l^2 + \beta^2 {h_0}^2,$

$\gamma_l^2 = l^2 + \left(\beta^2 - n^2\right){h_0}^2, \qquad M_l = \beta l \frac{\partial {h_0}^2}{\partial \theta} / \mathrm{F_l^2}$

Equations (B.16) and (B.17) represent a transmission line with “harmonics”. The exponents in the relations (B.16) and (B.17) on $V_S$and $I_S$are giving the harmonic order. In order to have real coefficients we can set $U_S = jV_S$ so that (B.16) and (B.17) become

$$\begin{cases} \frac{\partial U_S^l}{\partial \theta} = -\frac{\gamma_l^2 - nM_lF_l}{F_l} I_S^l - A\frac{(l-2)n}{F_{l-2}} I_S^{l-2} - A\frac{(l+2)n}{F_{l+2}} I_S^{l+2} \\ \qquad -A\beta\left[U_S^{l-2} + U_S^{l+2}\right] \end{cases}$$

Using also

$$\begin{cases} \frac{\partial I_S^l}{\partial \theta} = -F_l U_S^l + B\frac{(l-2)n}{F_{l-2}} I_S^{l-2} + B\frac{(l+2)n}{F_{l+2}} I_S^{l+2} + B\beta\left[U_S^{l-2} + U_S^{l+2}\right] \end{cases}$$

$A = \frac{ql}{F_l} B = \frac{\beta q}{n}$ we get

$$\begin{cases} \frac{\partial U_s^l}{\partial \theta} = -\frac{\gamma^2 - nMF}{F} I_s^l - \frac{lqn}{F}\left[\frac{(l-2)}{F_{l-2}} I_s^{l-2} + \frac{(l+2)}{F_{l+2}} I_s^{l+2}\right] - \frac{q\beta l}{F}\left[U_s^{l-2} + U_s^{l+2}\right] \\ \frac{\partial I_s^l}{\partial \theta} = -FU_s^l + q\beta\left[\frac{(l-2)}{F_{l-2}} I_s^{l-2} + \frac{(l+2)}{F_{l+2}} I_s^{l+2}\right] + \frac{q\beta^2}{n}\left[U_s^{l-2} + U_s^{l+2}\right] \end{cases} \quad \text{(B.18)}$$

We can follow the same procedure defining

$$V_{SS} = \frac{V_M}{n} + V_E I_{SS} = nI_M + I_E \ (I_{SS} = I_S n\ , V_{SS} = \frac{V_S}{n})$$

for the odd modes.